ABSTRACT

NARAYANAN, GANESH. Electrospinning of Poly (ε-caprolactone) Fibers Functionalized with Cyclodextrins and their Inclusion Complexes. (Under the direction of Prof.s Alan E. Tonelli and Bhupender S. Gupta).

Functionalization of polymeric nanofibers by cyclodextrins offers a novel way to enhance properties such as, small molecule encapsulation, efficient drug delivery, tissue engineering, improved mechanical and thermal behavior, in the resultant nanofibers. The advantage of using CDs, apart from their abundant availability from natural resources, biodegradability and biocompatibility, include their easy manipulation to obtain desired features in the nanofibers.

In the first study, a unique way to electrospin PCL nanofibers with α- and γ-CDs, without forming ICs was described. This was achieved by using a binary solvent mixture of chloroform/DMF, which is expected to hinder the formation of ICs. The resultant nanofibers were characterized by FTIR, DSC, TGA, SEM, water contact angle, and for the efficiency of PhP absorption. Based on the results, a simple model was proposed for both α- and γ-CD filled PCL nanowebs.

In the second study, electrospinning of PCL with β-CD was performed from mixture of chloroform/DMF, and the nanofibers were characterized using FTIR, WAXD, TGA, and SEM. An interesting application of this material, *i.e.*, as an absorbant for wound odors, was proposed, and subsequently the potential was studied by GC & XPS analysis. XPS indicated higher absorption of volatile fatty acids with higher CD loadings, whereas the absorption by the neat PCL nanofibers was little. The results found led to the suggestion that stabilizing CD

over PCL by cross-linking will enhance the wound odor absorption potential, and this idea should be explored by further experimentation.

In the third study, mechanically strong nanofibers were obtained from electrospinning PCL along with non-stochiometric inclusion complexes formed with PCL and α-CD, as a solution/suspension, from chloroform/DMF mixture. Non-stochiometric inclusion complexes were prepared from PCL and α-CD at various ratios, and were characterized by FTIR, DSC, and ^{1}H-NMR. The electrospun nanofibers were characterized by SEM, DSC, TGA, and their mechanical properties by Instron. It was observed that those nanowebs containing (n-s)-PCL-α-CD-ICs exhibited modulus values as high as six times more than that of the neat PCL, along with substantial decrease in elongation values. From these observations, it could therefore, be concluded that by using CDs and PCL, hybrid structures developed in this work has high potential for variety of biomedical applications.

Electrospinning of Poly (ε-caprolactone) Fibers Functionalized with Cyclodextrins and their Inclusion Complexes

by
Ganesh Narayanan

A dissertation submitted to the Graduate Faculty of
North Carolina State University
in partial fulfillment of the
requirements for the degree of
Doctor of Philosophy

Fiber and Polymer Science

Raleigh, North Carolina

2014

APPROVED BY:

_____	_____
Alan E. Tonelli Committee Co-Chair	Bhupender S. Gupta Committee Co-Chair
_____	_____
Russell E. Gorga Committee member	Saad A. Khan Committee member

DEDICATION

This work is dedicated to my parents, my older siblings, extended family, and my close friends from India and the US, who stood with me and motivated me to pursue a PhD degree. I certainly could not have done this without your support and love. Thank you all.

BIOGRAPHY

Ganesh Narayanan was born in, then sleepy little rail town of Perambur in Southern India, and was raised in nearby Ambattur, both suburbs of Madras, Tamil Nadu, India. He completed his high school education in Madras, and decided to pursue a Bachelor of Technology degree in Polymer Engineering from Mahatma Gandhi University at Kottayam, Kerala, India. After completing his Bachelor's degree in the year 2004, he gained some valuable research experience in the Rubber Research Institute of India, Kottayam, Kerala. In the fall of 2006, he decided to emigrate to the US to pursue a MS degree in Material Science & Engineering from New Jersey Institute of Technology. After gaining some industrial experience, he joined the PhD program in Fiber & Polymer science at North Carolina State University, under the mentorship of Prof.s Alan.E.Tonelli & Bhupender.S.Gupta.

Aside from academic pursuits, he is an avid reader, especially interested in history, political science, fiction and economics. One of his extracurricular ambition is to publish a legal thriller at some point in his life.

ACKNOWLEDGMENTS

First and foremost, I would like to thank Prof Bhupender S. Gupta, for recruiting me and providing the financial, emotional, intellectual support, and for introducing me to Prof Alan E. Tonelli and his research. Without your guidance and willingness to share your past research and ideas, I would have never have come so far in my Ph.D. research. Prof Tonelli, you are one of the best scientists I had ever interacted with. Thank you for all the patience you had with me, and for giving key inputs to my research. The best thing, I felt working for you was the immense freedom that you gave me to pursue my individual thoughts. I would also like to thank my committee members, Prof Saad A. Khan, and Prof. Russell E. Gorga, for their support, and willingness to pass down valuable knowledge in their fields of expertise, and for letting me use their instruments.

I would like to express my special thanks to a set of faculty that includes: Drs Wendy E. Krause, Richard A. Venditti, Michael Jaffe, Melissa Pasquinelli, Bryan Ormond, Stephen Michielsen, Martin W. King, Jon Rust, and Nelson Vinueza, who have shown a great interest in my research over the years, and have provided guidance, encouragement, and ideas pertaining to their field of expertise.

Birgit Anderson and Judy Elsen, my relationships with you have been special, and I would like to offer special thanks to both of you for helping me in equipment training, and novel ideas that I used for my research. Without your help, my PhD research certainly could have derailed.

During my graduate studies, I have had the opportunity to meet and interact with a group of intelligent, creative, and highly motivated students. I appreciate the opportunity to talk about a variety of subjects with the following: Ramiz Boy, Yongxin Wang, Hammad Cheema, Jialong Shen, Nagarajan Thoppey, Maqbool Hussain, Jen Leary, Farzad Rezaei, Nasim Farah, Maryam Mazloumpour, and Kun Fu.

During the summer of 2013, I had a great opportunity to work for Invista S.à r.l., and would like to thank my colleagues: Drs Steven Smith, Hong Liu, Dutch Waldbauer, Mick Lambert, Achille Bivigou, and my managers, Steve Huffer and Bill Bender. Thank you folks for constant motivation both during and after my internship, it was certainly a memorable time in my life.

Finally, I would like to thank my parents, siblings, non-NC State friends in the US, including Venkat, Anand, Mangesh, Narendra, Aditya, Bhagat, and Siddharth; former undergraduate classmates: Reji, Nadersha, Shaiju, Jameel, Shameem, Thomas, Suresh, Binu; and my extended family, for their constant motivation and encouragement throughout my graduate studies. Last but not the least, I would like to thank the TECS and COT administrative staff: Traci Figura, Amanda Holbrook, Vicki Stocksdale, Angie Brantley & Kathryn Collie, for taking care of chemical orders, grad school paper work, and for providing timely information.

Thank you all,

Ganesh Narayanan

October 2014.

TABLE OF CONTENTS

LIST OF TABLES

LIST OF FIGURES

Chapter 1: Introduction to Cyclodextrins and their Inclusion Complexes:

Cyclodextrins (CDs) belong to a group of cyclic α-1, 4-linked oligosaccharides. The most widely used CDs are α-, β-, and γ-CD which have 6, 7, and 8 glucopyranose units, respectively. The CDs were first observed in 1891, by French scientist, A. Villiers, when he isolated a crystalline substance from the bacterial digestion of starch. The composition of the crystalline substance was unknown then and was later estimated to be $(C_6H_{10}0_5)_2$. $3H_2O$. The crystalline material was named "cellulosine", since it was similar to cellulose in its resistance to acid hydrolysis.

Though unknown at that time, we now know, the two different crystalline substances that were isolated were a mixture of α- and β-CDs. Schardinger's research group was instrumental in distinguishing two forms of crystalline cyclodextrins by iodine reaction: α-CDs turn blue under wet conditions, and grey under dry conditions, whereas β-CDs are brownish in both damp and dry conditions [1, 2, 3**]**. The structure of the most widely used CDs, α, β and ɤ-CDs, are shown in Figure 1.1 [4a-4b].

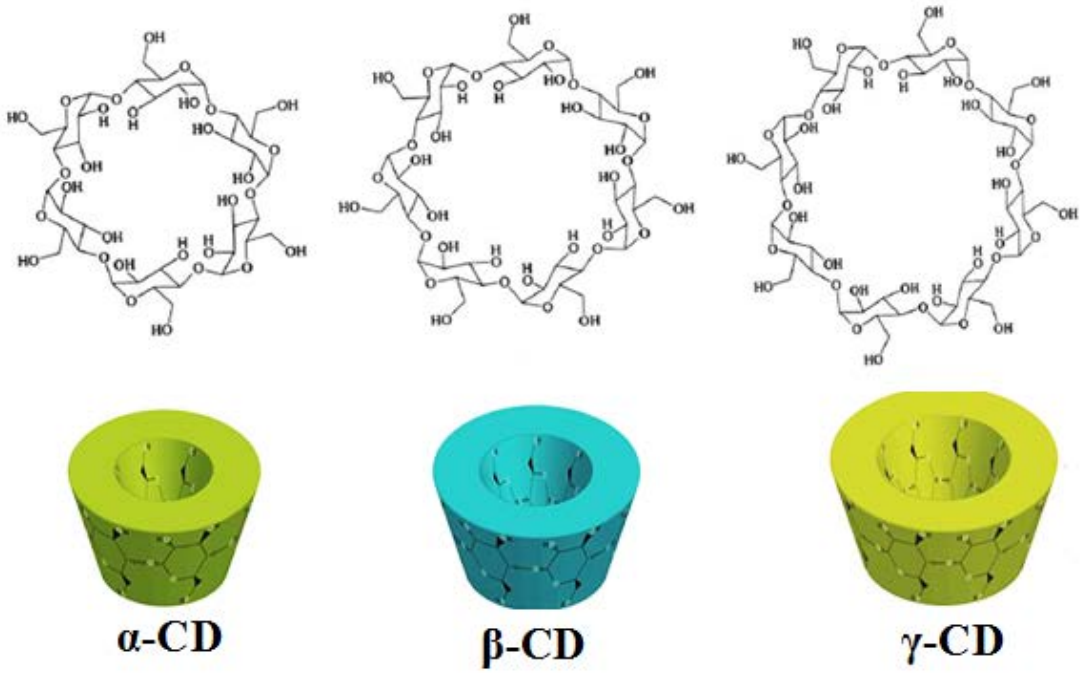

Figure 1.1: Chemical structures and schematic representation of α, β, ɤ-cyclodextrins.

Pringsheim's research group played a leading role in CD research and published extensively till 1935, yet there was no significant progress made until ɤ-CD was discovered in the 1940's and structure of the three CDs elucidated subsequently.

Figure 1.2, shows the total no of publications including conference proceedings and patents put out in the last century. It can be seen that after 1970, there is a clear explosion in the number of CD publications, with the main reason being decreased cost in producing CDs. Initially, the price of β-CD was around $2000 per kg and the prices of α- and ɤ-CDs were even higher due to their expensive purification process. With the advent of cheaper

purification techniques, the price of the CDs went down sharply and production increased many fold from hundreds to several thousands of tons, the latter further decreasing the CD costs. Meanwhile, modified CDs were being commercialized for various specialty applications, thereby fueling the growth of CD production and hence indirectly decreasing the costs.

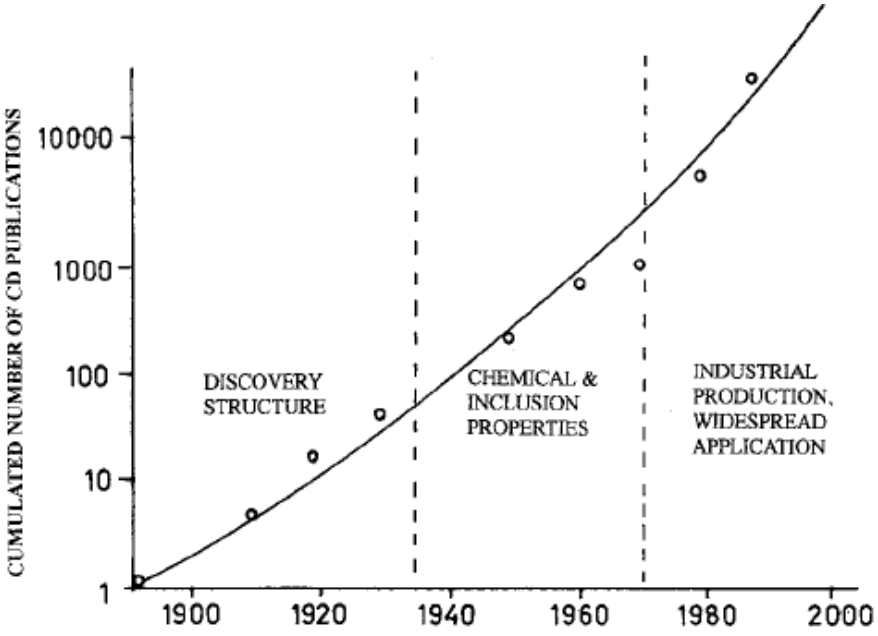

Figure 1.2: Total no of publications regarding CD in the last century.

1.1 Cyclodextrin Chemistry and properties:

CDs are cyclic oligosaccharides derived from starch sources containing six to virtually any number of (α-1, 4) – linked α-D-glucopyranose units, though those containing 6-10 glucose units are widely used. They are named α-, β-, ɤ-, δ-, ε-CDs for containing

respectively, 6,7,8,9 and 10 (α-1,4)- linked α-D-glucopyranose units [5]. Some of the properties of α-, β-, and ɤ- CDs are shown in Table 1.1.

Table 1.1: Basic properties of α-, β-, and ɤ-Cyclodextrin [6].

Property	*α-CD*	*β-CD*	*γ-CD*
Number of glucopyranose units	6	7	8
Molecular weight (g/mol)	972	1135	1297
Solubility (% w/v in water, 25 C)	14.5	1.85	23.2
Outer diameter (Å)*	14.6	15.4	17.5
Cavity diameter (Å)	4.7-5.3	6.0-6.5	7.5-8.3
Height of torus (Å)	7.9	7.9	7.9
Cavity volume (Å)	174	262	427

Due to the chair conformation of glucopyranose units, CDs have a truncated cone like structure. The primary hydroxyl groups are present on one side of the rim and the secondary hydroxyl groups are present on the other side (in Figure 1.3). The inner cavities of CDs are lined with, CH and CH_2 carbons, and ether oxygens, whereas the outer edges are lined with hydroxyl groups, making the outer surface hydrophilic and the inner cavity hydrophobic. The CD cavity structure is shown schematically in Figure 1.3 [7].

Figure 1.3: 3D structures of Cyclodextrin [7].

1.2 Solubility of CDs:

α-, β-and ɤ-CDs have a depth of ~7-8 Å and inner diameters of ~ 5, 7, 9 Å, respectively (Figure 1.4) [8]. The aqueous solubility of α, β, ɤ-CDs are generally lower compared to linear dextrins, due to the strong intra and inter molecular forces (H-bonding) in CD molecules in the solid state.

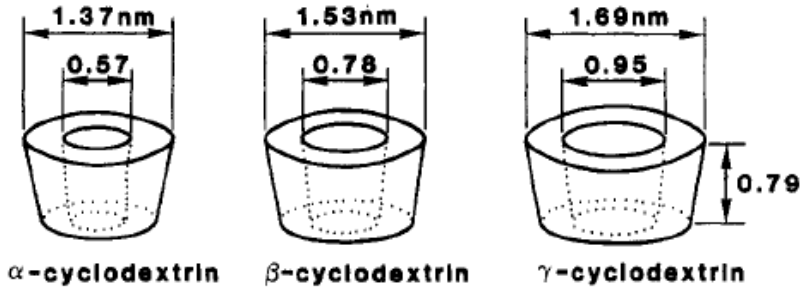

Figure 1.4: Inner and outer diameters of α, β, ɤ-Cyclodextrins [8].

Unlike α- and γ-CDs, β-CDs form stronger intra molecular hydrogen bonds resulting in diminished capability to form external hydrogen bonds with water molecules. To overcome its low solubility in water, CDs in general and β-CD in particular, are modified. Due to the

amorphous nature of the modified CDs, their solubility is enhanced [9]. Comparison of solubilities of some modified CDs with their parent CDs in water is shown in Table 1.2. It can be seen that the substitution of the hydroxyl groups present in CDs even by hydrophobic groups like methoxy functions results in dramatic increases in water solubility till about 2/3 of the hydroxyl groups are substituted, and then further increase in hydrophobic moieties results in decreased solubility.

Table 1.2: Solubilities of modified CDs and their parent CDs in water [9]

Cyclodextrin	Substitution of glucose unit	MW(Da)	Solubility in water (mg.ml)	Pharmacopoeia		
				Ph.Eur	USP/ NF	JPC
α-CD	-	972	145	Yes	No	Yes
β-CD	-	1135	18.5	Yes	Yes	Yes
[a]HP-β-CD	0.65	1400	>600	Yes	Yes	No
[b]RM-β-CD	1.8	1312	>500	No	No	No
[c]SBE-β-CD	0.9	2163	>500	No	No	No
ɤ-CD	-	1297	232	In progress	Yes	Yes
HP-ɤ-CD	0.6	1576	>500	No	No	No

[a]HP-β-CD- (2-Hydroxypropyl)- β-CD.

[b]RM-β-CD- Randomly methylated β-CD.

[c]SBE-β-CD- Sulfobutylether β-cyclodextrin sodium salt.

1.3 CD-Inclusion complexation [IC]:

When CDs are dissolved in aqueous solvent, their inner cavities are occupied by water molecules. As mentioned before, the inner cavity of CD is lined with CH and CH_2 carbons and ether oxygens, and therefore tend to prefer hydrophobic moieties. The substitution of high enthalpic water molecules present in CD cavity by appropriate guest molecule takes place; this results in the formation of CD inclusion complexation (IC) as shown schematically in Figure 1.5.

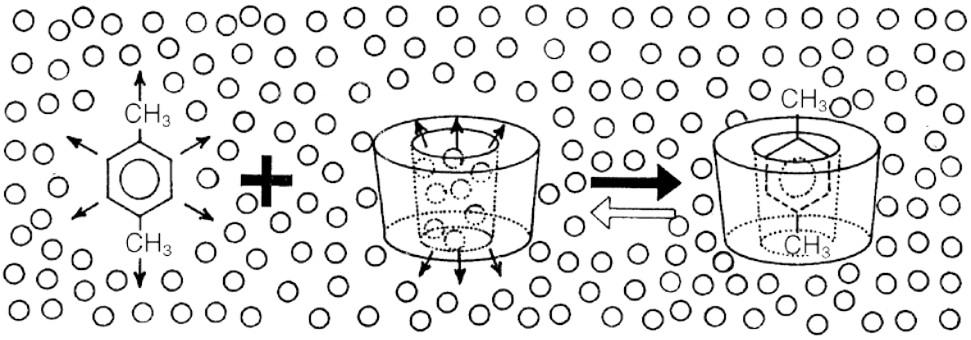

Figure 1.5: Schematic representation of IC formation between p-xylene and α-CD. Small circles represent the water molecules in the cavity of the CD that are displaced by hydrophobic p-xylene.

The thermodynamics of IC formation are primarily manifested by the stability constant K_a, which is defined as the equilibrium ratio established between dissociated and associated species of the complexes when they are dissolved. Usually, one CD molecule contains one or more guest molecules and this is the essence of molecular encapsulation. In a typical equilibrium equation like the one represented above, 1:1 represents the host: guest ratio,

although in some cases higher order equilibrium like 2:1 or 3:1 and so forth can exist [12]. Apart from energetically favored formation of inclusion complex by apolar-apolar interaction between guest and the cavity, other effects can also play vital roles, including the released strain in the CD rings on complexation, van der waals interactions and hydrogen bonds between host and the guest [13].

$$CD + D \underset{}{\overset{K_a}{\rightleftharpoons}} CD.D$$

$$K_{1:1} = \frac{[CD.D]}{[CD.][D]}$$

1.4 Crystal structure of CDs and CD-ICs:

α, β and ɤ-CDs, when crystallized as hydrates typically form cage-type crystal structures. Their IC crystal structures depend on the size of the molecular guest and type of CD. For example, α-CD forms a herringbone like cage structure with smaller guests like krypton, iodine, acetic acid, and a columnar structure with larger guests resulting either in head to head or head to tail arrangements. B-CD forms herringbone type cage structures with water and small sized alcohols, but for larger guests, the preferred structure is like a basket between two β-CD molecules that are hydrogen bonded. ɤ-CD forms herring bone type cage structure with only water as guests, for all other guest molecules, it crystallizes into channel type columnar structures [10].

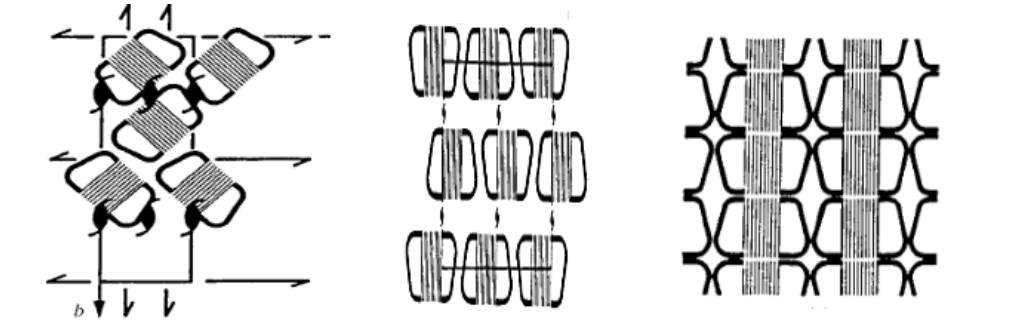

Figure 1.6: Structures of CD and Inclusion Complex [10].

When polymers, instead of small molecules are included as guests, they inherently form columnar structures (shown in Figure 1.6c), where the polymer chains are confined to the cavities of the CDs and separated from neighboring chains by stacks of adjacent CDs [10a]. Our group has been studying polymer chains that are confined in such CD nanocavities and these will be discussed in detail later.

1.5 IC formation:

1.5.1 Preparation techniques:

When a molecule of CD comes in contact with a guest molecule, it may result in IC formation with water being the key driving factor. According to Hedges et al [16], there are four methods commonly employed for IC formation, namely; co-precipitation, slurry, paste, and dry mixing methods. In principle, all four methods are similar except for the differing quantities of water involved.

In the co-precipitation method, guest compound is dissolved in an appropriate solvent (typically organic), is added to a CD-water solution. Once the precipitation occurs, the precipitate is filtered and dried to yield crystalline IC powders.

In the slurry method, CD is not dissolved completely; instead a slurry is obtained by suspending 40-45% w/w concentration (depending on viscosity of slurry and room for mixing). As the complex precipitates, more CDs dissolve into water producing more IC. Though less solvent is used to make IC through this process, it is time consuming and IC formation depends on the vigor of stirring and the thermodynamics and kinetics of the complexing guests and CD.

In the paste method, 20-30% w/w of water is used, so high shear force has to be applied to compensate for the high viscosity. Since so little water is added, this method is not ideal in a laboratory set up.

The last method is the dry mixing method. In this method, CD is mixed with guest with no water present. Since no water is added, this method generally is inefficient and mixing time is very long. This method is not practical except for a few liquid guest molecules like lemon oil, where ICs form within a few minutes [11].

1.6 Application of CD Inclusion complexes:

1.6.1 Food Industry:

CDs are predominantly used in the food industry for stabilization of food flavors and fragrances. The other major applications include elimination or prevention of undesirable

odors and tastes, preparation of antifungal complexes and improved product shelf life. It is also frequently used in households, hospitals and in tinned food and meat industries as preservatives owing to its unique advantages of forming ICs with various guest molecules [14].

CDs, especially β-CD, have the capability to form inclusion compounds with components like cholesterol; which is frequently found in animal products like eggs, lard, and tallow. When these foods are mixed in water, cholesterol forms a suspension which can complex with CD and can thus be centrifuged and separated to yield low fat food products [15-16]. Table 1.3 below shows an example of cholesterol removed from egg yolk, cream and butter after treatment with β-CD and its various derivatives.

It is seen from Table 1.3 that except for modified β-CD (b), the efficiency of removing cholesterol from egg yolk is relatively higher in unmodified β-CD, whereas, the same trend is not observed in the cases of cream and butter. The above example indicates that with the right choice of CDs it is possible to eliminate or remove, for example, the undesirable fatty acid molecules from food sources.

Table 1.3: Cholesterol removed from food after treatment with β-CD and its derivatives. [16].

Cyclodextrin	% Cholesterol removed		
	Egg yolk	Cream	Butter
β-CD	80	76	24
a*	17	25	10
b*	98(1)	95(2)	23

Table 1.3 Continued

c*	27	79	24
d*	7(3)	96	34
e*	23	52	9
h(polymer)	6	9	26

* More details about the type of derivatives (a to e in Table 1.3) or polymer type (h in Table 1.3) used were not reported in this article.

Apart from its ability to remove fatty molecules like cholesterol, components, found in food, like caffeine and strong flavor oils, can be separated and also removed. CDs are also widely used to preserve food ingredients that go rancid or that are sensitive to light or heat. For example, Vitamins like A and D are highly sensitive to light, heat and air, and, therefore, undergo oxidation and lose efficacy. When vitamin A is included in the cavity of CD, it does not undergo oxidation for prolonged times. In the case of light sensitive vitamin D_3, uncomplexed vitamin D_3 was found to lose all activity in one day, whereas in the complexed state, 49% of its activity was found to be retained after 43 days at high temperature [16, 17].

1.6.2 Drug/Pharma applications:

In the pharmaceutical industry, similar to the food industry, CDs are preferred where the water solubility of drugs is poor and they are soluble only in organic solvents. Being soluble only in organic solvents, the drugs might irritate the tissues and taste bitter, and without complexation they might also be sensitive to light or air [5]. To overcome these drawbacks, drugs and CDs are complexed to improve drug delivery. Figure 1.7 depicts a schematic representation of CD-drug IC formation and some proposed models of CD-Drug ICs [18].

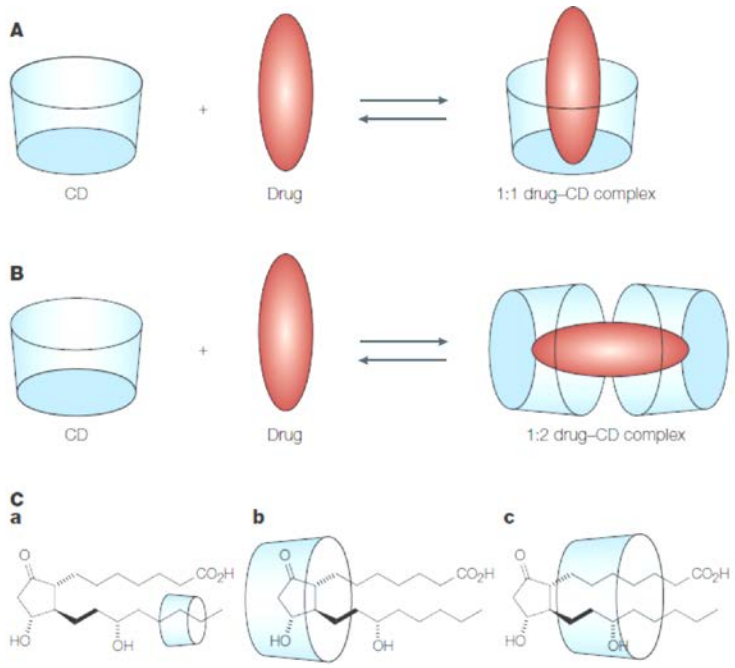

Figure 1.7: Schematic of 1:1 drug-CD complex formation (A),1:2 drug-CD complex (B), proposed models of drug-CD complex involving α-CD (a), β-CD (b) and ɤ-CD(c) [18].

1.7 Application of CDs to polymers:

1.7.1 Nucleating agents:

Nucleating agents are added to reduce the induction time and enhance the transformation from the liquid to solid crystalline state [19]. The nucleating agents provide the sites for the crystallization process. In slow crystallizing polymers, like poly (ethylene terephthalate) or poly (3-hydroxybutyrate), if nucleating agents are not used it usually results in the formation of samples with a heterogeneous distribution of large spherullites leading to poor mechanical properties. Typically used nucleating agents are talc, boron nitride, potassium chloride and

iodine. The main drawbacks of using these nucleating agents are their poor biocompatibility and hence their inapplicability in biomedical applications [20].

Because CDs are biocompatible/biodegradable, nontoxic and are readily available from renewable sources, they could be a great alternative to, for example, talc or boron nitride as nucleating agents. The application of CDs as nucleating agents have been studied for various polymers including poly (3-hydroxybutyrate) (PHB), polycaprolactone (PCL) and poly (ethylene terephthalate), to name a few. It was observed by Inoue et al, that the nucleation and crystallization kinetics of poly (3-hydroxybutyrate) (PHB) containing α-CDs were similar to those obtained when talc was used as nucleant. The crystallization times observed in DSC were found to be similar for both the CD and talc nucleated systems [21].

Inoue et al in their subsequent study compared the nucleating effects of various cyclodextrins and its combinations with talc as nucleants for PHB and they observed that neat PHB had a broad crystallization exotherm and addition of any CD type tended to make the crystallization peak narrower. It was also observed that α-CD had a better nucleating capability compared to that of other CDs [22].

1.7.2 Nonstoichiometric polymer-cyclodextrin Inclusion complexes [(n-s)-polymer ICs]:

The (n-s)-polymer-ICs are formed when the polymer chains are not completely covered by the host molecules and some portion of the guest polymer chains “dangle” outside the CD cavity. They have a CD: polymer ratio much less than needed to completely cover all of the guest polymer chains. A typical application of (n-s)-polymer ICs is their capability to act as

melt nucleating agents for bulk polymers [23]. For example, when 2 wt% 3:1-(n-s)-Nylon 6-α-CD-IC was used as a nucleant for bulk Nylon 6 (N6), it was observed by Mohan *et al.* that this (n-s)-IC served as an effective nucleant for bulk N6. Composite films pressed from the melt exhibited increased crystallization temperatures compared to neat N6 film (185 vs 170°C), even after annealing for a significant period of time in the melt. Another interesting observation made by them was, when the neat N6 and 3:1-(n-s)- N6- α-CD-IC films were heated beyond the melting temperature of neat N6, neat N6 flowed completely whereas the 3:1-(n-s)- N6- α-CD-IC didn't flow but sagged (without any weight), and it started to flow only after the addition of a small load. The 3:1-(n-s)-N6-α-CD-IC, also retracted almost completely to its original dimension once the weight was removed, whereas the neat N6 didn't retract significantly, indicating shape memory effects imparted to films of these supramolecular structures [24-25].

Inoue *et al.* had previously reported the enhanced crystallization of various polymers [poly (ε-caprolactone) [PCL], polyethylene glycol [PEG], polybutylene succinate [PBS] by their (n-s)-polymer-α-CD-ICs. Their general observation was that the (n-s)-polymer-α-CD-IC caused an enhanced interfacial interaction between the neat polymer and the (n-s)-polymer-α-CD-IC, resulting in the nucleation of the bulk polymer. It was also observed, that the α-CD in its uncomplexed state was far less capable of nucleating polymers compared to (n-s)-polymer-α-CD-ICs, due to the limited mobility of polymer chains inside the CD cavity and the absence of their contact with molten bulk polymer chains [26].

In Figure 1.8 are shown, the spherullitic morphologies of neat PBS (a), PBS containing α-CD (b), talc (c), and (n-s) PBS-α-CD-IC (d). It is seen clearly that the diameters of the spherullites is less with nucleants because of the presence of greater number of nuclei. Those nucleated by (n-s) ICs exhibited the smallest spherullite diameters followed by talc and α-CD. The same trend was however not observed for other polymers (PCL and PEG) and this could possibly be due to reduced surface energy barrier between the protruding chains from the CD cavity and neighboring chains (neat polymer), observed for PBS, but not PCL and PEG [26-27]. Inoue *et al.* in their later study examined the mechanical properties of

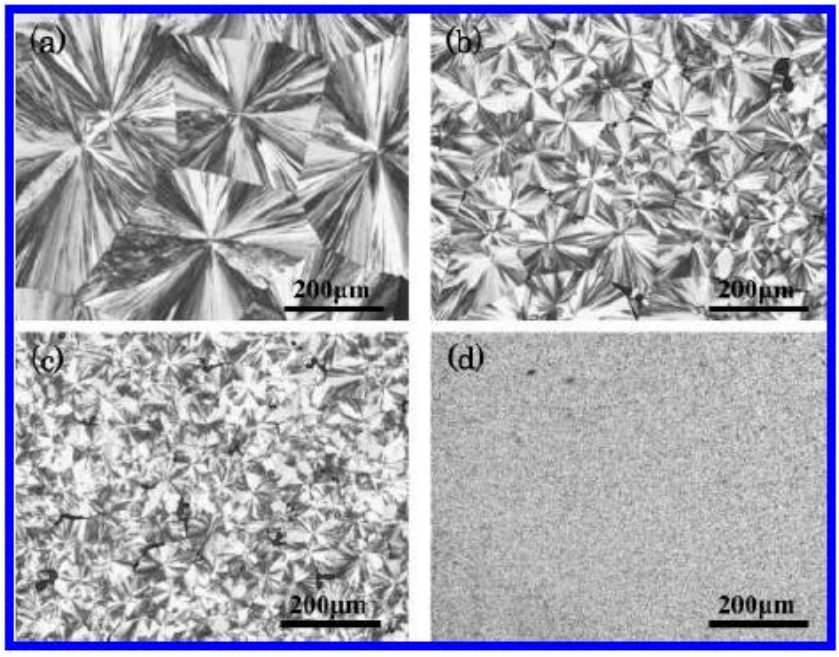

Figure 1.8: Polarized optical images of (a) PBS, (b) PBS containing 2 wt% α-CD, (c) talc, (d) (n-s) PBS-α-CD-IC.

composite films made of PCL reinforced with (n-s)-PCL-α-CD-IC. It was observed (See Figure 1.9) that there were significant increases in the storage moduli of the composite films containing (n-s)-PCL-α-CD-ICs. The increase in modulus was found to be directly correlated to the (n-s)-PCL-α-CD-IC. Though there wasn't significant difference in storage modulus observed for neat PCL and composites in the first phase (glassy to rubbery plateau), significant difference was observed for the second phase (rubbery to melting) caused by the agglomeration of (n-s)-PCL-α-CD-IC giving rise to the formation of hard domains which resulted in higher storage modulus.

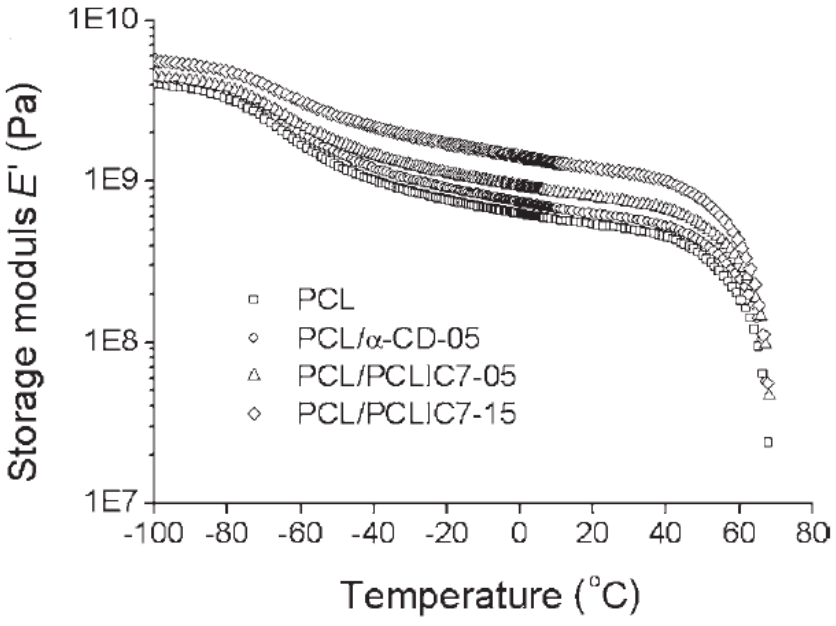

Figure 1.9: Storage modulus vs T plots of neat PCL films and composite films nucleated with (n-s)-PCL-α-CD-ICs.

A similar trend was also seen in the tensile modulus values observed through tensile testing. Tensile modulli (490 vs 250 MPa) were consistently seen to be higher for those containing (n-s)-PCL-α-CD-ICs and the increase was proportional to % content and stochiometry of (n-s)-PCL-α-CD-IC (smaller the coverage, higher the modulus) [28].

PHB is a biodegradable polymer made by various bacteria, and is an interesting material for biomedical applications, but is very brittle and crystallizes slowly, making it unsuitable for melt processing into fibers. BrÜnig et al, reported the formation of composite fibers composed of PHB nucleated with (n-s)-α-CD-PHB-IC that showed enhanced and faster crystallizability. Another critical observation made by the authors was the fiber's resistance to sticking to the winding bobbin, which is usually observed in neat PHB fibers due to their poor crystallizability. The mechanical behavior trend of the melt spun fibers was found to be similar to those observed by Inoue *et al.*, for the complexed material, the tensile modulli were higher (4.94 vs 4.45 MPa) and elongation at break sharply lower (18 *vs* 50%) [29].

1.7.3 Polymer-Cyclodextrin Inclusion complexes (CD-IC):

CD-IC formation with long chain guest molecules was first demonstrated by Harada *et al.* in 1990. They were successfully able to prepare ICs with α-CD and PEG with molecular weights of 400 to 10,000, but they were unable to make an IC using β-CD [30]. It was also noted by them that the rate at which IC forms decreases with increase in molecular weight of the guest PEG. Initial pioneering research in the formation, characterization and

conformational understanding of polymer-CD-IC was done by the Tonelli and Harada research groups [31-33].

Figure 1.10, illustrates the formation of CD-ICs and the subsequent process of coalescing the guest polymer chains from the CD-IC. Polymer-CD-ICs are typically made by dissolving polymer preferably in organic solvent and CDs in aqueous medium. The CD solution is then added drop wise into the polymer solution and is allowed to mix for some time, resulting in accumulation of a white precipitate, and the white precipitate thus obtained, is filtered and dried [34]. Polymer-CD-ICs cannot be used as such since they don't melt or dissolve and the films obtained by casting technique are brittle. Their applicability is generally low except for potential use as nucleating agents, and another important use of these polymer CD-ICs would be to form mutually compatible blends, when CD-ICs are simultaneously formed with two mutually incompatible polymers and the CDs are removed from their common IC [35-36]. The CDs present in ICs can be removed by a process called coalescence, and it was reported by Tonelli *et al.*, that these coalesced polymers (c-polymer) exhibit enhanced crystallinity, melting temperatures, and mechanical properties, and can be used as melt nucleants [37].

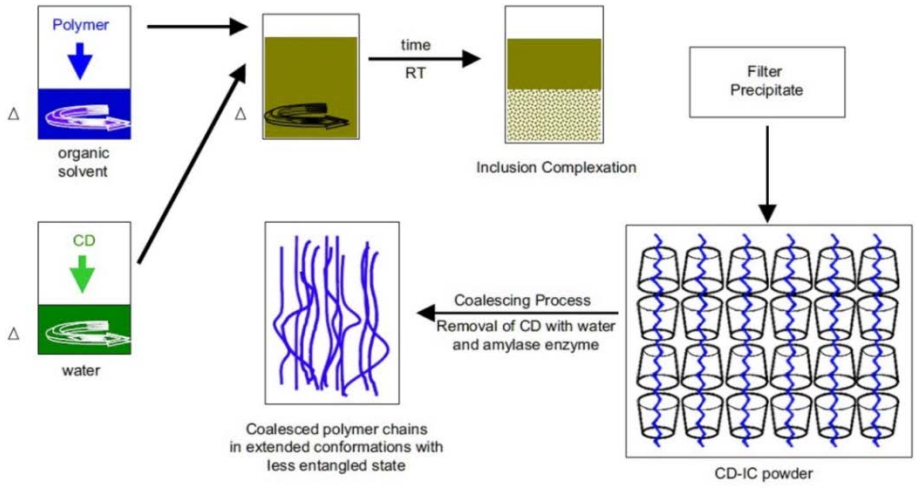

Figure 1.10: Schematic representation of IC formation.

A typical coalescence process involves, washing the polymer-CD-IC with hot water aided by enzymes; recently, it was reported by Williamson *et al.*, that a small quantity of concentrated HCL could be used for the process without causing degradation to the polymer [38].

Though schematic and not a true representation, from Figure 1.10, it is clear that the polymer chains which usually adopt random coil conformations, retain the extended un-entangled chain morphology even after CDs are removed by the coalescence process. This phenomenon of extended chain morphology in the case of coalesced polymers was first observed by Uyar *et al.*, when they coalesced poly (methyl methacrylate) (c-PMMA) from its γ-CD-IC. From their FTIR spectra shown in Figure 1.11 [39], it is seen there are two peaks

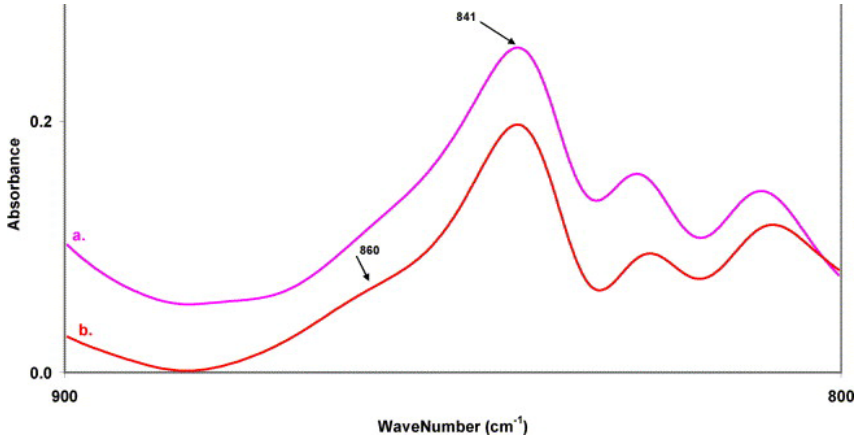

Figure 1.11: FTIR images of (a) as received PMMA (b) coalesced PMMA.

observed for c-PMMA at 860 and 841 cm^{1}, and a single peak at 841 cm^{-1} for asr-PMMA. The additional peak observed at 860 cm^{-1} in the case of c-PMMA corresponds to all trans and combined trans and gauche± conformations, indicating the retention of some extended chain morphology after coalescing, whereas the single peak at 841 cm^{-1} observed for asr- PMMA indicates the gauche± random coil conformations of polymer chains.

It is expected that the mechanical and thermal properties of these c-polymers will be superior to those of as-received polymers by virtue of the existence of some extended chain morphology. Mohan *et al.*, compared the crystallization behavior of c-Nylon 6 (N6) and (n-s)- α-CD-N6-ICs as nucleants for neat N6. They reported that, c-N6 nucleated N6 films exhibited a very similar nucleating behavior compared to that of (n-s)-αCD-N6-ICs, with significant increase (185 *vs* 170° C) in crystallization temperatures compared to neat N6 [25].

Williamson *et al.*, recently reported the thermal, mechanical and nano-indentation properties of c-PCL obtained from its stoichiometric PCL-α-CD-IC. The non-isothermal melt crystallization DSC curves and storage modulus *vs* T plots of c-PCL are shown in Figures 1.12 & 1.13, respectively. From the crystallization patterns of c-PCL and asr-PCL, it is evident that T_cs of c-PCL are significantly higher than that of as-received PCL at all cooling rates. As expected, higher T_cs are observed for both c-PCL and asr-PCL at low rates of cooling and lower T_cs at higher cooling rates, however the differences in T_cs with increase in cooling rates is higher in asr-PCL than in c-PCL (39.2 to 11.4° C *vs* 47.30 to 36.76° C).

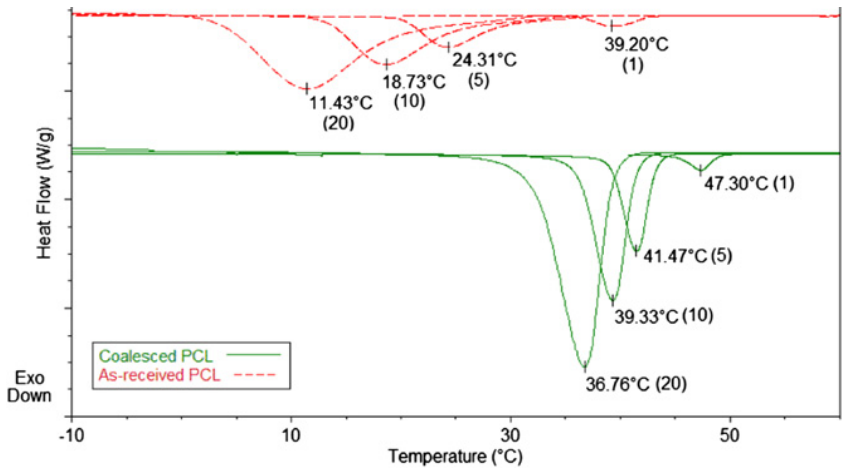

Figure 1.12: Melt crystallization curves of c-PCL (green) and asr-PCL (red).

Another interesting observation made that is, the crystallization exotherms of c-PCL are narrower at all cooling rates compared to asr-PCL, indicating the ability of c-PCL to transition from random coiled to un-entangled extended chain morphology. Though it might

seem odd, it is only expected because the c-PCL chains in amorphous domains are already in extended conformations with very little entanglement causing the polymer chains to readily crystallize from its melt.

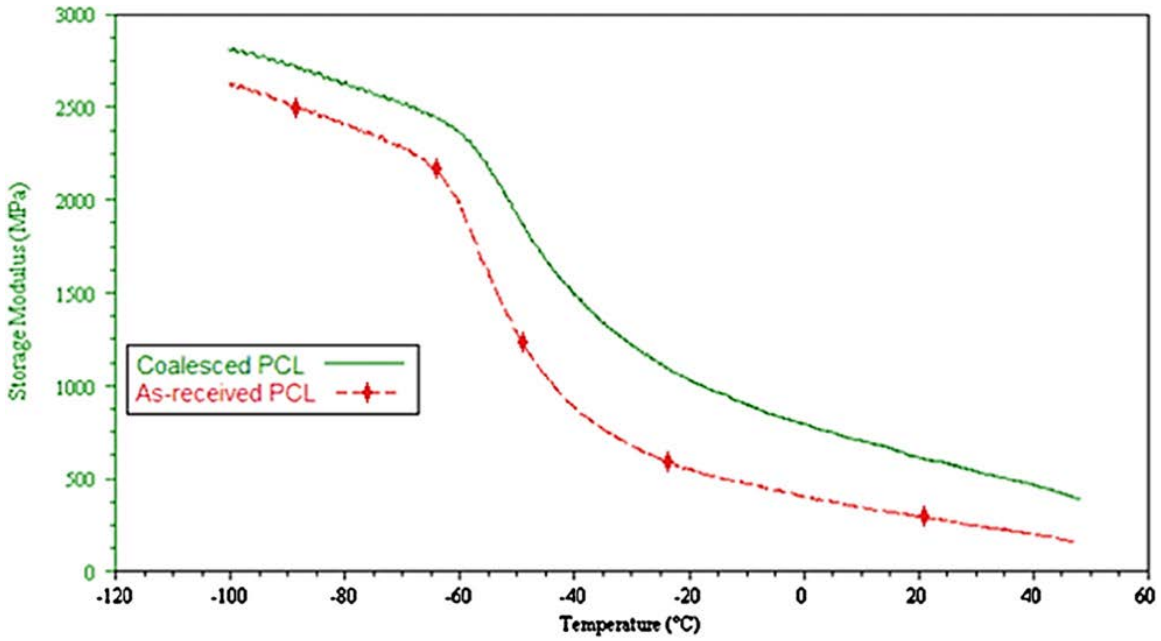

Figure 1.13: Storage modulus of asr-PCl and c-PCL.

Both storage (Figure 1.13) and loss modulli of c-PCL above Tg were observed to be significantly higher compared to asr-PCL, though higher storage modulus was expected, but higher loss modulus was not expected. The loss modulus of asr-PCL below Tg was observed to be higher indicating significant molecular motion of PCL chains, whereas c-PCL possibly didn't experience molecular motion to the same extent and thus had a lower loss modulus. However, when the temperature was raised above Tg, c-PCL, by virtue of lower

entanglements in the amorphous domains, permitted the PCL chains to move more freely without constraints causing the increase in loss modulus above Tg [38].

1.7.4 CDs as additives:

CD-ICs containing smaller molecules are thermally stable irrespective of the thermal stability of the small molecule guests; thereby volatile guests can be safely protected. Our group recently has been investigating the addition of CD-ICs by embedding them in polymers and providing various functionalities. We have successfully made functional CD-ICs containing a spermicidal, an antibacterial and antimicrobial, a flame retardant and an insect repellant agent by embedded them in various polymers, using melt processing or solution techniques [40-44]. It was noted that triclosan for example, an antibacterial/antimicrobial material , that melts between 55-60 °C, can be made thermally stable inside CDs and can be incorporated safely into polymers that melt at elevated temperatures.

CD-ICs have great prospects of application in the textile industry, where they can be used to impart functionalities that are harder to achieve by any other means. For example, fragrance molecules have high vapor pressures, but when included in CD cavities they tend to have lower vapor pressures, thereby delaying their molecular dispersal. When CDs are incorporated into textile surfaces, it has been seen that they can absorb foul odors in cavities, which can subsequently be washed away [45].

1.7.5 Polymerization inside CD channels:

Uyar et al polymerized styrene in the cavities of ɤ-cyclodextrin and were able to form rotaxanated polystyrene using two different polymerization techniques. The first method was to form a suspension in aqueous medium and using a water soluble initiator and the second was to carrying out a solid state polymerization technique that resulted in unusual microstructures [46-47]. Prior to the work of Uyar et al, different monomers like methyl methacryalate, pyrolle, bithiophene, aniline have been solution complexed in aqueous environment inside the cavities of various CDs and their polymerization studied [48-51].

Ding et al polymerized highly hydrophobic helical poly (N-Propargylamide), in aqueous solutions of HP-β-CD and HP-ɤ-CD IC. Through dichroism and UV-Vis spectroscopy, it was seen that the polymer assumed helical conformations. A major advantage of using such a system is that harmful toxic solvents can be avoided resulting in green polymerization technique. The CDs can be removed by washing and can then be reused [52].

Xu et al synthesized polystyrene microspheres coated with β-CD by a ɤ-irradiation emulsion polymerization technique using solid styrene-β-CD-IC as stabilizer of the emulsion; such a system was seen to have exceptional hydrophilicity considering the fact that polystyrene is highly hydrophobic [53].

1.8 IC Characterization:

The most widely used techniques to characterize ICs are Fourier transform infrared spectroscopy (FTIR), differential scanning calorimetry (DSC), wide angle X-ray diffraction analysis (WAXD), thermogravimetric analysis (TGA) and nuclear magnetic resonance

spectroscopy (NMR). FTIR provides information about the vibrational and or stretching behavior of chemical bonds and groups in a material. When we have fully covered IC for example, we will be able to observe the presence of both host CDs and guest polymers. Due to the possible secondary interaction or steric hindrance of polymers inside the CD cavity, there might be changes or shifts in some of the polymer guest peak frequencies, which indicate the presence of IC instead of a physical mixture. Another observation generally noted is the decrease in the intensity of the peaks corresponding to polymer chains as the coverage of polymer chains increase [54].

An example of the FTIR spectra observed with varying stochiometries of PCL and α-CD are shown in Figure 1.14. The peaks at ~3350 and 1721 cm^{-1} indicate the presence of secondary hydroxyl groups and carbonyl groups, present in α-CD and PCL, respectively.

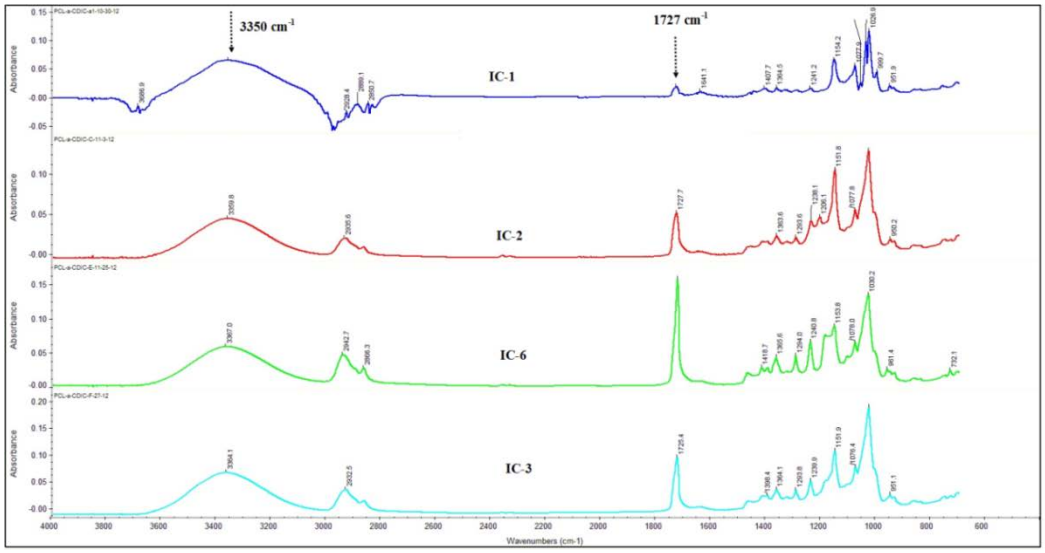

Figure 1.14: FTIR spectrum of PCL-α CD-ICs with varying stoichiometry.

It is seen clearly that as the coverage of polymer chains by CD increases, the intensity of the carbonyl peaks decreases (indicated by the black arrow). FTIR provides qualitative information about ICs, but, unfortunately, quantitative information usually cannot be obtained [55].

DSC provides information about the physical structure and thermal transitions unique to the material observed. Thermal transitions commonly observed for polymers include glass transition, melting, and crystallization. Upon forming a stoichiometric IC, since there are no polymers chains present outside the CD cavity, no melting or crystallization or glass transition peaks are observed for polymer in heating and cooling cycles in the DSC. DSC thermograms of ICs formed with low molecular weight PEG, hexatriacontane (HTC) and CDs reported by Tonelli *et al.* are shown in Figure 1.15. It is seen that PEG and HTC melt at about 25 and 75° C respectively, but when they are completely covered with CDs, their melting is suppressed,*i.e.*, not observed [56].

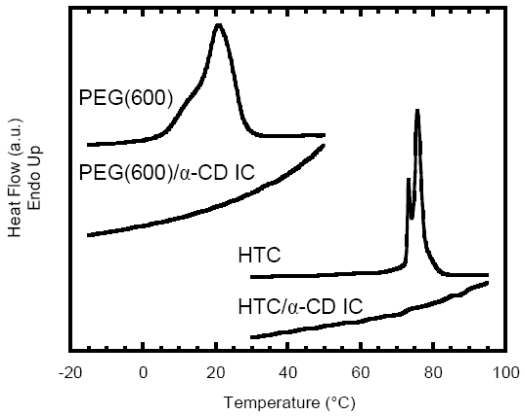

Figure 1.15: DSC thermograms of PEG, hexatriacontane (HTC) and their ICs.

When the polymer chains are partially covered as in (n-s)-ICs, depending on the coverage, melting behavior is observed. It is possible from the melting enthalpies to estimate the stochiometries of polymer chains and CDs present in their (n-s)-ICs.

Wide angle X-ray diffraction (XRD) analysis is widely performed to understand the crystal structure of materials. As mentioned earlier, when forming ICs with guest molecules, CDs change their crystal structures, especially when the guests are made of long chain molecules, like polymers. When ICs are formed with polymers, naturally observed cage structures of neat CDs and small molecules transforms into columnar structures. Figure 1.16 shows the XRD patterns of nylon 6, α-CD, nylon 6/α-CD mixtures, and nylon 6-α-CD-IC. The crystalline α-CD (a) in cage form, exhibits a series of peaks at 2θ=9.6, 12.03, 19.5 and 21.8°, nylon 6 (d) exhibits a broad peak at about 22° which corresponds to a combination of the α- and γ-crystal polymorphs. When nylon-6 and α-CD form an IC, they exhibit a unique

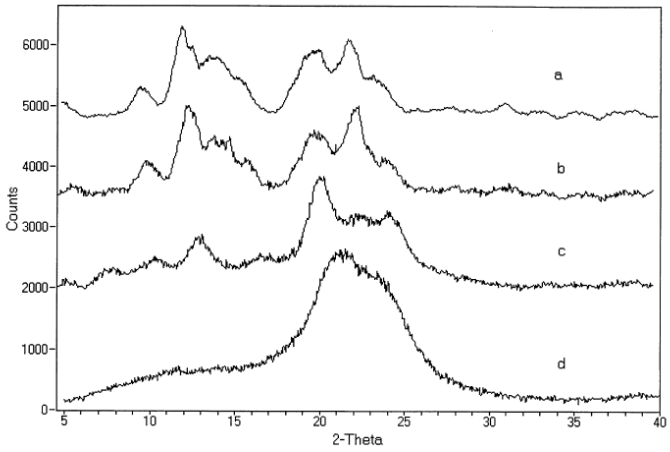

Figure 1.16: Wide-angle X-ray diffraction of (a) α-CD, (b) α-CD and nylon 6 mixture, (c) nylon 6-α-CD-IC, and (d) nylon 6.

peak at 2θ=20° which is not observed for either of its pure components, indicating the formation of a new crystal structure. It has been widely reported that this unique peak is due to the presence of long chain molecules inside CD cavities, which results in the formation of columnar structure [57]. Similar to α-CD, when γ-CD forms ICs with polymers, they exhibit a characteristic peak, but at 2θ=7.8°, thus polymer-γ-CD- ICs can be characterized [58].

Guest molecules inside the CD cavities exhibit enhanced thermal stability due to the crystalline nature of the ICs. By observing the degradation pattern with TGA of the IC compared to that of individual components (guest polymer and host CD) or their mixtures, it was concluded by Tonelli *et al*. that the IC made from PEO and α-CD decomposes at significantly higher temperature (334° C) compared to α-CD (315° C).

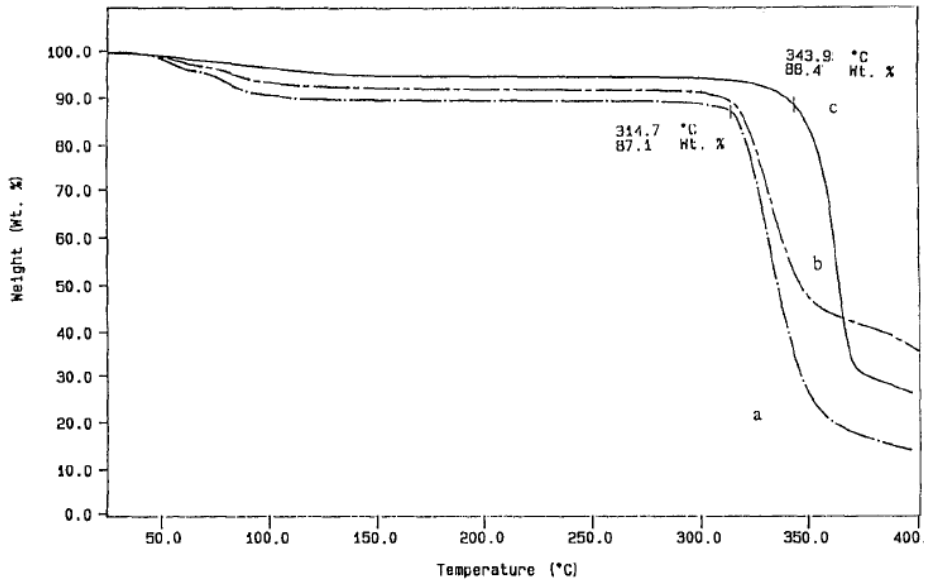

Figure 1.17: TGA scans of (a) α-CD, (b) physical mixture of PCL and α-CD, (c) PCL-α-CD-IC, at 10° C/min.

The same TGA behavior was observed for PCL (Figure 1.17). The presence of guest molecule in the IC causes an enhanced stability irrespective of its neat volatility [59].

Nuclear magnetic resonance spectroscopy is widely used for structural elucidation of materials including polymers. The main reason it is so powerful compared to other methods is because of its capability to unravel the microstructures of materials. The resonance phenomenon observed is uniquely characteristic of particular microstructures [60]. Upon IC formation, there are shifts in both CD and guest molecule resonance frequencies, which can be observed in either proton (^{1}H-NMR) or carbon (^{13}C NMR) spectra, However, ^{13}C NMR is highly preferred over proton NMR, because of its higher sensitivity to ICs. It should be noted that chemical shifts observed upon complexation are specific to each component of the IC (host and guest) [61].

When ^{13}C spin-lattice relaxation times of a semi-crystalline polymer like PCL or its block copolymer with PEO were observed, the crystalline chains were found to have long spin-lattice relaxation times, however when the small chains were included in the columnar CD cavities, they were observed to have a 2-3 orders of magnitude decrease in relaxation times.

The reduction in relaxation times was found to be independent of chain length of the homo or block copolymer or of type of chains, if more than one polymer chain was included in a CD cavity (γ-CD instead of α-CD) [62]. Table 1.4 summarizes the relaxation times of PCL and its block copolymer with PEO included in the cavities of α-CD or γ-CD, as observed by Tonelli *et al.*

Table 1.4: The relaxation times of PCL, PCL-PEO-PCL in the cavities of α-CD and γ-CD.

Carbon	PCL	PCL–α-CD-IC	PCL–γ-CD-IC	PCL–PEO–PCL	PCL–PEO–PCL–α-CD-IC	PCL–PEO–PCL–γ-CD-IC	PCL–PS	PCL–PS–α-CD-IC	PCL–PS–γ-CD-IC
a	169.8 3.28	0.24	0.22	185.9 2.6	0.28	0.29			
b	160.6 1.23	0.26	0.19	181.7 0.7	0.24	0.41			
c	161.5 1.22	0.31	0.28	221.9 1.2	0.29	0.23	0.78	0.58	0.38
d	161.5 1.22	0.31	0.28	221.9 1.2	0.29	0.23	0.78	0.58	0.38
e	223.6 1.68	0.29	0.17	328.2 4.0	0.24	0.22			
f	–			379.1			43.7	28.0	55.2
m				0.35	0.19	0.27			
h							155.3 12.35	69.38 1.95	21.6
g							20.7 23.3	64.54 0.48	40.2

2D-NMR techniques are widely used to observe the spatial interaction that occurs through non bonded protons. This interaction is known as the nuclear overhauser effect (NOE) and can be generally examined through one of two techniques; namely, nuclear overhauser effect spectroscopy (NOESY) or rotating frame nuclear overhauser spectroscopy (ROESY). NOESY can detect spatial interaction between protons that are separated by only a few angstroms; such an interaction can occur only if the CD and polymer exist closely as in their soluble IC. If the host and guest are separated further, as expected in their non complexed solution, they would not have any interaction and hence no NOESY effect will be present [63].

1.9 Electrospinning:

Electrospinning, also known as electrostatic spinning, is a process widely used to make ultrafine micro to nanofibers from polymer solutions or melts [64]. When a drop of polymer

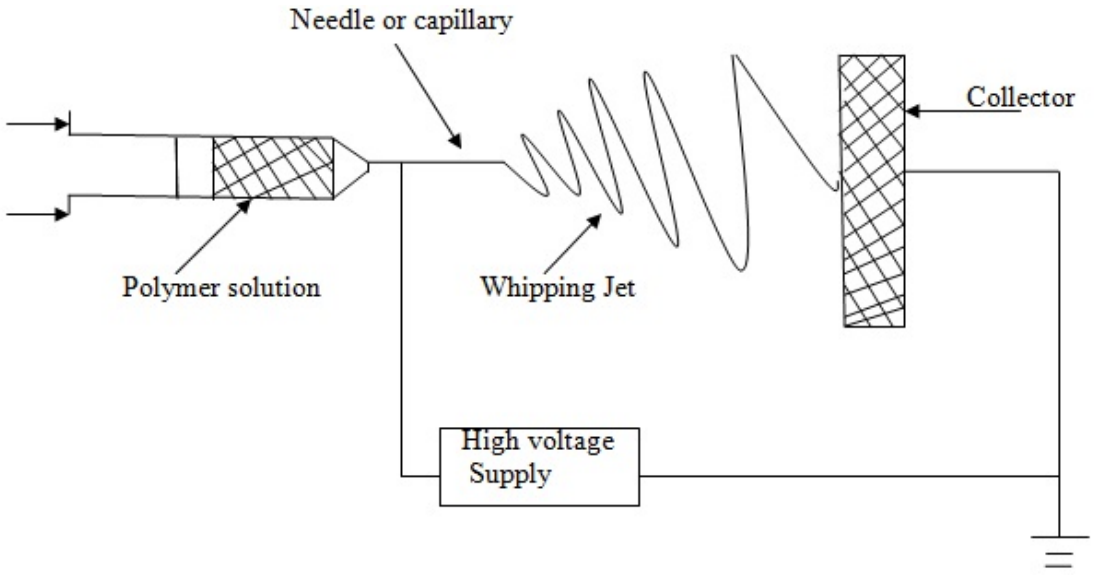

Figure 1.18: Typical electrospinning setup.

solution is subjected to a strong electrostatic potential, it accelerates towards the grounded collector due to the movement of charge carriers that are present in the solution [65].

Figure 1.18 illustrates a typical electrospinning setup; it consists of a blunted needle connected to a syringe filled with polymer solution, a high voltage power supply between needle and grounded collector, and a pump to deliver solution at a predefined rate. When the electric field is applied, excess charges are produced which causes spherical droplets to form. These spherical droplets undergo distortion and eventually form a conical shape, known as a

Taylor cone [66]. The conical shape thus attained is highly unstable and undergoes a whipping motion that causes a reduction the fiber diameter [67]. The resulting jet continues to elongate till it gets deposited on to the collector in the form of a non-woven mat [68]. Solution properties like viscosity, conductivity and surface tension play key roles in determining final fiber diameter and morphology [69]. Operational parameters, including feed rate, potential difference applied, tip to collector distance, diameter of the orifice, humidity etc, also impact fiber diameters and morphology [70].

1.9.1 Electrospinning of CD and CD-IC functionalized nanofibers:

The first article on electrospinning of CD functionalized polymeric nanofibers was reported by Ramakrishna *et al.* in 2006. They reported the formation of PMMA/β-CD functionalized fibers. It was observed by them that the average fiber diameter of the were about 900 nm and they exhibited structural integrity over a period of time [71]. Uyar *et al.*, successfully prepared various CD functionalized polymeric nanofibers including polystyrene (PS), polymethylmethacrylate (PMMA), polyethylene oxide (PEO) and polyethylene terephthalate (PET) [72-75]. Meanwhile various other researchers reported the preparation of CD functionalized nanofibers by electrospinning. Diao *et al.*, for example, reported the preparation of CD functionalized polyvinyl alcohol (PVA) nanofibers [76] and Mokhtari *et al.*, reported the formation of CD functionalized chitosan/PVA nanofibers [77]. These functionalized nanofibers can be ideal substrates for filtration and drug delivery applications.

Uyar's research group additionally successfully electrospun polymer fibers containing CD-ICs. ICs with various functionalities were electrospun including antibacterial, antifungal and food fragrances like vanillin, to name a few [78-81]. Though a wide variety of research combining electrospinning of polymers and CDs or their ICs has been performed, there are a few areas of related research that have not been undertaken. My dissertation intends to explore some of the gaps in research based on electrospinning of nanowebs containing CDs and their ICs.

1.10. Motivation for my work:

1. To the best of my knowledge, poly (ε-caprolactone) (PCL), a polymer widely used in biomedical applications, hasn't been functionalized with CDs, which is for two main reasons. Firstly, CD functionalized polymeric nanofibers, for the most part, have been electrospun from a single solvent. PCL and CDs do not have a common solvent, and, therefore such a system can be electrospun only from a binary solvent mixture, which makes the process complicated. Secondly, the capability of PCL to form ICs with CDs is well known and, thus, electrospinning such a system to form functionalized fibers without forming ICs can be challenging. It would be of interest to learn how to form functionalized nanofibers for PCL and CD perform, and what effect CDs have on PCL hydrophobicity?

2. β-CD, has been found not to form ICs with PCL. One main reason is its stable cavity, which hinders the formation of ICs with PCL. Although, α- and γ-CDs functionalized PCL nanofibers can be electrospun, as done in a subsequent chapter, some of the α- and γ-CDs might also have been threaded by PCL chains, which will hinder their small molecular

encapsulation ability. Hence, β-CD functionalized PCL nanofibers would provide a greater opportunity for encapsulating small molecules, e.g. there one may want to use for absorbing wound odor. CDs have been known to form ICs with small molecules such as butyric acid and propionic acid, frequently observed in wound exudates. Will the efficacy of these functionalized materials in masking these foul odors be better compared to neat PCL nanofibers? Since commercial testing is not feasible, alternative method to conduct the testing would be explored in this research.

3. CD-ICs, especially (n-s)-CD-ICs have been shown to greatly improve the mechanical properties of bulk polymers, especially storage modulus when observed in a dynamic mechanical analyzer (DMA). Though PCL has some ideal characteristics for bone tissue engineering applications, it has undesirably poor mechanical properties. If one uses (n-s)-PCL-CD-ICs as reinforcing filler for bulk PCL nanofibers; will it enhance the resulting mechanical properties enough to make it a better material for bone tissue engineering application? This will be one of the questions explored in this research.

References:

1. Villiers A. Sur la Fermentation de la Fécule par l'action du Ferment Butyrique, Compt. Rend.1891; 112:536.

2. Loftsson T, Duchéne D. Cyclodextrins and their Pharmaceutical Applications. Int. J. Pharm.2007; 329:1−11.

3. Szejtli J. Introduction and General Overview of Cyclodextrin Chemistry. Chem. Rev.1998; 98: 1743-1753.

4a. Harada A, Takashima Y. Macromolecular Recognition and Macroscopic Interactions by Cyclodextrins. The Chemical Record.2013; 13:420-431.

4b. Astray G, Gonzalez-Barreiro C, Mejuto JC, Rial-Otero R, Simal-Gandara J. A Review on the use of Cyclodextrins in Foods**.** Food Hydrocolloids. 2009; 23:1631-1640.

5. Vyas A, Saraf S. Cyclodextrin Based Novel Drug Delivery Systems. J. Inclusion Phenom.Macrocyclic.Chem.2008; 62: 23-42.

6. Delwalle, EM. Cyclodextrins and Their uses: A Review. Process. Biochem.2004; 39: 1033-1046.

7. Szejtli J, Cyclodextrin Technology. Boston: Kluwer Academic Publishers, 1988. P. 1-15

8. Li S, Purdy WC. Cyclodextrins and Their Applications in Analytical Chemistry. 1992; 92:1457-1470.

9. Loftsson T, Duchéne D. Cyclodextrins and their Pharmaceutical Applications.Int. J. Pharm. 2007; 329: 1−11.

10. Saenger W, Steiner T. Cyclodextrin Inclusion Complexes: Host-guest Interactions and Hydrogen-Bonding Networks. Acta Crystallogr.1998; A54:798-805.

10a.Tonelli AE. Nanostructuring and Functionalizing Polymers with Cyclodextrins. 2008; 49:1725-1736.

11. Hedges AR. Industrial Applications of Cyclodextrins. Chem.Rev.1998; 98:2035-2044.

12. Szejtli J. Utilization of Cyclodextrins in Industrial Products and Processes. J.Mater.Chem. 1997; 7:575-587.

13. Astray G, Gonzalez-Barreiro C, Mejuto JC, Rial-Otero R, Simal-Gandara J. A Review on the use of Cyclodextrins in Foods**.** Food Hydrocolloids. 2009; 23:1631-1640.

14. Szejtli J. Cyclodextrins in Food, Cosmetics and Toiletries.Starch.1982; 34:379-385.

15. Vollbrecht,H.-R,Cully J, Wiesmuller J. United States Patent 5,063,077,1991.

16. Hedges AR, Shieh WJ, Sikorski CT. Use of cyclodextrins for encapsulation in the use and treatment of food products. In S. J. Risch, & G. A. Reineccius (Eds.), Encapsulation and controlled release of food ingredients, ACS symposium series 590 (pp. 60–71). Washington DC: American Chemical Soc.

17. Shaw PE, Wilson CW. Debittering Citrus Juices with β-Cyclodextrin Polymer. J. Food Sci.1983; 48:646-647.

18. Davis ME, Brewster ME. Cyclodextrin-based pharmaceutics: past, present and future. Nature reviews. 2004; 3:1023-1035.

19. Menczel J, Varga J. Influence of nucleating agents on crystallization of polypropylene. J. Therm. Anal.1983; 28:161-174.

20. Mohan A. Modification of Nylon 6 Structure via Nucleation. PhD Thesis, North Carolina State University.2009.

21. He Y, Inoue Y. α-Cyclodextrin-Enhanced Crystallization of Poly(3-hydroxybutyrate). Biomacromolecules.2003; 4:1865-1867.

22. Dong T, He Y, Zhu B, Shin KM, Inoue Y. Nucleation Mechanism of α-cyclodextrin-Enhanced Crystallization of some Semicrystalline Aliphatic Polymers. Macromolecules.2005; 38:7736-7744.

23. Williamson B, Tonelli AE. Constrained Polymer Chain Behavior Observed in their Non-stoichiometric Cyclodextrin Inclusion Complexes. J Incl Phenom Macrocycl Chem.2012; 72:71-78.

24. Mohan A, Joyner X, Kotek R, Tonelli AE. Constrained/Directed Crystallization of Nylon-6. I. Nonstoichiometric Inclusion Compounds Formed with Cyclodextrins Macromolecules.2009; 42:8983-8991.

25. Mohan A, Gurarslan A, Joyner X, Child R, Tonelli AE. Melt-Crystallized Nylon-6 Nucleated by the Constrained Chains of its Non-stoichiometric Cyclodextrin Inclusion Compounds and the Nylon-6 Coalesced From Them. Polymer.2011; 52:1055-1062.

26. Dong T, He Y, Zhu B, Shin KM, Inoue Y. Nucleation Mechanism of α-cyclodextrin-Enhanced Crystallization of some Semicrystalline Aliphatic Polymers. Macromolecules.2005; 38:7736-7744.

27. Dong T, Shin K-M, Zhu B, Inoue Y. Nucleation and Crystallization Behavior of Poly(butylene succinate) Induced by Its α- Cyclodextrin Inclusion Complex: Effect of Stoichiometry.Macromolecules.2006; 39:2427-2428.

28. Dong T, Mori T, Pan P, Kai W, Zhu B, Inoue Y. Crystallization Behavior and Mechanical Properties of Poly (ε-caprolactone)/Cyclodextrin Biodegradable Composites. J.Appl.Polym.Sci.2009, 112, 2351-2357.

29. Vogel R, Tandler B, Haussler L, Jehnichen D, Brunig H. Melt Spinning of Poly (3-hydroxybutyrate) Fibers for Tissue Engineering Using α-Cyclodextrin/Polymer Inclusion

Complexes as the Nucleation Agent. Macromol. Biosci.2006; 6:730–736.

30. Harada A, Kamachi M. Complex Formation Between Poly (ethylene glycol) and α-Cyclodextrin. Macromolecules.1990; 23:2821-2823.

31. Harada A, Li J, Kamachi M. Preparation and Properties of Inclusion Complexes of Polyethylene Glycol with .Alpha.-Cyclodextrin.Macromolecules. 1993; 26:5698.

32. Rusa CC, Wei M, Bullions TA, Rusa M, Gomez MA, Porbeni FE, Wang X, Shin D, Balik CM, White JL, Tonelli AE. Controlling the Polymorphic Behaviors of Semicrystalline Polymers with Cyclodextrins. Crystal Growth and Design.2004;4: 1431-1441.

33. Harada A, Suzuki S, Okada M, Kamachi M. Preparation and Characterization of Inclusion Complexes of Polyisobutylene with Cyclodextrins.Macromolecules.1996; 29, 5611-5614.

34. Huang L, Tonelli AE. Inclusion Compounds Formed between Cyclodextrins and Nylon 6.Polymer. 1999; 40: 3211-3221.

35. Wei M, Tonelli AE. Compatiblization of Polymers via Coalescence from Their Common Cyclodextrin Inclusion Compounds.Macromolecules.2001; 34:4061-4065.

36. Wei M, Shuai X, Tonelli AE. Melting and Crystallization Behaviors of Biodegradable Polymers Enzymatically Coalesced from Their Cyclodextrin Inclusion Complexes. Biomacromolecules.2003; 4:783-792.

37. Vedula J, Tonelli AE. Reorganization of Poly (ethylene terephthalate) Structures and Conformations to Alter Properties. J. Polym. Sci., Part B: Polym. Phys.2007; 45:735-746.

38. Williamson BR, Krishnaswamy R, Tonelli AE. Physical Properties of Poly(ε-caprolactone) Coalesced from its α-Cyclodextrin Inclusion Compound.Polymer.2011;52: 4517-4527.

39. Uyar T, Rusa CC, Hunt MA, Aslan E, Hacaloglu J, Tonelli AE. Reorganization and Improvement of Bulk Polymers by Processing with their Cyclodextrin Inclusion Compounds. Polymer.2006; 46:4762-4775.

40. Huang L, Gerber M, Lu J, Tonelli AE. Formation of a Flame Retardant-Cyclodextrin Inclusion Compound and its Application as a Flame Retardant for Poly (ethylene terephthalate). Polym. Degrad. Stab. 2001; 71: 279-284.

41. Huang L, Taylor H, Gerber M, Orndorff PE, Horton JR, Tonelli AE. Formation of antibiotic, biodegradable/bioabsorbable polymers by processing with neomycin sulfate and its inclusion compound with beta-cyclodextrin. J. Appl. Polym. Sci.1999; 74:937-947.

42. Lu J, Hill MA, Hood M, Greeson DF, Horton JR, Orndorr PE, Herndon AS, Tonelli AE. Formation of Antibiotic, Biodegradable Polymers by Processing with Irgasan DP300R (Triclosan) and its Inclusion Compound with Beta-cyclodextrin,J.Appl.Polym.Sci.2001; 82:300-309.

43. Whang HS, Hunt MA, Wrench N, Hockney JE, Farin CE, Tonelli AE. Nonoxynol-9-Alpha-Cyclodextrin Inclusion Compound and its Application for the Controlled Release of Nonoxynol-9 Spermicide. J. Appl. Polym. Sci. 2007; 106:4104-4109.

44. Whang HS, Tonelli AE. Release Characteristics of the Non-Toxic Insect Repellant 2-Undecanone From its Crystalline Inclusion Compound with α-Cyclodextrin. J.Incl. Phenom. Macrocycl Chem.2008; 62:127-134.

45. Buschmann H-J, Knittel D, Schollmeyer E. New Textile Applications of Cyclodextrins. J.Incl. Phenom. Macrocycl Chem.2001;40:169-172.

46. Uyar T, Rusa M, Tonelli AE. Polymerization of Styrene in Cyclodextrin Channels: Can Confined Free-Radical Polymerization Yield Stereoregular Polystyrene? Macromol. Rapid Commun, 2004; 25:1382-1386.

47. Uyar T, Gracz HS, Rusa M, Shin ID, El-Shafei A, Tonelli AE. Polymerization of Styrene in γ-Cyclodextrin Channels: Lightly Rotaxanated Polystyrenes with Altered Stereosequences.2006; 47:6948-6955.

48. Storsberg J, van Aert H, van Roost C, Ritter H. Cyclodextrins in Polymer Synthesis: A Simple and Surfactant Free Way to Polymer Particles having Narrow Particle Size Distribution. Macromolecules.2003; 36:50-53.

49. Storsberg J, Ritter H, Pielartzik H, Groendaal L. Cyclodextrins in Polymer Synthesis: Supramolecular Cyclodextrin Complexes of Pyrrole and 3,4-Ethylenedioxythiophene and Their Oxidative Polymerization. Adv.Mater.2000; 12:567-569.

50. Takashima Y, Oizumi Y, Sakamoto K, Miyauchi M, Kamitori S, Harada A. Crystal Structure of the Complex of b-Cyclodextrin with Bithiophene and Their Oxidative Polymerization in Water. Macromolecules.2004; 37:3962-3964.

51. Wang B, He J, Sun D.H, Zhang R, Han B.X, Huang Y. Preparation of β-cyclodextrin–

Polyaniline Ccomplex in Supercritical CO_2.Euro.Polymer.J.2005;41(10), 2483-2487.

52. Ding L, Li Y, Deng J, Yang W, Polym.Chem. Preparation of Hydrophobic Helical Poly(*N*-propargylamide)s in Aqueous Medium *via* Monomer/Cyclodextrin Inclusion Complex. Polym.Chem. 2011; 2:694-701.

53. Xu D, Wang M, Ge X, Lam MHW. Synthesis and Characterization of β-CD-Coated Polystyrene Microspheres by γ-Ray Radiation Emulsion Polymerization. Macromol. Rapid Commun. 2012; 33:1945-1951.

54. Narayanan G, Gupta BS, Tonelli AE. Poly(ε-caprolactone) Nanowebs Functionalized with α- and γ-Cyclodextrins. Biomacromolecules.2014; 15:4122-4133.

55. Tonelli AE. Nanostructuring and Functionalizing Polymers with Cyclodextrins. Polymer. 2008; 49:1725-1736.

56. Hunt MA, Tonelli AE, Balik CM. The Effect of Water and Guest Hydrophobicity on the Complexation of Oligomers with Solid α-Cyclodextrin, Polymer.2008;49 , 985-991.

57. Rusa CC, Luca C, Tonelli AE. Polymer−Cyclodextrin Inclusion Compounds: Toward New Aspects of Their Inclusion Mechanism. Macromolecules,2001; 34:1318-1322.

58. Shuai X, Porbeni FE, Wei M, Bullions T, Tonelli AE. Formation of Inclusion Complexes of Poly(3-hydroxybutyrate)s with Cyclodextrins. 1. Immobilization of Atactic Poly(R,S-3- hydroxybutyrate) and Miscibility Enhancement between Poly(R,S- 3-hydroxybutyrate) and Poly(epsilon-caprolactone). Macromolecules. 2002; 35:2401-2405.

59. Huang L, Allen E, Tonelli AE. Study of the Inclusion Compounds Formed Between α-Cyclodextrin and High Molecular Weight Poly(ethylene oxide) and Poly(ϵ-caprolactone) Polymer.1998; 39:4857-4865.

60. Tonelli AE, NMR Spectroscopy and Polymer Microstructure: The Conformational Connection, VCH 1989.

62. Lu J, Mirau PA, Tonelli AE. Chain Conformations and Dynamics of Crystalline Polymers as Observed in their Inclusion Compounds by Solid-State NMR.Prog. Polym.Sci.2002; 27:357-401.

63. Williamson B. Processing Polymers with Cyclodextrins. Ph.D Thesis. North Carolina State University. 2010.

64. Li D, Xia Y. Electrospinning of Nanofibers: Reinventing the Wheel? Adv. Mater.2004;

16:1151-1170.

65. Fong H, Reneker D, Electrospinning and the Formation of Nanofibers", In Structure Formation in Polymeric Fibers; Salem, DR., Ed.; Hanser Gardner: Cincinati, Chapter 6, 2001.

66. Deitzel JM, Kleinmeyer J, Harris D, Beck Tan, NC. The Effect of Processing Variables on the Morphology of Electrospun Nanofibers and Textiles. Polymer.2001; 42:261-272.

67. Reneker D, Yarin A, Fong H, Koombhongse SJ. Bending Instability of Electrically Charged Liquid Jets of Polymer Solutions in Electrospinning. Appl. Phys. 2000; 87:4531-4547.

68. Frenot A, Chronakis IS, Polymer Nanofibers Assembled by Electrospinning. Curr. Opin.Colloid Interface Sci. 2003; 64-75.

69. Subbiah T, Bhat GS, Tock RW, Parameshwaran S, Ramkumar SS. Electrospinning of Nanofibers. J. Polym. Sci.2005; 96: 557–569.

70. Bhardwaj N, Kundu SC. Electrospinning: a Fascinating Fiber Fabrication Technique. Biotechnol. Adv 2010; 28:325–347.

71. Kaur S, Kotaki M, Ma Z, Gopal R, Ramakrishna S, Ng SC. Oliosaccharide Functionalized Nanofibrous Membrane.Int. J. Nanosci.2006; 5:1-11.

72. Uyar T, Besenbacher F. Electrospinning of Uniform Polystyrene Fibers: The Effect of Solvent Conductivity. Polymer.2008; 49:5336-5343.

73. Uyar T, Balan A, Toppare L Besenbacher F. Electrospinning of Cyclodextrin Functionalized Poly (methyl methacrylate)(PMMA) Nanofibers. Polymer.2009; 50:475-480.

74. Uyar T, Besenbacher F. Electrospinning of Cyclodextrin Functionalized Polyethylene oxide (PEO) Nanofibers. Euro.Polym.J.2009; 45:1032-1037.

75. Kayaci F, Ertas Y, Uyar T. Surface Modification of Electrospun Polyester Nanofibers with Cyclodextrin Polymer for the Removal of Phenanthrene from Aqueous Solution. J. Hazard. Mater.2013; 261:286-294.

76. Zhang W, Chen M, Diao G. Electrospinning β-Cyclodextrin/Poly(vinyl alcohol) Nanofibrous Membrane for Molecular Capture.Carbohydr Polym. 2011; 86: 1410-1416.

77. Bazhban M, Nouri M, Mokhtari J. Electrospinning of Cyclodextrin Functionalized Chitosan/PVA Nanofibers as a Drug Delivery System. Chin. J. Polym. Sci.2013; 31:1343-1351.

78. Kayaci F, Uyar T. Solid Inclusion Complexes of Vanillin with Cyclodextrins: Their Formation, Characterization, and High-Temperature Stability. J. Agric. Food Chem. 2011; 59:11772–11778.

79. Kayaci F, Uyar T. Encapsulation of Vanillin/Cyclodextrin Inclusion Complex in Electrospun Polyvinyl alcohol (PVA) Nanowebs: Prolonged Shelf-Life and High Temperature Stability of Vanillin, Food chemistry. 2012; 133:641-649.

80. Kayaci F, Umu OCO, Tekinay T, Uyar T. Antibacterial Electrospun Polylactic acid (PLA) Nanofibrous Webs Incorporating Triclosan/Cyclodextrin Inclusion Complexes. J. Agric. Food Chem. 2013; 61:3901-1908.

81. Celebioglu A,Umu OCO, Tekinay T, Uyar T. Antibacterial Electrospun Nanofibers from Triclosan/Cyclodextrin Inclusion Complexes. Colloids Surf., B.2013; 116:612-619.

Chapter 2: Poly (ε-caprolactone) Nanowebs Functionalized with α- and γ-Cyclodextrins.

Abstract:

The effects of alpha and gamma-cyclodextrins (α- and ɤ-CDs) on the thermal properties and crystal nucleation behavior of electrospun PCL nanofibers have been investigated. PCL/CD composite nanofibers were obtained for the first time by electrospinning the mixture from chloroform/ N,N-dimethylformamide (60:40). SEM analyses indicated that neat PCL nanofibers had an average diameter of 400 nm, which increased with the addition of CDs. The presence of CDs on/in the electrospun PCL fibers in the electrospun mats were investigated using Fourier transform infrared spectroscopy (FTIR), thermogravimetric analysis (TGA) and wide angle diffraction analysis (WAXD). DSC showed that the PCL/CD composite fibers exhibit higher crystallization temperatures and sharper crystallization exotherms with increased CD loading, indicating the ability of CDs to serve as nucleants for PCL crystallization. Water contact angle (WCA) measurements indicate an inverse relationship between WCA and α- or ɤ-CD concentration, up to 30% loading. Phenolphthalein (PhP) being an ideal compound to study kinetics of IC formation, was utilized to study the kinetics of IC formation with neat PCL, and CDs containing PCL nanofibers. Unexpectedly, γ-CD functionalized nanowebs performed better than α-CD. This might be because at elevated loadings, some α-CDs may have threaded over PCL chains and formed inclusion compounds (ICs), whereas ɤ-CD did not do so. With their encapsulation capabilities and their lowered hydrophobicity, PCL/CD composite fibers might have

potential uses in medical applications, in particular, as wound odor absorbants in dressings. This is because, it is well known that CDs can form ICs with these small molecule odorant compounds, thereby effectively removing them.

2.1 Introduction:

Electrospinning is a simple but effective and inexpensive method for preparing micro- to nanosized fibers. Owing to their smaller diameters, these fibers have enormous potential in applications such as scaffolds for tissue engineering, filtration membranes, and functional materials for delivering drugs [1-5]. Electrospun webs tend to have lower crystallinity compared to fibers and films, made by extrusion methods and, therefore, decreased mechanical properties [6]. In order to improve their properties and therefore, functionalities, various materials have been added to nanowebs, including carbon nanotubes, modified nanoclays, nanowhiskers and hydroxyapatite, to name a few [7-10]. In this study, we employed CDs to nucleate PCL fibers and study their effects on the thermal behavior, fiber morphology, surface wettability and small molecular absorption/ encapsulation in the nanowebs so produced.

Cyclodextrins (CDs) are a group of cyclic α-1,4-linked oligosaccharides, most widely used among which are α, β-, and γ-CD, containing 6, 7, and 8 glucopyranose units, respectively. The chemical structures and schematic representations of these are shown in Figure 2.1 [11-14a]. It has been found that CDs can function as nucleating agents for polymers used in biomedical applications, such as PCL, polyethylene glycol, poly (butylene succinate) and

poly(3-hydroxy butyrate) [15-16]. The advantages of using CDs include their biocompatibility, biodegradability and ready availability from renewable natural resources.

PCL is a linear aliphatic and flexible polyester, which is biodegradable and used extensively in the form of films or fibers for medical applications. At room temperature, it is semi-crystalline with 60-70% crystallinity [17]. The main drawbacks of PCL include: low

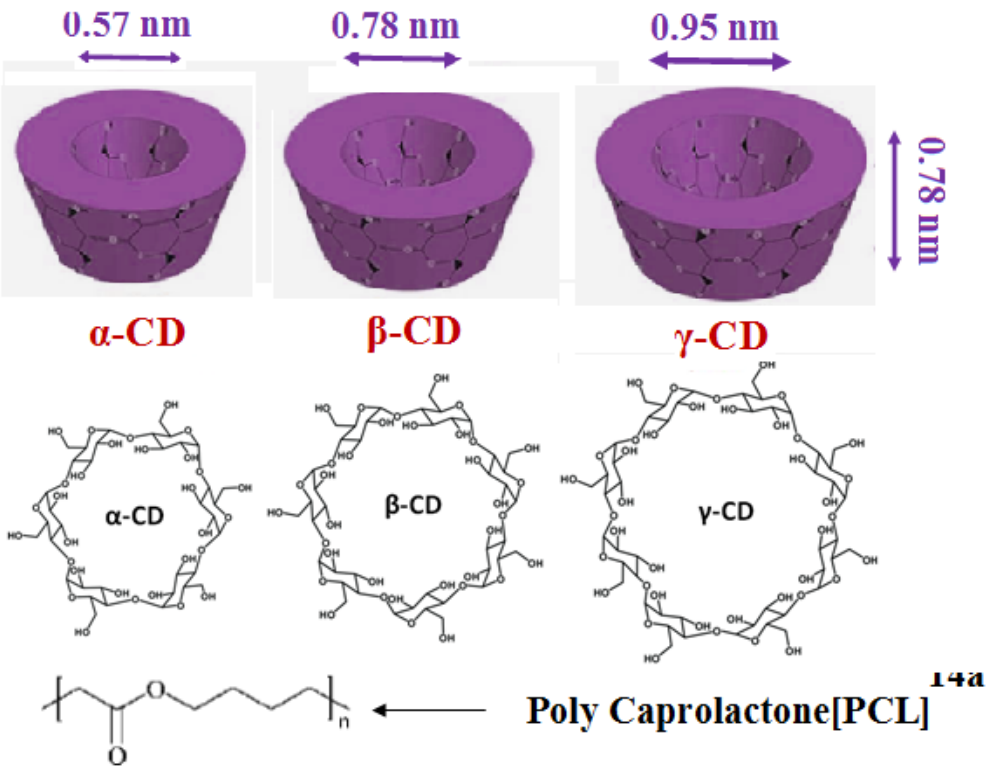

Figure 2.1: Chemical structures of α, β, ɤ-cyclodextrins, and poly (ε-caprolactone) [PCL] [14a].

melting point (~ 60˚ C), which limits its applications; rapid degradation at elevated temperatures; and poor wettability, due to its hydrophobic nature, which limits cell attachment and biological interaction. To improve surface hydrophilicity, a variety of approaches have been tried including plasma treatment, chemical treatment, coating with extra cellular matrix proteins or by blending PCL with biologically active materials [18]. Most tissue engineering/biomedical applications typically require biomaterials that have low contact angle (or high hydrophilicity) to promote cell adhesion and differentiation, and aid in the formation of new extracellular matrix (ECM) [19-22]. However, there are some applications, as for example, wound odor absorption, where some hydrophobicity can be an advantage as it can impart structural integrity to the material (wound dressing in this case).

CDs are used in a variety of applications, including pharmaceuticals, food, packaging, cosmetics, and for physically nanostructuring polymers [28-30]. CDs have also been used to functionalize electrospun fibers for potential application in molecular filtration, enhanced cell growth, controlled drug delivery and food applications. Most research has been focused on electrospinning polymer mixtures with CDs from a single solvent. Uyar *et al*, have successfully electrospun functionalized poly (methyl methacryalate) (PMMA), polystyrene (PS) and polyethylene oxide (PEO) fibers containing CDs. In all these cases, both polymer and CDs were dissolved in a common solvent; for example, PMMA/CDs and PS/CDs in N,N-dimethylformamide and PEO/CDs in water [31-35].

The primary motivation for our study was to electrospin PCL nanowebs containing CDs even though they did not dissolve in a common solvent. An interesting question faced was, if

different solvents were used, will cyclodextrin form a non-stoichiometric IC with the polymer or will it remain unthreaded and be freely available for complexation? To the best of our knowledge, such a study has not been conducted. It is well known that PCL readily forms ICs with α-CD and coalescing the PCL out of the α-CD-IC crystals is an arduous task [36]. PCL and both α- and ɤ-CDs are soluble in N,N-dimethylformamide (DMF), however PCL (MW = 65,000 or above) cannot be dissolved beyond 5% in DMF [37]. Instead, PCL dissolution is facilitated by adding chloroform to DMF. When CD and PCL are dissolved in DMF/chloroform mixtures, the possibility of forming ICs decreases due to thermodynamic interference, *i.e.,* the preference for DMF and chloroform, respectively, by CDs and PCL. Hence, such a combination of solvents should ideally result in α- and ɤ-CDs present on the fiber surfaces, *i.e*., without being threaded by and forming ICs with PCL. Availability of relatively free CDs within the nanofiber web can be an advantage for some applications, such as for wound dressings, wherein selective absorption of exudates, in particular odor causing molecules, is desirable.

A secondary motivation for our study was to improve PCL hydrophilicity and correlate the water contact angle of the nanowebs with CD loadings. A tertiary motivation was to study the molecular encapsulation capability of CD functionalized PCL nanowebs for phenolphthalein (PhP), which is a model compound typically used for studying IC formation. PhP absorption tests should indicate the availability of free CDs. No or limited absorption would indicate the some PCL chains have threaded CDs and are included in their cavities.

2.2 Experimental details:

2.2.1 Materials:

Poly (ε-caprolactone) (PCL) with a molecular weight of 60-80,000 was purchased from Sigma –Aldrich, as were the solvents [chloroform (99.5% pure) and N,N-dimethylformamide (anhydrous 99.8%)]. CDs (Pharma grade) were obtained from Wacker Chemie, Michigan US.

2.2.2 Solution preparation:

PCL solutions were prepared by dissolving appropriate quantities of PCL in 6 ml of chloroform, and CD solutions were prepared by dissolving appropriate quantities of CD in 4 ml of DMF. PCL and CD solutions were then mixed together. To serve as control for the electrospinning experiments, neat PCL solutions were also made by dissolving PCL in a mixture of chloroform and DMF (60:40). Once the solutions were prepared, they were stirred overnight at room temperature. Control PCL/CD films were obtained by evaporation of the solvent, *i.e.*, 60:40 chloroform: N/N-dimethylformamide solution.

2.2.3 Solution characterization:

Rheological measurements of electrospinning solutions were performed at 25° C using a Stresstech HR instrument with a 4.5 cm parallel plate geometry. Surface tension measurements were performed at 25° C with a data physics DCAT instrument using a Wilhemy plate method. The instrument has a motor speed of 1mm/s and the operation is automatically stopped when the standard deviation within each sample is less than 0.03

mN/m. Electrical conductivity measurements were made on an Orion model 162 at 25° C and the results are reported in μS/cm.

2.2.4 Preparation of PCL-CD Composite Nanowebs:

Polymer solutions were placed in a commercial 10 ml syringe (Becton Dickinson & Company) to which was attached a blunted 21 G needle. Electrospun mats were formed using a high precision pump (New era pump systems) that delivers the fluid at a preset rate. High voltage was applied between the tip of the needle and the collector using a Gamma High Voltage Research instrument. A rotating drum made of stainless steel, with an outer diameter of 1.5 inches and rotating at 280 rpm, was placed 30 cm from the tip of the needle, and used as the collector. The electrospinning process was carried out at a potential difference of 15 KV and with a solution feed rate of 0.5 ml/hr.

Cyclodextrin concentrations were varied from 0% to 50% by weight relative to PCL. Once the electrospun mats were obtained, they were allowed to dry for a week in a clean vacuum oven to remove unevaporated solvents.

2.2.5 Characterization of nano-webs:

The electrospun mats were characterized using Fourier Transform infrared spectroscopy (FTIR), thermogravimetric analysis (TGA), differential scanning calorimetry (DSC), scanning electron microscopy (SEM), and wide-angle x-ray diffraction (WAXD). Infrared spectral studies were conducted using a Nicolet 470 FTIR infrared spectrophotometer in the range of 4000-400 cm^{-1} with a resolution of 4 cm^{-1}, and 64 scans were collected for each

sample. A diamond probe, instead of the standard germanium probe, was used for FTIR, because of its better sensitivity to vibrations on such nanosurfaces.

TGA was performed using a Perkin Elmer Thermogravimetric analyzer. Nitrogen gas was used to purge the furnace. Samples were heated from 25 to 600° C at a rate of 10° C per minute and Pyris software was used to analyze the data. Thermal transitions of the neat and composite PCL nanofibers were determined using a Perkin Elmer diamond 7 DSC instrument with heat-cool-heat cycles between 0 to 80° C. First heating was carried out at 20° C/min and successive heating and cooling cycles were carried out at 10° C/min.

Scanning electron microscopy was performed using a phenom world G1 model microscope at an acceleration voltage of 10 KV to study fiber morphology. Samples were cut and attached onto a metal stub with double sided carbon tape and coated with gold using a Polaron SC7620 Mini Sputter Coater (Quorum technologies) for about 45 seconds that yielded a 10nm coating. SEM images were obtained at various resolutions and the fiber diameters were calculated using ImageJ software (freely downloadable from NIH). Diameters of a minimum of 100 fibers were measured and their average fiber diameters are reported.

WAXD analyses were performed on electrospun neat and composite PCL/CD mats, and on powdered samples of CDs using a Philips type-F X-ray diffractometer with a Ni-filtered Cu Kα radiation source (λ = 1.54 Å). CD powders were held in a glass cup, and gently patted. In the case of electrospun mats, small pieces were sliced off and held on the sample

holder and taped. The applied voltage and current used were 35 KV and 25 mA, respectively, and the diffraction intensities were measured from $2\theta = 10$ to 30°, at the rate of 0.05°/second.

The hydrophilicity of the electrospun mats were measured using a Data Physics OCA goniometer equipped with a high speed camera. A small sample measuring 1 x 5 cm was cut from the electrospun web and placed and held firmly on the stage using double sided tape. The DI water with bulk resistivity of 14 MΩ·cm was dispensed using a 50 µL syringe, attached to a 0.18 µm needle. The DI water was dispensed at a speed of 1.5 µL/s, and the contact angles between the water droplet and the surface upon immediate contact were measured and calculated automatically by the computer software. Average of five measurements were taken and reported as water contact angle (WCA).

The uptake of phenolphthalein (PhP) by the electrospun webs was observed visually and the images were captured using a Canon high definition camera. The PhP solution was made using the procedure described by Uyar et al [32]. Briefly, 4×10^{-4} M PhP solution was made by dissolving 0.0127 g of PhP in 100 ml absolute ethanol. The pH was then adjusted to 11 by adding a few drops of pH = 12.7 buffer solution. Small rectangular pieces weighing about 0.1 g were sliced from the electrospun webs and placed in 10 ml of PhP solution. As absorption of the PhP by nanofibers took place over time, the solution color changed from purple to colorless. This was monitored visually as well as recorded digitally.

2.3 Results:

Various solvents and their combinations have been described for successfully electrospinning PCL. The most widely used solvents include chloroform, acetone, dichloromethane, tetrahydrofuran, trifluoroethanol, and hexafluoroethanol. Sometimes, minor proportions of solvents like methanol or DMF are also added to improve spinnability or conductivity [23-27]. In this work, a mixture of chloroform and DMF was chosen as the solvent (60:40 ratio) due to the fact that chloroform is a good solvent for PCL, and DMF a good solvent for CDs. It is well known that three solution parameters, viscosity, surface tension, and electrical conductivity, generally affect the morphology of electrospun mats. PCL has been successfully electrospun in the concentration range from 10-20%, and in some cases even beyond 25% [19-27].

To identify suitable conditions for spinning from our chosen solvent combination, zero shear viscosity sweeps were performed in the Newtonian region and are shown in Figure 2.2. It is seen that viscosity sharply increases beyond ~14% PCL concentration, indicating that critical entanglement could begin around 12-14%. Hence, successful electrospinning was most likely to happen around this concentration, which needed to be examined and refined. Fibers were produced in the broad range of 10-16 % concentration and were studied further by SEM (discussed later).

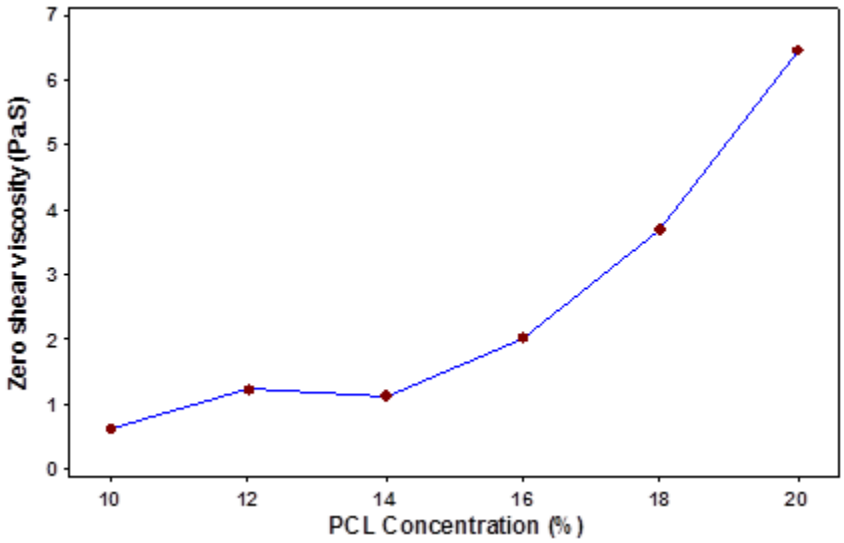

Figure 2.2: Zero shear viscosity sweeps of PCL solutions in 60:40 chloroform: DMF.

In addition to concentration, two other solution characteristics that can have an impact on the electrospinning process and the quality of the resulting web are surface tension and conductivity. It is well known that as a general rule, solutions with low surface tension lead to beaded fiber structures, whereas those with relatively higher surface tensions lead to finer bead-free or less beaded fibers [27, 38]. To examine the effect of solution concentration on surface tension, surface tension measurements were performed on different PCL solutions, and the results are shown in Figure 2.3. It is evident that varying the PCL concentration did not significantly change the surface tension of the solution. The same trend is observed in the case of electrical conductivity, as seen in Figure 2.4.

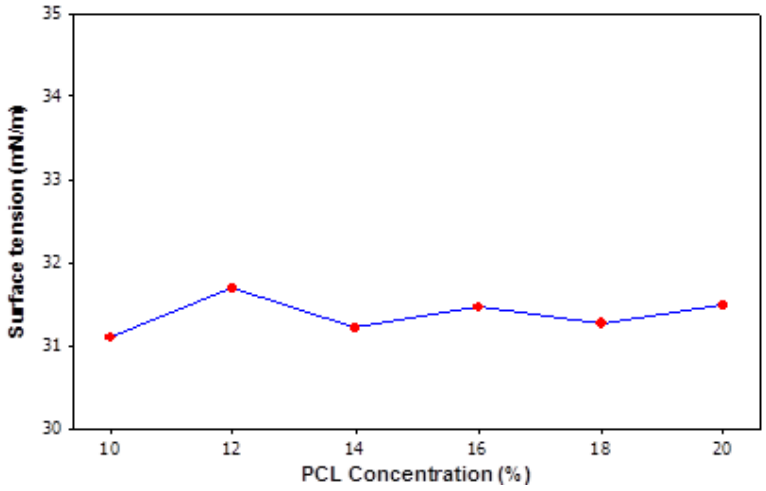

Figure 2.3: Surface tension of PCL solutions at varying concentrations.

It is generally known that conductivity of PCL alone is very poor, and use of solvents like DMF or additives like salt, improve the solution conductivity [28,29]. Uyar et al reported that the conductivity of solutions increased when CDs, especially β-CD, were added [31-35]. But this did not happen in our case, most likely because of the lower loadings, and types of CDs (α-CD & γ-CDs) used in our research were different from theirs (β-CD).

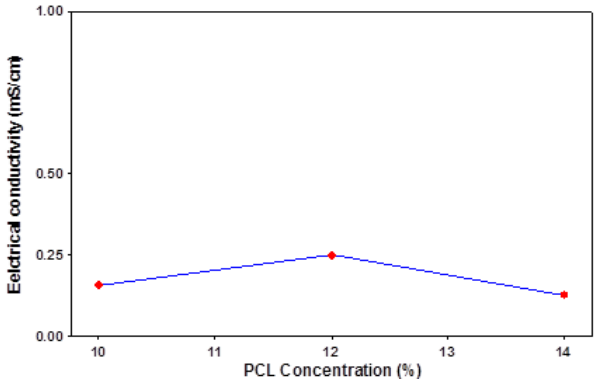

Figure 2.4: Electrical conductivity of PCL solutions.

The morphologies of the neat electrospun PCL webs and the corresponding values of fiber diameters are shown in Figures 2.5 & 2.6. It is seen that finer fibers were obtained at 12% concentration (Figure 2.6), and average fiber diameter increased as the concentration increased up to 14%. Also noted is that beyond 14% PCL, although the average fiber diameters remained similar, fiber diameter variability increased, with upper values reaching into the micrometer range, which is not desirable for most applications. As there was little or no change in surface tension and conductivity values with PCL concentration, the change in fiber morphology was most likely due to changes in viscosity (Figure 2.2).

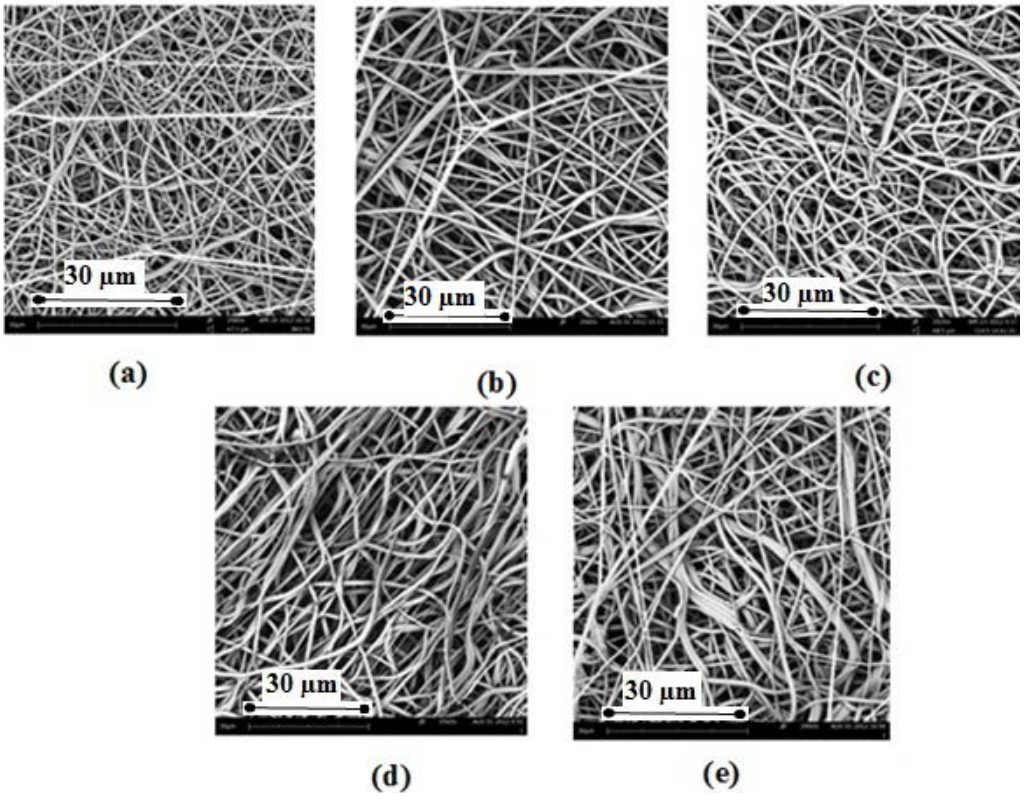

Figure 2.5: SEM images of electrospun PCL fibers at (a) 12% PCL, (b) 13.5 % PCL, (c) 14.5% PCL, (d) 15% PCL, (e) 15.5 % PCL.

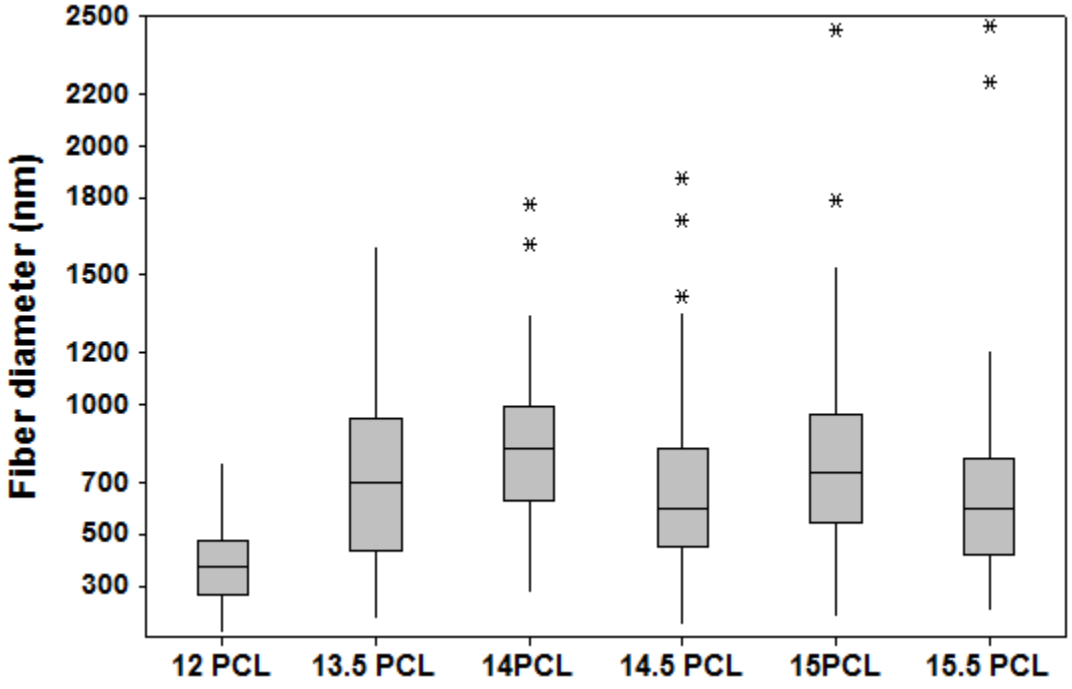

Figure 2.6: Fiber diameters of neat electrospun PCL nanofibers.

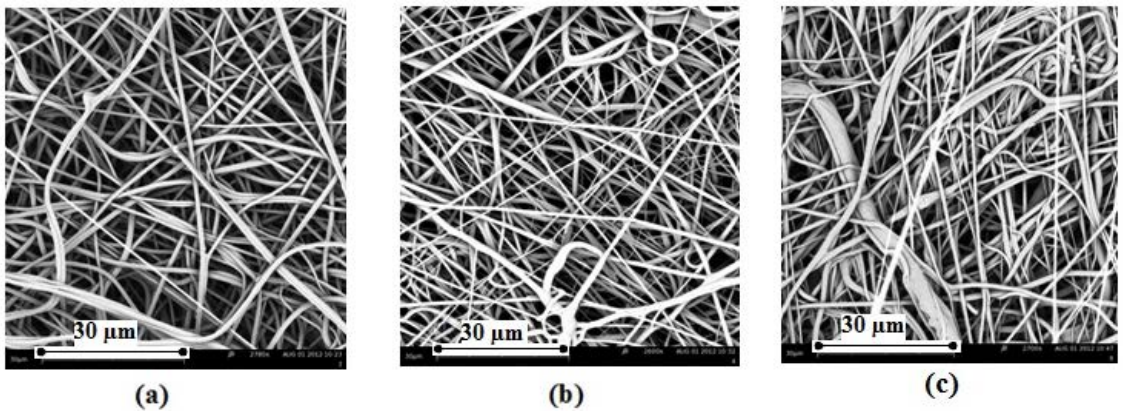

Figure 2.7: Representative SEM images of (a) 14% neat PCL nanofibers and PCL nanofibers functionalized with (b) 5% ɤ-CD and (c) 10% ɤ-CD.

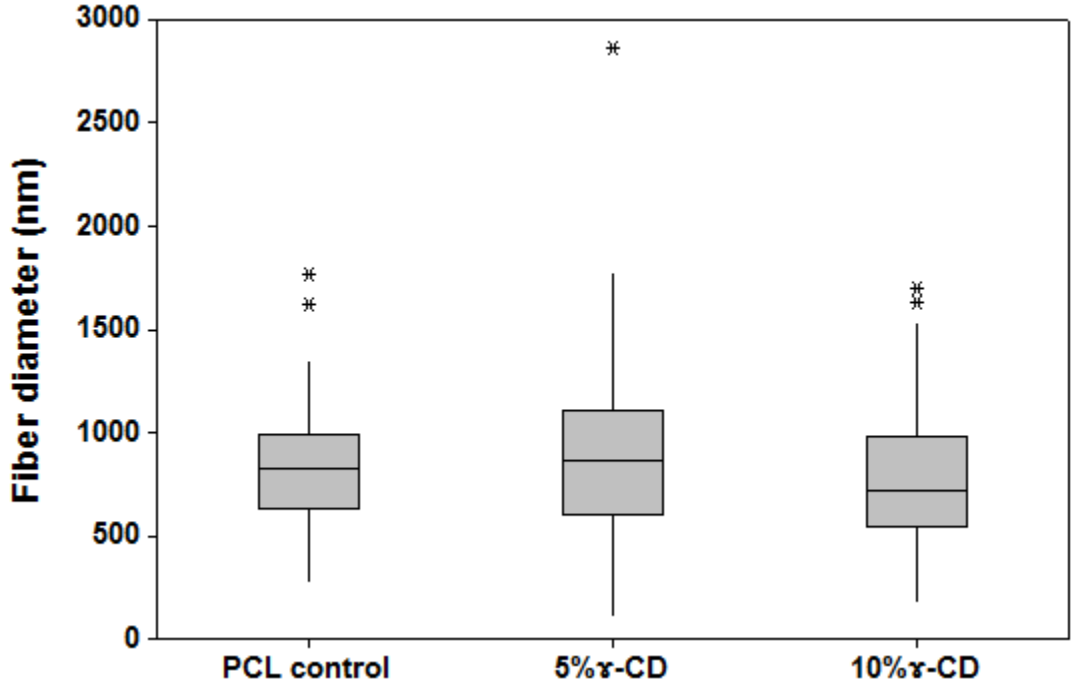

Figure 2.8: Average fiber diameters of control PCL fibers (14%), PCL functionalized with ɤ-CD.

For the CD functionalized fibers, the concentration of PCL was varied from 12 to 14%, and the CD concentration was varied from 5 to 40% with respect to PCL. The morphology and average fiber diameters of PCL and ɤ-CD functionalized PCL fibers (5 and 10% ɤ-CD) at 14% PCL concentration are shown in Figures 2.7 and 2.8, respectively. Average fiber diameters of the neat PCL nanoweb and ɤ-CD functionalized PCL fibers were about 800 nm.It was seen that a maximum of 15% ɤ-CD loading was possible when the concentration of PCL was 14%. To study if higher loading of ɤ-CD was possible, the concentration of PCL was reduced to 12% and the loading of ɤ-CD was varied from 5 to 40%; representative images and calculated fiber diameters are shown in Figures 2.9 & 2.10. As found with

nanowebs obtained with a concentration of 14% PCL, it is seen that the smallest fiber diameter is obtained at a loading of 5% ɤ-CD, and it increases only slightly with increased loading. Also, it is interesting to note, that with PCL concentration of 12% (instead of 14%), a loading of up to 30% ɤ-CD was possible.

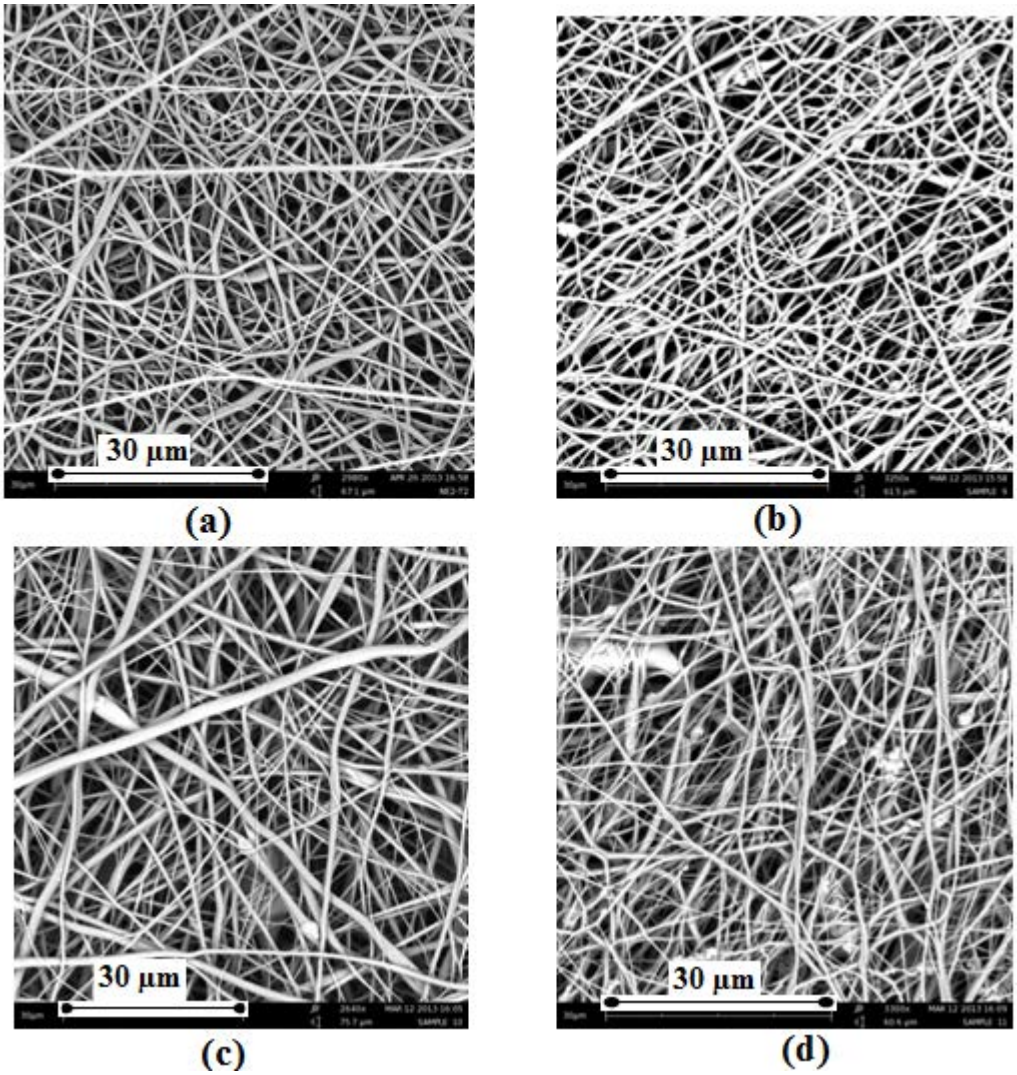

Figure 2.9: Representative images of PCL nanofibers functionalized with ɤ-CD. (a) control (12%PCL), (b) 5% ɤ-CD, (c) 15% ɤ-CD, (d) 30% ɤ-CD.

From SEM images (not shown) it was found that beyond 30% ɤ-CD loading, substantial agglomeration of CD occurred that resulted in highly non-uniform and beaded fibers. We concluded that for our solvent system and spinning parameters, PCL concentration of 12% and ɤ-CD loading of up to 30% yield the best results.

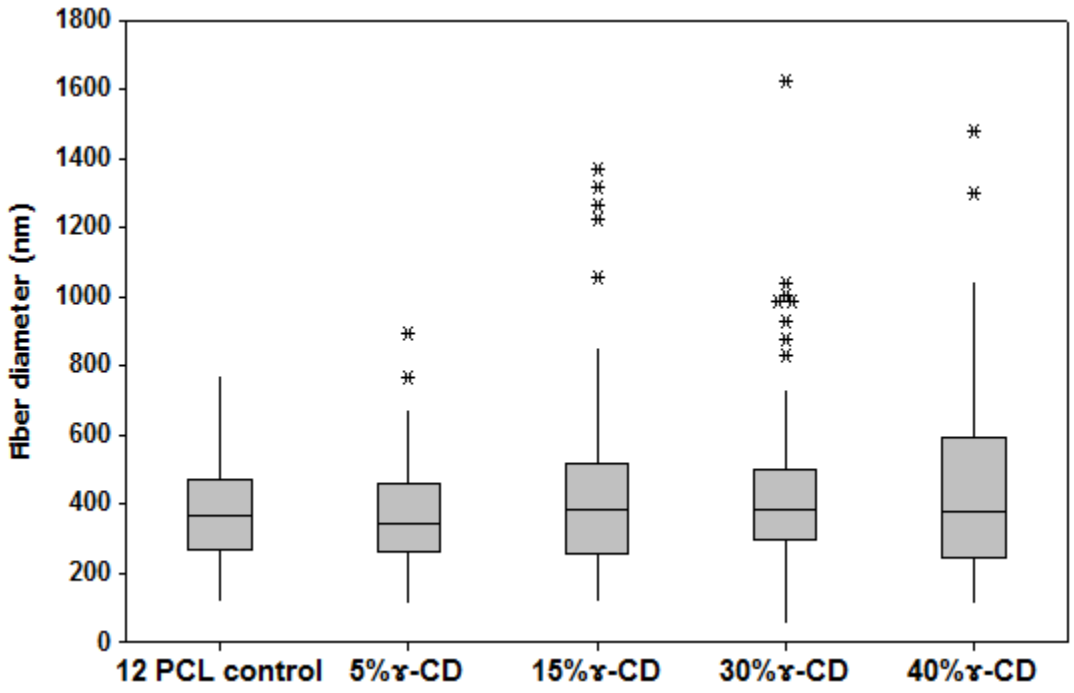

Figure 2.10: Average fiber diameters of ɤ-CD functionalized PCL(concentration=12%).

In our study of α-CD functionalized PCL fibers, using 12 % PCL concentration, finer fibers were obtained (not shown) only at α-CD loading of about 15%, whereas a loading greater than 15% resulted in beaded fibers. Unlike ɤ-CD functionalized PCL nanofibers, beyond

15% loading, there is a higher agglomeration of α-CD resulting in beaded fibers. Hence we could conclude that at both the 12 & 14% PCL concentration, the maximum possible loading of α-CD was only about 15%.

To confirm the presence of CDs on PCL nanofiber surfaces, electrospun mats were subjected to FTIR analysis and the spectra obtained are shown in Figure 2.11. The presence of strong carbonyl peaks at 1728 cm^{-1} indicates the presence of PCL and, though not intense, the hydroxyl peak at 3356 cm^{-1} indicates the presence of cyclodextrin. However, FTIR as noted by Tonelli *et al.*, doesn't indicate whether PCL is threaded through the cavities of CDs or remain outside of the unthreaded CDs [41].

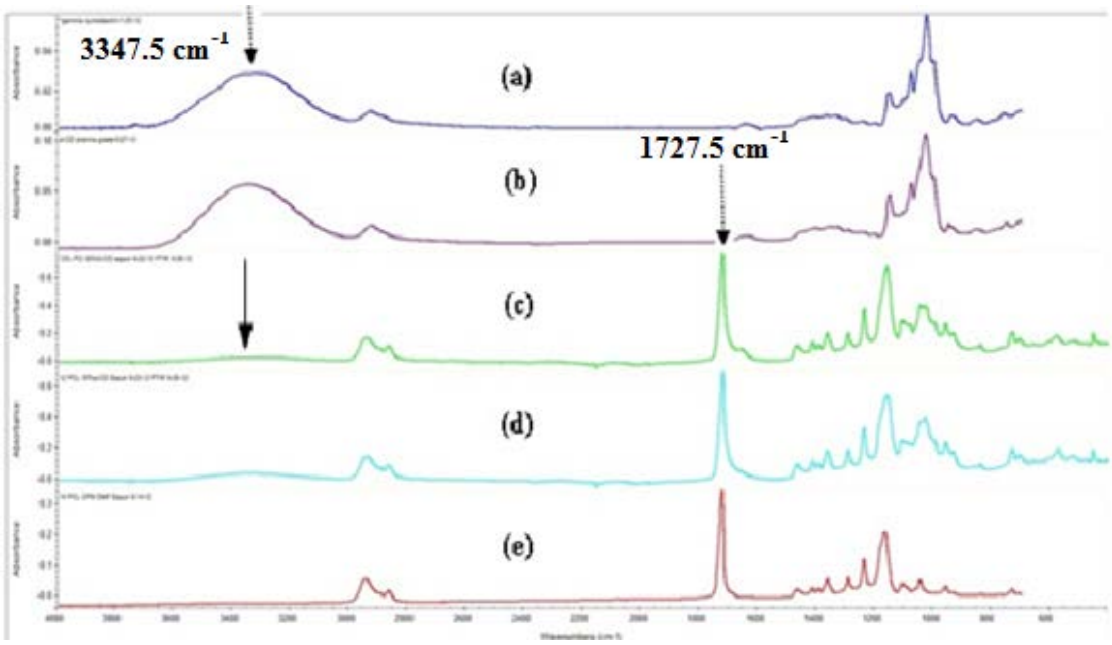

Figure 2.11: FTIR of electrospun mats. (a) ɤ-CD, (b) α-CD, PCL webs functionalized with 30% ɤ -CD (c) and 30% α–CD (d), and (e) electrospun PCL control.

Thermal transitions seen with DSC provide valuable information about the physical structure and hence properties of materials. It is known that completely covered polymer chains in an inclusion complex do not exhibit melting peaks, as seen for neat semi-crystalline polymers. In the case of non-stoichiometric inclusion complexes, depending on the ratio of dangling chain to covered chain, the presence of melting peaks are observed. From the first heating scans of electrospun fibers shown in Figure 2.12, it is seen that all electrospun webs exhibit similar melting peaks, though the melting points (T_m's) for those containing CDs seems to be slightly lower than that for pure PCL. Their crystalline contents are estimated from the DSC data using the equation X% = $\frac{\Delta H_m}{\Delta Hm^\circ}$, where ΔH_m is the melting enthalpy observed from DSC and ΔH_m° is the melting enthalpy of a reference PCL with 100% crystallinity, reported in the literature.

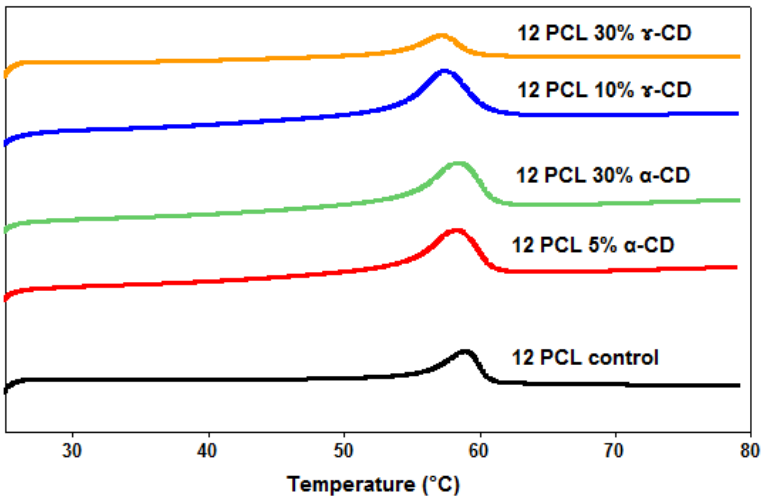

Figure 2.12: First heating cycle of electrospun PCL and functionalized PCL fibers.

For convenience, the reference $\Delta H_m°$was taken as 135.6 J/g as observed by Price et al [40]. The melting temperatures and their enthalpies, the crystallization temperatures and their enthalpies (Figure 2.13), and calculated crystalinities of the webs are reported in Table 2.1.The neat electrospun PCL fibers have a crystallinity of 43.5% which is lower than that of PCL films or powders as reported in the literature [42]. This is expected because polymers electrospun from high concentration solution tend to have lower crystallinity and lower molecular orientation. However, those containing CDs exhibit higher than usual crystallinities (up to 65% for those containing 30% ɤ-CD); this result is consistent with the capability of the CDs to nucleate the melt crystallization of PCL [15].

From Table 2.1, it is seen that neat electrospun PCL fibers have a crystallization temperature (T_c) and corresponding enthalpy of ~25°C & -54.4 J/g, respectively, whereas addition of a mere 5% α-CD results in an increase in T_c of about 7° C. As the % CD loading increased, the crystallization temperatures increased for all samples irrespective of the CDs used, and the crystallization peaks became more intense (Figure 2.13). At higher loading (30%), though crystallization temperatures remained higher, the intensity of the crystallization peaks became smaller than those containing lower loadings of CDs (Figure 2.13). This could possibly be due to the agglomeration of the CDs producing a slightly lowered nucleating effect on PCL.

Table 2.1: Thermal characteristics of PCL and PCL-CD composite fibers.

Material	T_m (°C)	T_c (°C)	ΔH_m (J/g)	ΔH_c (J/g)	X_c (%)
12 PCL control	59.0	24.97	75.3	-54.4	43.5
12 PCL 5% α-CD	58.3	31.73	67.5	-57.1	52.0
12 PCL 30% α-CD	57.3	34.31	56.7	-44.2	59.7
12 PCL 10% ɤ-CD	57.5	29.36	64.6	-51.5	53.0
12 PCL 30% ɤ-CD	57.2	32.58	61.9	-45.8	65.2

It was reported by Inoue *et al.* [42], that the carbonyl absorption peak seen for PCL at 1728 cm^{-1} could be resolved into two components; namely, crystalline and non-crystalline phases. Although not determined here, it would be of interest to know if there was any change in the ratio of crystalline to non-crystalline phases in the PCL webs containing CDs. From the DSC trends, it appears that due to the nucleation effects of CDs, the intensity of the non-crystalline domain peak would decrease or vanish. It would also be of value to examine the degree of molecular orientation existing in the composite fibers by polarized-FTIR or WAXD. The DSC trends seem to suggest that these functional composite fibers would have enhanced molecular orientation.

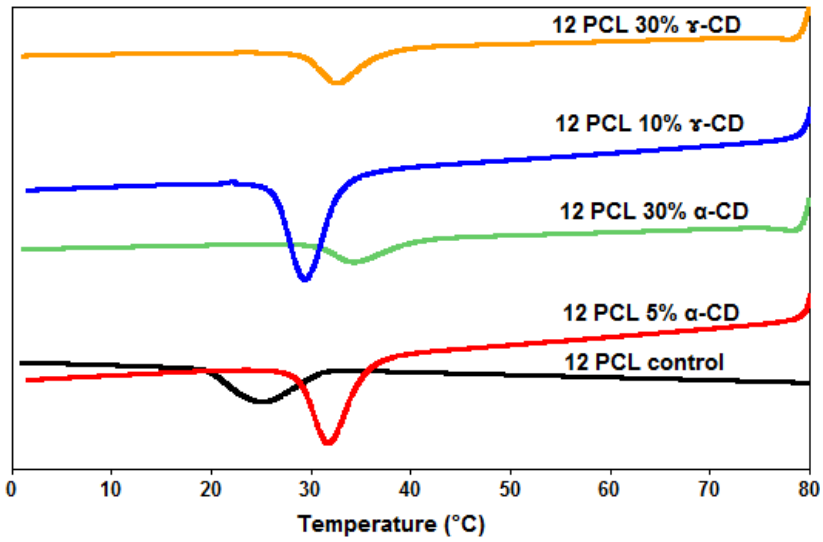

Figure 2.13: Cooling curves of PCL and composite fibers.

Figures 2.14a and 2.14b show the TGA plots of electrospun neat and composite nanofibers There is no weight loss observed in neat PCL fibers upto around 100° C (not shown), as expected because they are highly hydrophobic and hence no moisture was present on their surfaces. However, those containing CDs (both types) exhibit weight loss at temperatures up to about 100° C (shown by the arrow in Figure 2.14a), which is most likely due to the evaporation of moisture present on the surface. It is also observed that the composite fibers having higher loading of CDs lost more moisture, indicating moisture loss was somewhat directly proportional to that of CD loading.

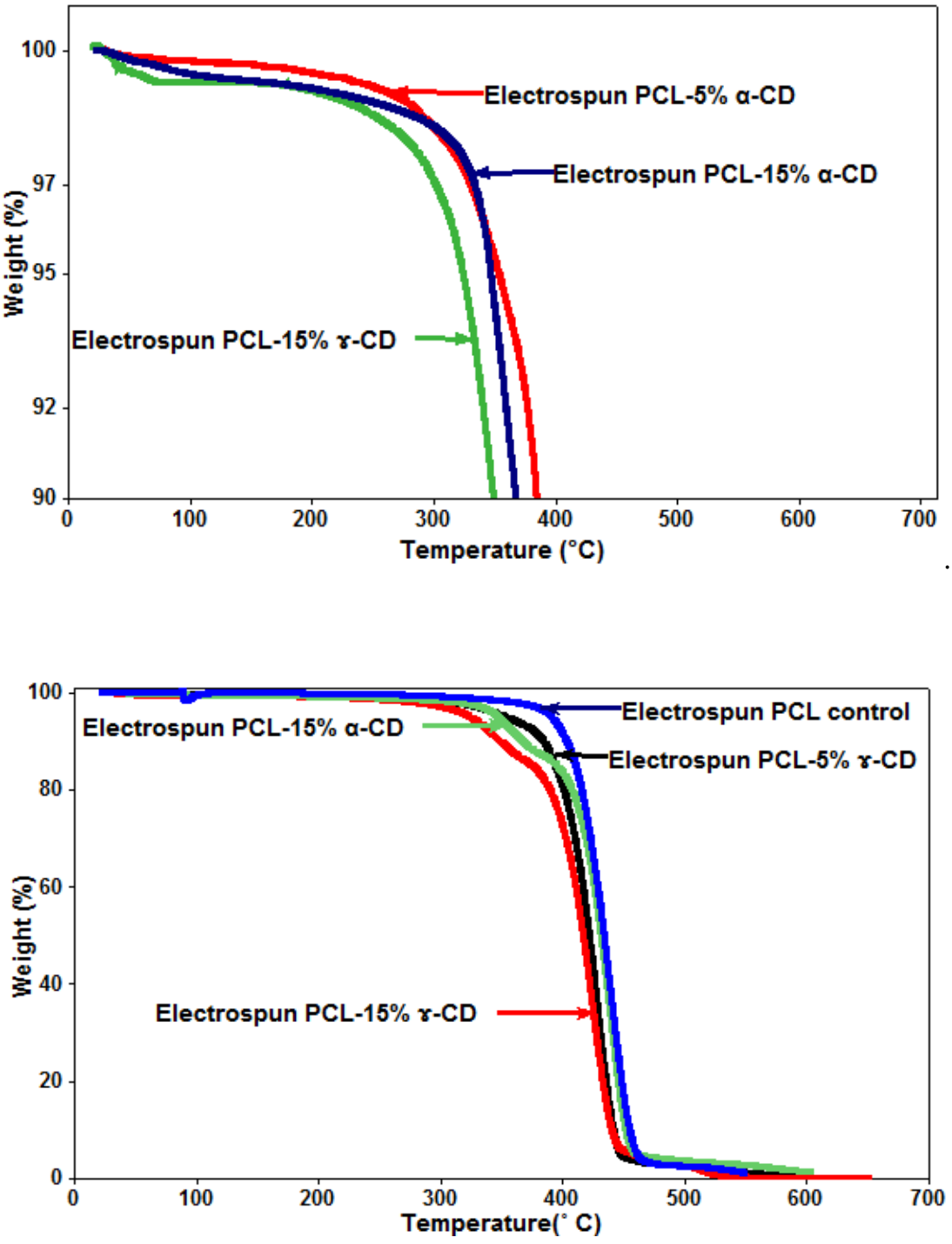

Figure 2.14: TGA plots of electrospun neat PCL, PCL/γ-CD, and PCL/α-CD composite fibers (25-400° C) (upper).TGA plots of electrospun neat PCL, PCL/α-CD, and PCL/ɤ-CD composite fibers (0-700° C).

α-CD has been reported to degrade at about 315° C [43] and PCL tends to degrade significantly beginning at 370° C. It is seen from Figure 2.15 that by about 370° C most of the ɤ-CD in functionalized composite fibers had already degraded reflecting a loss of 5% and 15% in the two materials, whereas in α-CD functionalized composite fibers, the loss observed was only about 10%, indicating that the remaining α-CDs might have formed inclusion complexes with PCL.

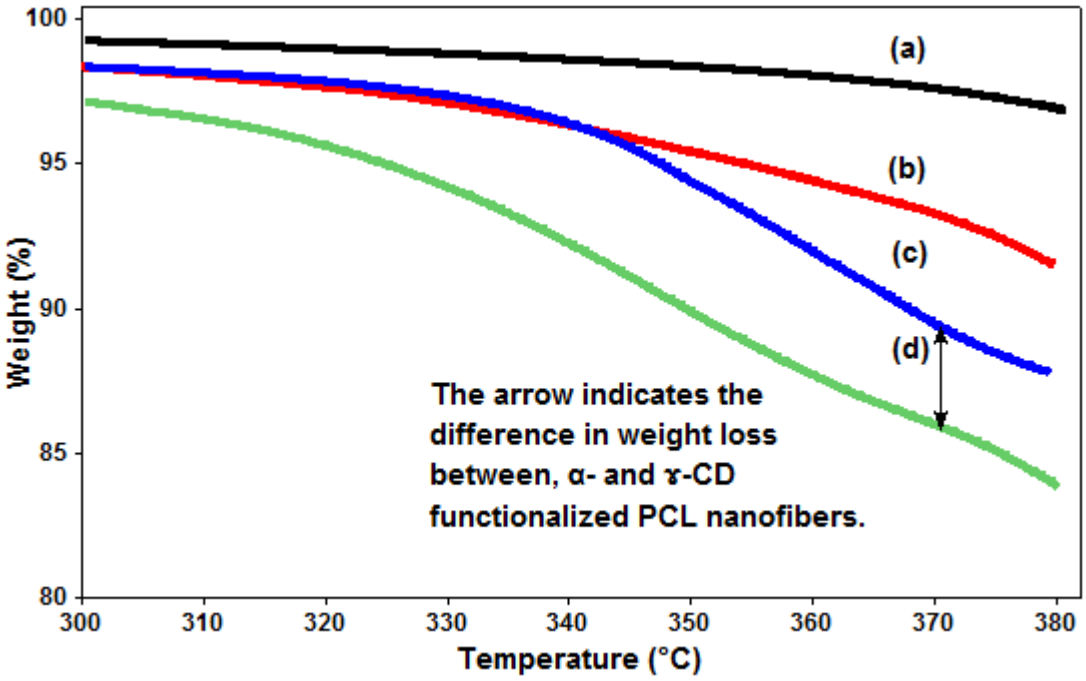

Figure 2.15: TGA plots of, (a) Electrospun PCL, (b) Electrospun PCL-5% α-CD, and (c) Electrospun PCL-15% α-CD, (d) Electrospun PCL-15% ɤ-CD(300-380°C).

It was shown by Tonelli et al [43] and Li et al [44] that polymer-cyclodextrin inclusion complexes tend to have higher degradation temperatures than neat cyclodextrins, because of the highly crystalline nature of the ICs. This phenomenon was noticeable in the case of α-CD functionalized fibers, which exhibited three stages of thermal degradation (Figure 2.15). The first stage is the degradation of free α-CD, followed by degradation presumably of the crystalline CDs in CD-ICs, and lastly by degradation of PCL.

Although ɤ-CD functionalized composite fibers also exhibited three stages of degradation, as noted for α-CD functionalized fibers, the final stage of degradation, *i.e.*, of the IC, is much less evident (Figure 2.14b). From our TGA observations, it could be concluded that although most of the CDs (both α and ɤ) were freely available on the surface, some of the α-CD, especially at higher loading (15%) might have formed ICs with PCL, while such IC formation with ɤ-CD was, by comparison, less.

The WAXD patterns of the control electrospun PCL, PCL-α-CD-IC film, and the α-CD functionalized electrospun PCL, webs are shown in Figure 2.16. PCL, a semicrystalline polymer, has approximately 60% crystallinity and has an orthorhombic crystal structure with a = 0.748 nm, b = 0.498 nm, and c = 1.729 nm, respectively. It has strong characteristic 2θ peaks at 22 and 24˚ that are attributed to (110) and (200) reflections [45]. α-CD typically exhibits a series of characteristic peaks at 2θ = 9.6 , 12.03 , 19.5 and 21.8° indicating a cage structure for its neat powder. When CDs form ICs with polymers, they assume columnar structures and these α-CD-ICs exhibit a unique peak at 2θ = 20˚ which is not observed for either the electrospun PCL, or the physical mixture of PCL and α-CD [43].

As seen in Figure 2.16, the electrospun webs containing 10% α-CD also do not exhibit this unique peak, which indicates the α-CDs that are present are either available freely on the surface or buried deep within the fiber without forming ICs. However, the PCL nanoweb and control film, both containing 40% α-CD, exhibit a weak but observable columnar IC peaks at 2θ = 20˚, indicated by arrows in the diffractograms. This indicates that perhaps some of the α-CDs might have formed ICs with PCL. PCL-α-CD films that were made directly from solution, also exhibit the same peak for the IC, indicating that the duration and nature of PCL and CD interaction was of less importance than their corresponding concentrations.

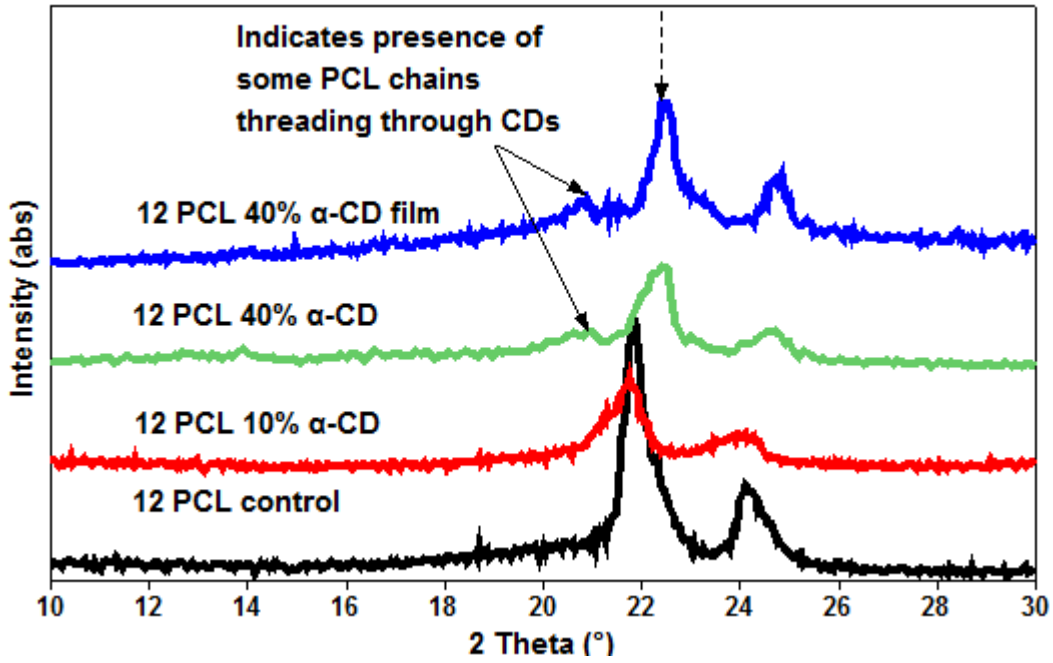

Figure 2.16: WAXD patterns of the electrospun PCL, α-CD functionalized electrospun PCL nanofibers and PCL-α-CD film cast from solution.

Another interesting observation is that in both the film and the web containing 40% α-CD, the strong peaks that correspond to (110) and (220) PCL reflections shift to higher 2θ values (~23˚), indicating possibly a change in crystal structure, over that observed for neat PCL control webs. The mixture of PCL and α-CD ideally should exhibit superimposed diffractograms of the two. The functionalized webs containing 10% α-CD do not exhibit the characteristic peaks of α-CD, indicating that the α-CD might not have agglomerated enough, whereas those containing 40% α-CD do exhibit them, although their intensities are low.

The WAXD patterns of ɤ-CD, electrospun PCL, and ɤ-CD functionalized electrospun PCL webs are shown in Figure 2.17. As found for α-CD, ɤ-CD, exhibits a series of peaks between 2θ = 5 and 30°.

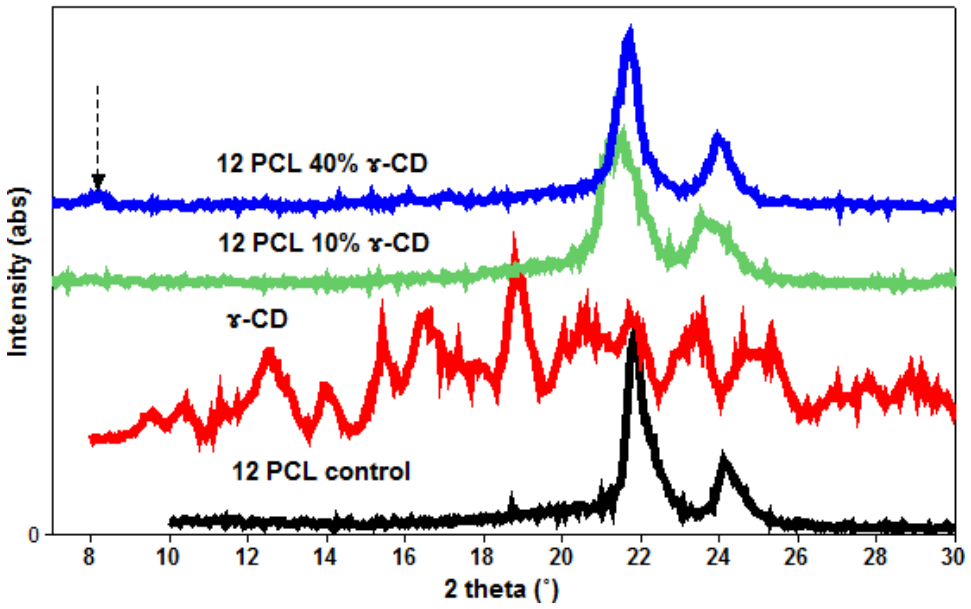

Figure 2.17: WAXD patterns of electrospun PCL, ɤ-CD functionalized electrospun PCL nanofibers with ɤ-CD.

These peaks are not observed in the case of functionalized PCL nanofibers containing 10% ɤ-CD, indicating that ɤ-CD might not have agglomerated and are only individually available on the surface. As observed in the case of α-CD, ɤ-CD, when formed into ICs with polymers, exhibit a unique X-ray peak (at 2θ = 7.8°), in addition to the peaks arising from the two superimposed materials.

As suggested by TGA, some functionalized fibers containing higher loadings of ɤ-CD seem to exhibit a peak at 2θ = 7.8°, indicating some might have formed inclusion complexes with the PCL. The peak tends to be less intense suggesting that only a small percentage of available ɤ-CD might have formed ICs with PCL chains.

Water contact angle (WCA) measurements were performed on electrospun neat webs that were electrospun from 10-16% polymer solutions and were observed to have values of 132 ±7°. PCL concentration was not found to have a significant effect on WCA. In Figure 2.18, representative images of WCA measurements on PCL and functionalized PCL nanofibers with α- and γ-CDs are shown, and in Figure 2.19, plots of WCA values against CD loading for 12% PCL nanofibers are presented. From both Figures, it is evident that the WCAs of functionalized nanofibers are considerably lower than that of neat PCL fibers. The inverse relationship suggests that the reduction in WCAs could be due to the presence of the CD hydroxyl groups on the fiber surface. It is noted that addition of as small as 5% CD caused reduction in WCA by about 18°. The minimum WCAs observed were about 100° for both functionalized fibers.

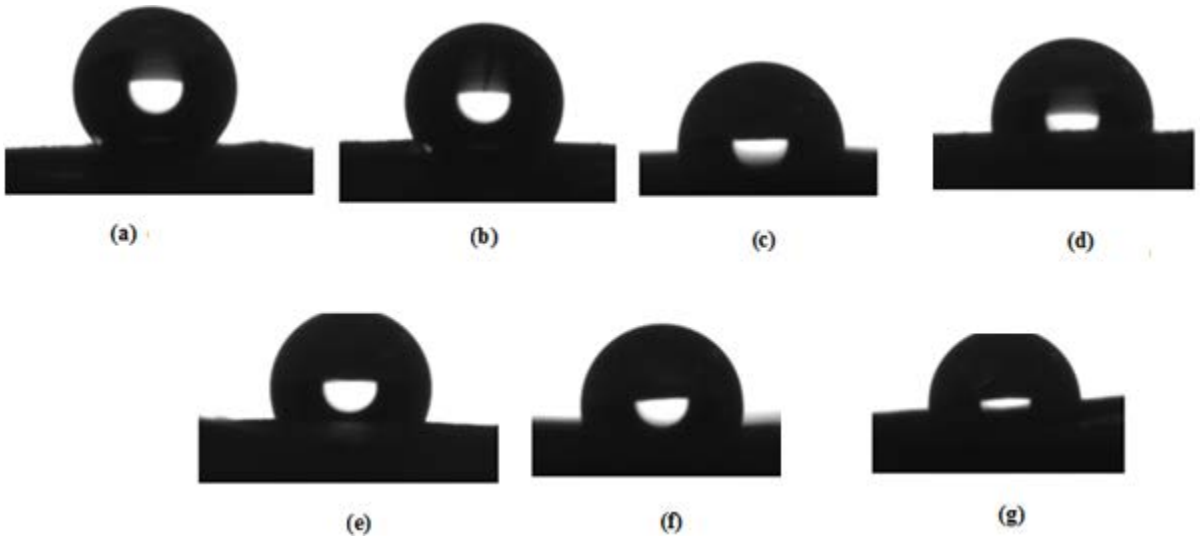

Figure 2.18: Representative WCA images of, (a) neat PCL nanoweb, PCL nanowebs with α-CD at (b) 5% , (c) 10%, and (d) 15% ; PCL nanowebs with γ-CD at 5% (e), 10% (f) and (g) 30%.

One of the most desirable features for a fiber based wound odor absorbant is that it has a level of hydrophobicity, as opposed to hydrocolloid wound dressings, which must necessarily have high hydrophilicity. Due to the presence of some minimal hydrophobicity, the structural integrity of the wound absorbant material would be expected to be retained over a period of time and hence frequent dressing changes would not be required. WCA results indicate that the CD functionalized PCL fibers can meet the structural requirement for wound odor absorbants, provided CDs present on the nanosurface are able to absorb the malodorous molecules.

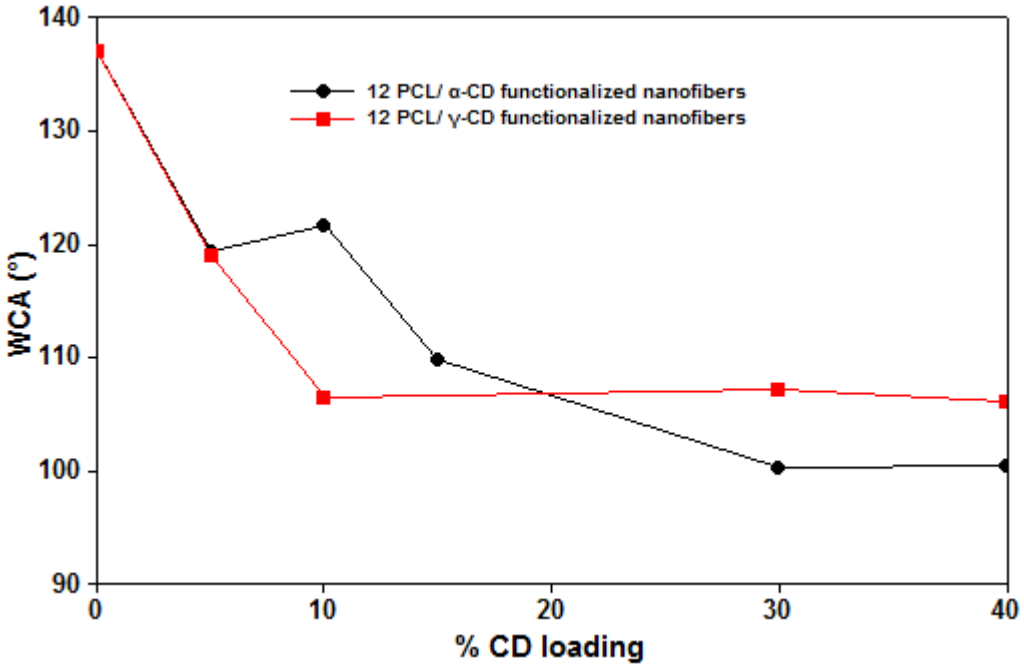

Figure 2.19: WCA measurements of neat and CD functionalized PCL nanofibers.

As mentioned earlier, the presence of free CDs can be expected to aid in the absorption of PhP. The motivation for performing the PhP absorption experiment was to determine the efficiency of PhP uptake of α- and γ-CD functionalized PCL webs, and also to compare our results with those reported in the literature. The uptake of PhP by neat PCL fibers, and α- and γ-functionalized PCL fibers (10 and 40% loading), observed over a period of time, are illustrated in Figures 2.20-2.24. Although the results are only qualitative, some critical observations can be made. Over a short period of time, the neat PCL nanofibers showed insignificant rate of absorption, while even 10% functionalized PCL nanofibers absorbed noticeable quantities of PhP (not shown). After 144 hours, however, the 10% functionalized

nanofibers performed only slightly better than the neat PCL nanofibers. Between the two CDs, the γ-CD functionalized nanofibers performed better than the α-CD functionalized nanofibers.

Figure 2.20: Uptake of PhP by neat PCL nanofibers. (a) Initial condition after immersion, (b) after 24 hours, and (c) after 144 hours.

Figure 2.21: Uptake of PhP by α-CD (10% loading) functionalized PCL nanofibers. Initial condition after immersion, (b) after 24 hours, (c) after 144 hours.

Figure 2.22: Uptake of PhP by α-CD (40% loading) functionalized PCL nanofibers. Initial condition after immersion, (b) after 24 hours, (c) after 144 hours.

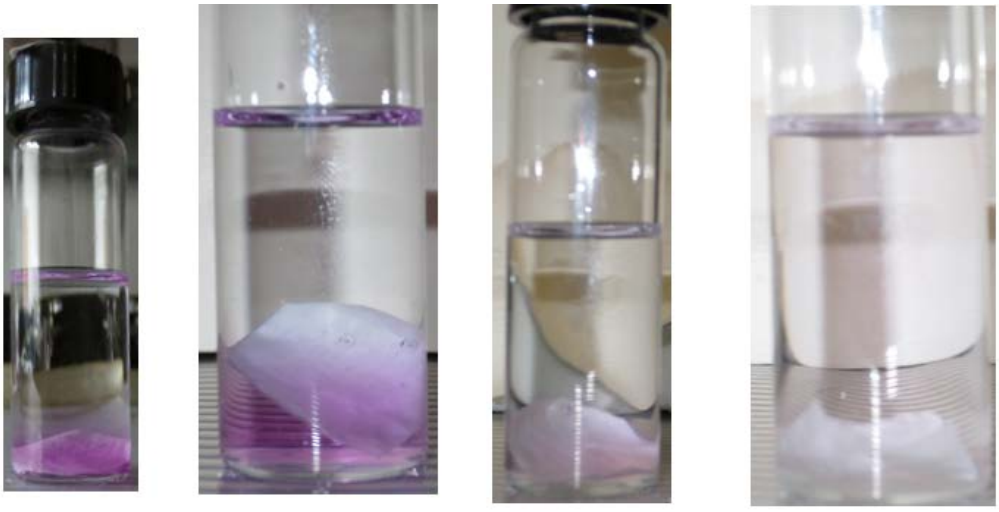

Figure 2.23: Uptake of PhP by γ-CD (10% loading) functionalized PCL nanofibers. (a) Initial condition after immersion, (b) after 24 hours, (c) after 72 hours, and (d) after 144 hours.

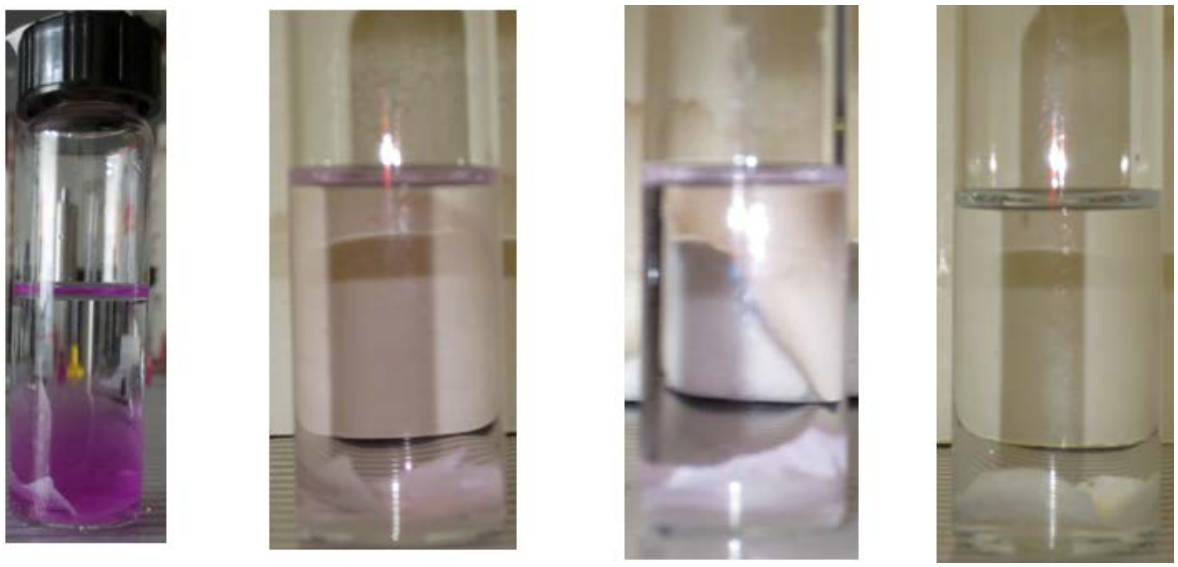

Figure 2.24: Uptake of PhP by γ-CD (40% loading) functionalized PCL nanofibers. (a) Initial condition after immersion, (b) after 24 hours, (c) after 72 hours (d) after 144 hours.

It was reported by Uyar et al [32], that α-CD functionalized polymeric nanofibers consistently performed better than β- and γ- CD functionalized fibers. For example, when the PhP absorption of the PS/CD fibers was examined, the order of absorption found was PS/α-CD > PS/β-CD > PS/γ-CD. Uyar et al also determined the saturation times for trapping PhP molecules in CD cavities in the functionalized PS nanowebs, and found the result to be 3 days. In our study, we observed that the CD functionalized PCL webs were able to absorb PhP efficiently only when the CD concentration was high (40%). Comparison of the results of 40% CD loading in Figures 2.22 and 2.24, we conclude that the saturation time for γ-CD functionalized PCL nanofibers lies close to 3 days, while that for α-CD functionalized fibers lies somewhere between 3 to 6 days. Uyar et al compared the molecular efficiency of PhP

absorption by PS nanofibers at CD concentration of 15%, which should not be significantly different from our results for 10% CD reported here.

Two possible reasons exist for differences in the performance of Uyar's PS/CD and our PCL/CD nanowebs. Either the distributions of γ-CDs are more homogenous than α-CDs, or, α-CD formed ICs with PCL significantly more than did γ-CD. PS and CDs are reported not to form complexes with each other [46-47]; whereas, both α- and γ-CD form ICs with PCL relatively easily [36]. As mentioned earlier, another possible reason, why γ-CD functionalized PCL nanofibers elicited a better response of trapping PhP molecules than did α-CDs functionalized fibers could be due to a larger presence of γ-CD molecules on the PCL nanofiber surfaces.

Although neat PCL nanofibers have lower fiber diameters as compared to those of the CD functionalized PCL nanofibers, the kinetics of PhP absorption has been observed to be dependent on both CD type as well as CD-concentration. From the observation in our study, we conclude the PhP absorption order to be: PCL/γ-CD (40%) > PCL/α-CD (40%) > PCL/γ-CD (10%) > PCL/α-CD (10%) > neat PCL.

2.4 Discussion:

Possible hypothetical structures that can develop when PCL and CD are electrospun from chloroform/DMF solutions are shown in Figure 2.25. With FTIR, we observed the peaks at 3347.5 and 1427.5 cm^{-1}, that corresponds to the hydroxyl groups in cyclodextrin, and

carbonyl peaks in PCL. Since the presence of CDs and PCL has been confirmed, the first model (a), wherein only PCL are available on the nanofiber surface, can be eliminated.

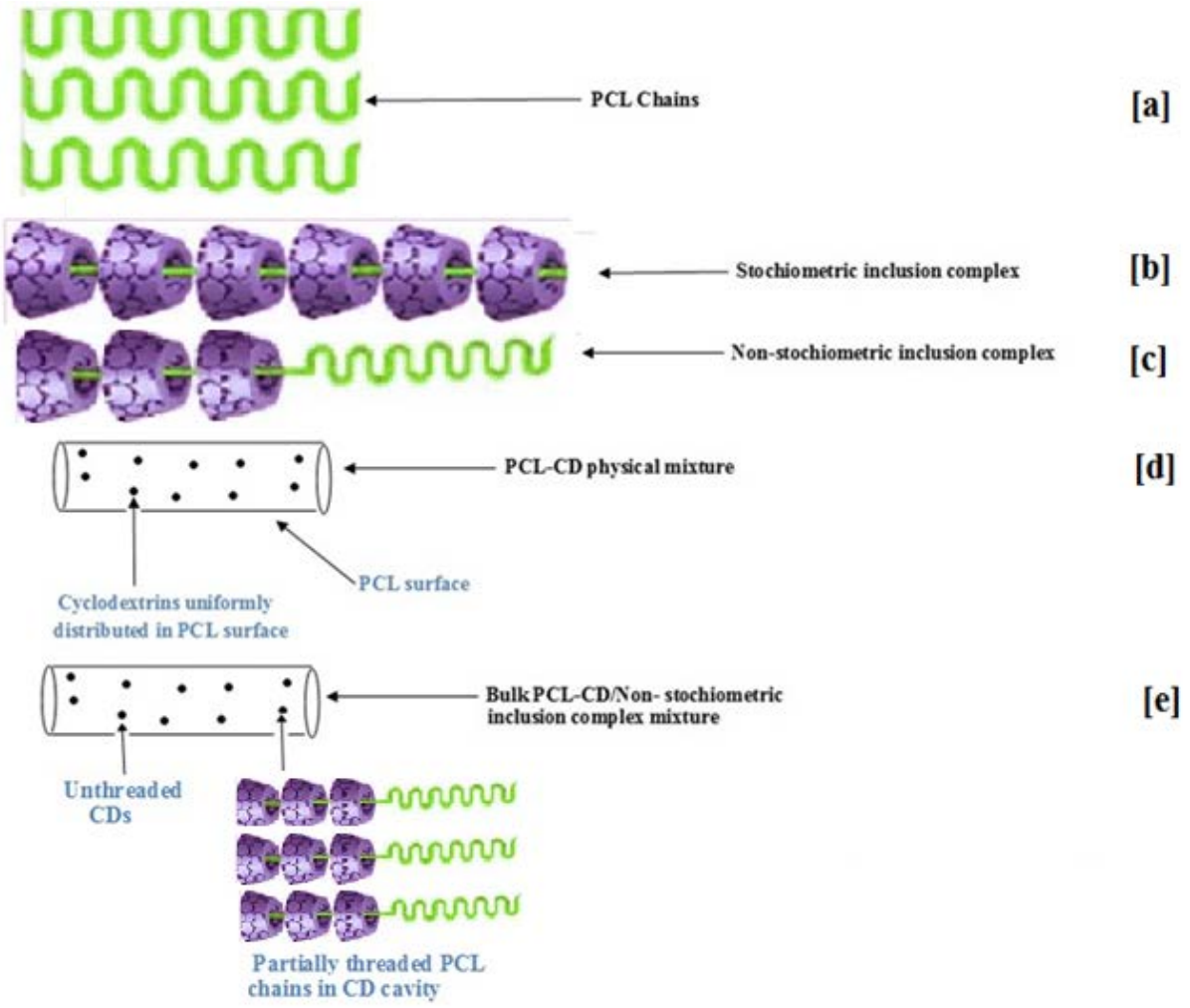

Figure 2.25: Suggested models of electrospun PCL-CD nanofibers. [a] PCL chains, [b].Stochiometric inclusion complex, [c]. Non-stochiometric inclusion complex, and [d] uniformly distributed CDs on PCL surface, [e]. Combinations of chains partially threaded in CD cavities and unthreaded PCL chains.

Furthermore, through TGA, initial mass loss was observed at 100° C, corresponding to moisture loss, which confirms the presence of CDs; as PCL is a highly hydrophobic material, and hence moisture loss is not expected. Stochiometric inclusion complexes do not elicit any thermal transitions corresponding to that of the included polymer. Since the DSC analyses indicated the presence of both melting and crystallization enthalpies for PCL, the absence of stochiometric inclusion complexes (b) is confirmed. Moreover, the mass of CDs added was insufficient for the formation of stochiometric inclusion complexes, which leaves only the possibilities [c], [d], and/or [e]. It is well known that CDs, as well as their ICs, including (n-s)-polymer-CD-ICs, can be efficient nucleants for the melt crystallization of PCL; hence, the DSC thermograms (Figures 2.12 and 2.13) by themselves cannot differentiate modes [c], [d], & [e].

Our XRD observations indicated at 10% loadings that for both CDs the diffractograms were mirror images of its constituents, i.e., CDs and PCL, indicating physical mixture of CDs and PCL; while at 40% CD loadings, diffractograms exhibited characteristic peaks at $2\Theta = 20°$ and $2\Theta = 7.8°$, for α- and γ-CD, respectively. These two peaks correspond to the formation of inclusion complexes, which indicate some of the CDs might have formed ICs with the PCL; however, the intensity of the peak corresponding to γ-CD-PCL-IC was much less intense compared with the PCL-α-CD-IC peak. Similar results were also observed through TGA analyses, in which at 15% CD loadings, three stage degradation was observed for both CDs. Through TGA & XRD analyses, presence of (n-s)-PCL-α-CD-IC alone (model [c]) can be discounted. Through further observation by TGA & XRD, we had concluded that α-CD

follows more closely model [e] and γ-CD model [d]. However, using either technique, determining an accurate ratio of free CD to that of CDs threaded by PCL chains is not feasible, especially, considering the fact that the molar ratios of CD:PCL, are rather low.

The above conclusion was further supported by the PhP absorption tests, which indicated, unlike those reported in the literature, but for different polymer the γ-CD functionalized nanofibers to be more efficient, compared to α-CD. Also, the maximum efficiency was observed at 40% γ-CD loading, which indicates that not all of the CDs would have formed IC with PCL. Because if this were the case, there would not be any PhP absorption. It should be noted that a similar trend was observed for the α-CDs, wherein, maximum absorption was observed at 40% CD loading, which indicates that CDs are substantially unthreaded, with a minor proportion threaded by PCLchains. Side-by-side comparison of the α- and γ-CD functionalized PCL nanofibers, however, it can be concluded that, γ-CD/PCL webs tend to follow model [d] with a minor proportion of model [e]; whereas, comparatively, α-CD/PCL webs have a higher proportion of model [e] structures.

Our water contact angle measurements were performed over multiple thin rectangular strips cut from various sections of the nanowebs, and a minimum of 10 samples were tested and their average reported (Figures 2.18 and 2.19). A low standard deviation indicates that there is no significant agglomeration of CDs, although, localized agglomeration cannot be completely discounted.

2.5 Conclusions:

Functionalized composite nanofibers containing PCL and CDs have been prepared for the first time using electrospinning of PCL/CD from a chloroform/DMF 6:4 mixture. Presence of CDs in the mats was verified using FTIR and TGA. Average fiber diameter of a neat PCL control web was found to be around 400 nm, while that of the composite web fibers was found to be more than 600 nm. Average fiber diameter tended to increase only slightly as the loading of CD was increased.

Addition of CD caused the crystallinity of the PCL composite to increase. The results from DSC showed that this increase in crystallinity greatly enhanced the crystallization temperature, indicating that the CDs cause crystal nucleation of PCL in the melt.

TGA observations indicate the degradation patterns of the α- and ɤ-CD functionalized composite fibers to be slightly different from each other, with a relatively greater number of α-CDs forming ICs with PCL. XRD analyses indicate the presence of PCL-CD-ICs as well as free CDs in the mats.

The surface wettability measurements of the CD functionalized nanofibers indicate significant reduction in WCA, even with additions of as small as 5% CD. The PhP absorption tests suggest that, γ-CD functionalized nanofibers absorbed PhP faster than did α-CD functionalized nanofibers at all CD loadings. This indicates γ-CD was more available in unthreaded form than was α-CD in their PCL nanowebs.

It would be desirable to study the absorption of simulated wound fluids containing malodorous compounds, for example butyric acid, in our PCL/CD nanowebs using gas chromatography. From our observations of PhP absorbance, we would expect that γ-CD functionalized nanofibers would perform better in such a study, compared to either α-CD functionalized or neat PCL nanofibers or films.

Acknowledgements:

Authors thank the Department of Textile Engineering, Chemistry and Science, College of Textiles, NC State University, Raleigh, NC. for partial funding of this research. GN would like to thank, Ms. Judy Elson, and Mrs. Birgit Andersen, for training him on the analytical instruments, and the data analyses used in this research.

References:

1. Bhardwaj N, Kundu SC. Electrospinning: a Fascinating Fiber Fabrication Technique. Biotechnol. Adv 2010; 28:325–347.

2. Pham QP, Sharma U, Mikos AG. Electrospinning of Polymeric Nanofibers for Tissue Engineering applications: a Review.Tissue Eng.2006; 12: 1197-1211.

3. Li D, Xia Y. Electrospinning of Nanofibers: Reinventing the Wheel? Adv. Mater.2004; 16:1151-1170.

4. Subbiah T, Bhat GS, Tock RW, Parameshwaran S, Ramkumar SS. Electrospinning of Nanofibers. J. Polym. Sci.2005; 96: 557–569.

5. Frenot A, Chronakis IS, Polymer Nanofibers Assembled by Electrospinning. Curr. Opin.Colloid Interface Sci. 2003; 64-75.

6. Liu D, Yuan X, Bhattacharya D. The Effects of Cellulose Nanowhiskers on Electrospun Poly(lactic acid) Nanofibers. J Mater Sci.2012; 47: 3159–3165.

7. Dror Y, Salalha W, Khalfin RL, Cohen R, Yarin AL, Zussman E. Single-Walled Carbon

Nanotubes Embedded in Oriented Polymeric Nanofibers by Electrospinning.Langmuir.2003; 19: 7012-7020.

8. Li L, Li J, Jiang J, Liu X, Luo L, Nan K.Electrospun Fibrous Scaffold of Hydroxyapatite/Poly (Epsilon-Caprolactone) for Bone Regeneration. J. Mater. Sci.: Mater.Med.2012; 23: 547–554.

9. Naebe M, Lin T, Wang X, Carbon Nanotubes Reinforced Electrospun Polymer Nanofibres,in Kumar, Ashok (eds), Nanofibers. InTech.2010, Rijeka, Croatia, pp.309-328.

10. Wan YQ, He JH, Yu JY. Carbon Nanotube-Reinforced Polyacrylonitrile Nanofibers by Vibration-Electrospinning. Polym. Int. 2007; 56: 1367–1370.

11. Villiers, A. Sur la Fermentation de la Fécule par l'action du Ferment Butyrique, Compt. Rend.1891; 112:536.

12. Loftsson, T, Duchéne, D. Cyclodextrins and their Pharmaceutical Applications.Int. J. Pharm. 2007; 329: 1−11.

13. Szejtli, J. Introduction and General Overview of Cyclodextrin Chemistry. Chem. Rev.1998; 98: 1743-1753.

14. Astray G, Gonzalez-Barreiro C, Mejuto JC, Rial-Otero R, Simal-Gandara J. A Review on the use of Cyclodextrins in Foods**.** Food Hydrocolloids. 2009; 23:1631-1640.

14a.Agarwal S, Chemistry, Chances and Limitations of the Radical Ring-Opening Polymerization of Cyclic Ketene Acetals for the Synthesis of Degradable Polyesters Poly. Chem.2010; 1:953-964.

15. Dong T, He Y, Zhu B, Shin KM, Inoue Y. Nucleation Mechanism of α-cyclodextrin-Enhanced Crystallization of some Semicrystalline Aliphatic Polymers. Macromolecules.2005; 38:7736-7744.

16. Dong T, Mori T, Pan P, Kai W, Zhu B, Inoue Y. Crystallization Behavior and Mechanical Properties of Poly (ε-caprolactone)/Cyclodextrin Biodegradable Composites. J. Polym. Sci.2009; 2351–2357.

17. Mark EJ. Polymer Data Handbook. Oxford University Press. 1999.

18. Cipitria A, Skelton A, Dargaville TR, Dalton PD, Hutmacher DW. Design, Fabrication and Characterization of PCL Electrospun Scaffolds – A Review.J. Mater. Chem.2011;

21:9381-9792.

19. Martins A, Pinho ED, Faria S, Pashkuleva I, Marques AP, Neves NM. Surface Modification of Electrospun Polycaprolactone Nanofiber Meshes by Plasma Treatment to Enhance Biological Performance. Small.2009; 5:1195–1206.

20. Pham QP, Sharma U, Mikos AG. Electrospun Poly(epsilon-caprolactone) Microfiber and Multilayer Nanofiber/Microfiber Scaffolds: Characterization of Scaffolds and Measurement of Cellular Infiltration. Biomacromolecules.2006; 7:2796–2805.

21. Venugopal J, Ma LL, Ramakrishna S. In vitro Study of Smooth Muscle Cells on Polycaprolactone and Collagen Nanofibrous Matrices.Cell Bio Int.2005; 29: 861–867.

22. Yoshimoto H, Shin YM, Terai H, Vacanti JP. A Biodegradable Nanofiber Scaffold by Electrospinning and its Potential for Bone Tissue Engineering. Biomaterials. 2003,24,2077–2082.

23. Mobarakeh LG, Prabhakaran MP, Morshed M, Nasr-Esfahani MH, Ramakrishna S. Electrospun Poly (ε-caprolactone)/Gelatin Nanofibrous Scaffolds for Nerve Tissue Engineering.Biomaterials.2008; 29:4532-4539.
24. Moura LIF, Dias AMA, Carvalho E, De Sousa HC. Recent Advances on the Development of Wound Dressings for Diabetic Foot Ulcer Treatment-A Review. Acta Biomater.2013;9:7093-7114.

25. Haslauer CA, Moghe AK, Osborne JA, Gupta BS, Loboa EG. Collagen-PCL Sheath-Core Bicomponent Electrospun Scaffolds Increase Osteogenic Differentiation and Calcium Accretion of Human Adipose-derived Stem cells.J. Biomater. Sci. Polym. Ed.2011; 22:1695-1712.

26. Moghe AK, Gupta BS. Co-axial electrospinning for nanofiber structures: Preparation and applications. Polym. Rev.2014; 48:353-377.

27. Moghe AK, Hufenus R, Hudson SM, Gupta BS. Effect of The Addition of a Fugitive Salt on Electrospinnability of Poly(ε-caprolactone). Polymer.2009;50:3311-3318.

28. Whang HS, Hunt MA, Wrench N, Hockney JE, Farin CE, Tonelli AE. Nonoxynol-9-α-Cyclodextrin Inclusion Compound and its Application for the Controlled Release of Nonoxynol-9 Spermicide. J. Polym. Sci.2007; 106:4104-4109.

29. Szente L, Szejtli J. Cyclodextrins as Food Ingredients. Trends Food Sci. Technol.2004; 15:137-142.

30. Tonelli AE. Restructuring Polymers via Nanoconfinement and Subsequent Release. Beilstein J. Org. Chem.2012; 1318-1332.

31. Uyar T, Havelund R, Nur Y, Balan A, Hacaloglu, J, Toppare F, Kingshott P. Cyclodextrin Functionalized Poly (methyl methacrylate) (PMMA) Electrospun Nanofibers for Organic Vapors Waste Treatment. J. Membr.Sci.2010; 1, 409-417.

32. Uyar T, Havelund R, Hacaloglu J, Besenbacher F, Kingshott P. Functional Electrospun Polystyrene Nanofibers Incorporating Alpha, Beta and Gamma Cyclodextrins: Comparison of Molecular Filter Performance. ACS Nano.2010; 4:5121-5130.

33. Uyar T, Hacaloglu J, Besenbacher F. Electrospun Polyethylene Oxide (PEO) Nanofibers containing Cyclodextrin Inclusion Complex. J. Nanosci. Nanotechnol. 2011; 11:3949-3958.

34. Uyar T, Havelund R, Nur Y, Hacaloglu J, Besenbacher F, Kingshott P. Molecular Filters Based on Cyclodextrin Functionalized Electrospun Fibers. J.Membr.Sci.2009; 332:129-137.

35. Uyar T, Besenbacher F. Electrospinning of Cyclodextrin Functionalized Polyethylene oxide (PEO) nanofibers. Eur. Polym. J.2009; 45:1032-1037.

36. Rusa CC, Fox J, Tonelli AE. Competitive Formation of Polymer−Cyclodextrin Inclusion Compounds.Macromolecules.2003;36:2742-2747.

37. Bordes C, Freville V, Ruffin E, Marote P, Gauvrit JY, Brianc S¸ Lantéria P. Determination of Poly(epsilon-caprolactone) Solubility Parameters: Application to Solvent Substitution in a Microencapsulation Process.Int. J. Pharm.2010; 383;236–243.

38. Liu Y, He JH, Yu.J, Zeng.H. Controlling Numbers and Sizes of Beads in Electrospun Nanofibers. Polym. Int.2008;57:632–636.

39. Schurren LV, Schoenmaker BD, Kalaoglu OI, De Clerk K. An Alternative Solvent System for the Steady State Electrospinning of Polycaprolactone. Eur. Polym. J.2011; 47: 1256-1263.

40. Ong C, Price FJ. Blends of poly(ϵ-Caprolactone) with Poly(vinyl chloride). I. Morphology. J. Polym. Sci., Polym. Symp. 1978; 63:45.

41.Williamson BR, Krishnaswamy R, Tonelli AE. Physical Properties of Poly(ε-caprolactone) Coalesced from its α-Cyclodextrin Inclusion Compound.Polymer.2011;52:

4517-4527.

42. Shin KM, Dong T, He Y, Inoue Y. Morphological Change of Poly (ε-caprolactone) with a Wide Range of Molecular Weight via Formation of Inclusion Complex with α-Cyclodextrin. J. Polym. Sci., Part B: Polym. Phys.2005; 43, 1433– 1440.

43. Huang L, Allen E, Tonelli AE. Study of the Inclusion Compounds Formed Between α-Cyclodextrin and High Molecular Weight Poly(ethylene oxide) and Poly(ϵ-caprolactone) Polymer.1998; 39:4857-4865.

44. Luo H, Liu Y, Yu Z, Zhang S, Li B. Novel Biodegradable Shape Memory Material \ Based on Partial Inclusion Complex Formation between α-Cyclodextrin and Poly(ϵ-caprolactone).Biomacromolecules.2008; 9:2573-2577.

45. Wang S, Ma D, Huang Y, Yao C, Xie A, Shen Y. Synthesis and Characterization of PCL/Calcined Bone Composites. J. Chil. Chem. Soc.2013; 58:1902-1906.

46. Hunt MA, Jung D-W, Shamsheer M, Uyar T, Tonelli AE. Polystyrenes in Channels. Polymer.2004; 45:1345-1347.

47. Uyar T, Gracz HS, Rusa M, Shin ID, El-Shafei A, Tonelli AE. Polymerization of Styrene in Gamma-Cyclodextrin Channels: Lightly Rotaxanated Polystyrenes with Altered Stereosequences. Polymer.2006; 47:6948-6955.

Chapter 3: Efficient Wound Odor Removal by β-Cyclodextrin Functionalized Poly (ε-caprolactone) nanofibers.

Abstract:

Polymer-cyclodextrin (CD) composite nanofibers, by virtue of hollow cavities and abundant hydroxyl groups present in CDs, have tremendous potential in variety of biomedical applications. However, in most cases, especially in aliphatic polyesters, polymer chains thread readily into CD cavities, therefore its potential has not yet been fully realized. Herein, we report the formation of poly (ε-caprolactone) (PCL)/β-CD functional nanofibers by electrospinning their mixture from chloroform/N, N-dimethylformamide (60:40). The fiber diameter of the neat PCL and β-CD functionalized fibers were measured from the images obtained from scanning electron microscope, and were found to be about 500 nm. As expected, due to incompatibility between the PCL and β-CD, β-CDs had aggregated on PCL surface. The efficiency of wound odor absorbance by these composite fibers was studied using simulated wound odor solution, consisting of butyric and propionic acids in ethanol. Immersion tests indicated, even in adversarial test condition, the nanofibers containing β-CDs were very efficient in masking the odor. These results were further confirmed by thermogravimetric analyses by unique degradation pattern, confirming the masking capability of the β-CD functionalized PCL nanofibers. These results indicate, the PCL/ β-CD nano-composite, by virtue of having its cavity free, could be an ideal substrate for removing wound odor through IC formation, while providing an ideal environment for the wound to heal. These results can serve as guidelines for tailoring polymer-CD nanostructures for

specific applications in wound odor absorbance, surface grafting of chemical moieties, vehicles for drug delivery.

Keywords: Polycaprolactone; β-cyclodextrin; Wound healing; Wound odor absorbance; wettability; XPS; TGA; XRD.

3.1. Introduction:

Although the electrospinning process for producing nanofibers in the range of 5-500 nm has been known to mankind for about a century, the last two decades has seen an explosion in utilizing this process to make nanofibers for innovative applications in filtration, wound dressing/healing, scaffolds, and so forth [1-5]. The advantage of using electrospinning, apart from being a simple method for fabrication, include its ability to form nano-sized fibers in various shapes, such as porous, hollow, and core-sheath structures [6-9]. There are two techniques commonly utilized to prepare porous nanofibers; the first technique is by choosing solvents with high vapor pressure, which evaporate faster during electrospinning resulting in the formation of porous nanofibers, and the second technique is to deliberately add salt to the polymer solution and leach the latter out once the fibers are dried; this results in the formation of porous nanofibers [10-11]. Because of their enhanced surface to volume ratios, the porous and hollow fibers are also highly desired for enhanced filtration applications, compared to the regular, cylindrical nanofibers.

Wound healing is a complicated process during which our body initially forms a fibrin plug to establish homeostasis, which is aided by the secretion of several growth factors. The

process of wound healing is complete when new extra cellular matrix (ECM) is formed, replacing the old ECM [12-14]. The wound healing process is, however, hindered in some patients, especially those suffering from diabetes or metastasized cancer, resulting in chronic wounds that are normally non-healing [15]. Other factors that affect wound healing include: the pH of wounded tissue, oxygen permeability, moisture of the wound environment, and non-adherence of the dressing to the wound [16-19]. When the wound does not heal properly and quickly, foul odors emanate from the exudates. The malodor from the wound is mainly due to the liberation of volatile fatty acids such as acetic acid, butyric acid, propionic acid, valeric acid, and amines, such as putrescine and cadaverine, which are produced by aerobic or anaerobic action of various bacteria on serum protein [24]. The composition of the wound, however, have been found to vary depending on the type/location of the wound, age and general health of the patient, and many other factors. Commonly used wound dressings include hydro-fibers, hydrocolloids, hydrogels, foams and films [20-23]. Apart from topical agents such as metronidazole, activated charcoal based dressings are widely used to absorb the malodor emanating from chronic non-healing wounds. But these dressings lose their efficiency when they come in contact with exudates with high moisture content [25]. Hence, there is a definite need for novel wound absorbent material which can absorb the volatile foul smelling compounds when in contact with moist exudates, and which simultaneously retain its structure, thereby necessitating infrequent changing of dressing.

Cyclodextrins (CDs) belong to a group of cyclic α-1, 4-linked oligosaccharides. Most widely used CDs are α, β-, and γ-CD, which have 6, 7, and 8 glucopyranose units

respectively, and their chemical structure is shown below in Figure 3.1. CDs have a truncated conical shape with a hollow interior that enables CDs to form inclusion complexes (ICs) with guest molecules. The size of interior cavities depends on the number of glucose units and are found to have diameters of 5.7, 7.8 and 9.5 Å, for α-, β-, and ɤ-CDs respectively [27]. Depending on the nature of guest molecules, cyclodextrins-inclusion complex (CD-IC) formation results in either of two crystalline forms: cage and columnar structures [28]. The cage structures are observed, when ICs are formed with small molecules as guests, and columnar structures are observed when long molecule like polymers or other small molecules such as long chain carboxylic acids like valeric acid are used as guests [29-31]. CDs are used

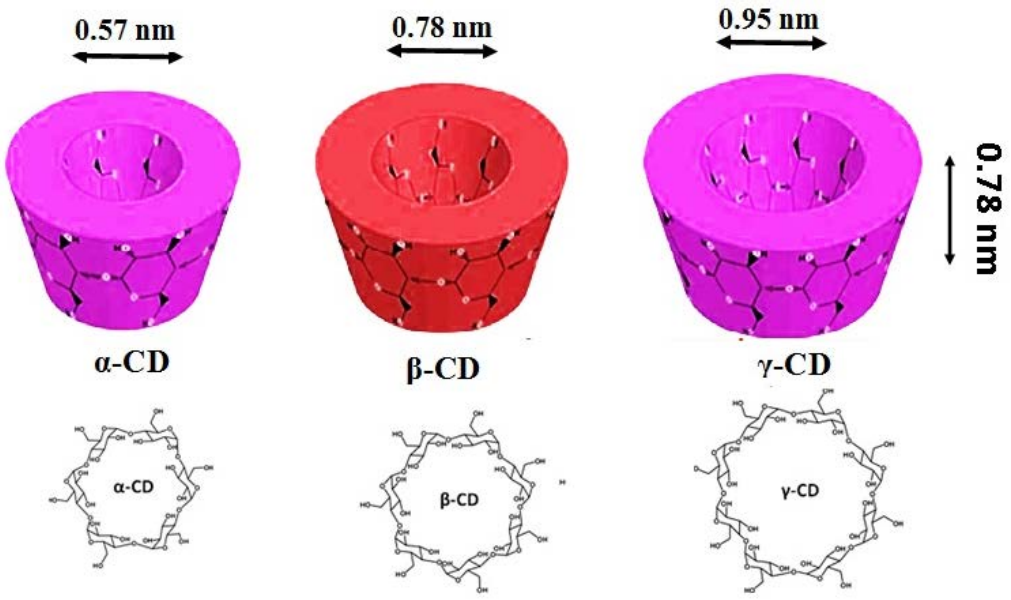

Figure 3.1: Chemical structure of cyclodextrins (CDs).

in a variety of applications including, pharmaceutical, food, packaging, cosmetics and in physically nanostructuring polymers [32-34]. A CD containing hydrocolloid dressing has been marketed under the trade name exuderm® odorshield® (Medline), and has been reported to be more effective than activated charcoal based dressings [25].

Recently, there has been growing interest in using cyclodextrin functionalized nanofibers for filtration, drug delivery, and food packaging. In a previous report, we had reported the successful formation of functional PCL nanofibers containing α- and γ-CDs [35]. It was observed that, α-CD, and to some extent γ-CD, had formed inclusion complex with the PCL; therefore its inclusion complex forming capability with small molecule guests are expected to be somewhat diminished, which was evident with the molecular encapsulation study of phenolphthalein as guest molecule. Although, α- and γ-CD have been known to form inclusion complex with PCL [36-38], the β-CDs, however, are not expected to form IC with PCL due to the size mis-match between the two [39-40]. This could then provide an opportunity to absorb small molecules.

In this report, we report the formation and characterization of functionalized PCL/β-CD nanofibers, and their subsequent capability to absorb wound odor components such as butyric and propionic acid determined by X-ray photoelectron spectroscopy (XPS). As mentioned before, butyric and propionic acid are only two of the many components typically found in wound exudate, and these experiments are proof of concept to compare the efficiency of absorption with respect to CD loadings. Also, since CDs are water soluble, instead of water, these tests were performed by diluting the acids in ethanol. Recently, Uyar et al reported the

crosslinking of electrospun PET/ β-CD nanofibers with citric acid, which is typically obtained from a renewable source [41]. With these advancements in cross-linked polymer/CD structures, it should be possible that CD functionalized nanofibers can be used for not only air and water filtration applications, but also biomedical applications such as wound odor removal.

3. 2. Materials and methods:

Poly (ε- caprolactone) with a molecular weight of 60,000 to 80,000 (M*n*), chloroform (99.5%), and N,N-dimethyl formamide (anhydrous 99.8%), butyric acid, propionic acid, ethyl alcohol (99%+ purity), were obtained from Sigma-Aldrich, St. Louis, Missouri, USA. β-CD was obtained as a gift from Wacker Chemie, Michigan, USA.

3.2.1 Electrospinning solution preparation:

PCL/β-CD solutions were prepared in accordance with our previous work, where PCL/α-CD and PCL/γ-CD solutions were prepared [35]. Briefly, PCL and β-CD solutions were prepared by dissolving them separately in chloroform and DMF, respectively, at 70º C on a hot plate under stirring. The two solutions were then mixed together to form combined PCL/β-CD solution/suspension in chloroform/DMF. Once the dissolution is complete, the solutions were allowed to stir overnight at room temperature. PCL concentration was set at 12% (m/v), and CD concentration was varied from 0-60%, with respect to that of PCL.

3.2.2 PCL/β-CD composite preparation:

PCL/β-CD solutions were electrospun according to the protocol we had used in our previous report [35]. Briefly, polymer solutions were held in a 10 cc syringe, to which a blunted needle (22G) was attached. A high precision pump (New Era Pump Systems, Farmingdale, NY) was used to deliver fluid at a rate of 1 mL/hr. In our previous report, we had used a feed rate of 0.5 mL/hr, which was observed to be unsuitable for PCL/β-CD solutions. The potential difference (15 kV) between the polymer solution and the collector was applied by Gamma High Voltage Research instrument (Ormond Beach, FL). A rotating roller (diameter 1.5 in), made of stainless steel was used as collector. The latter was rotated at 280 rpm (linear velocity of 28 m/min), and was placed at 30 cm from the tip of the needle.

3.2.3 PCL/β-CD nanowebs characterization:

The electrospun mats were characterized using Fourier Transform infrared spectroscope (FTIR), thermogravimetric analyzer (TGA), scanning electron microscope (SEM), gas chromatograph, X-ray photoelectron spectroscope, and wide-angle x-ray diffraction (WAXD). Infrared spectral studies were conducted using a Nicolet 470 FTIR infrared spectrophotometer in the frequency range of 4000-400 cm^{-1} with a resolution of 4 cm^{-1} and, 64 scans were collected for each sample. The degradation patterns of the nanowebs were observed through a TA Q500 v6.7 thermogravimetric analyzer. The samples were heated from 25 ° to 500 ºC at the rate of 20 ºC under nitrogen atmosphere, and the data was analyzed using TA universal analysis software. The fiber morphology was studied by a Phenom world G1 model scanning electron microscope at an acceleration voltage of 10 kV.

Since the samples are non-conductive, prior to SEM analyses, the samples were coated with gold, using a Polaron SC7620 Mini Sputter Coater (Quorum technologies). SEM images were obtained at various resolutions, and the fiber diameters were calculated using ImageJ software. Diameters of a minimum of 100 fibers were measured, and their average fiber diameters are reported. WAXD analyses were performed on electrospun neat PCL, PCL/β-CD composites, and powdered samples of CD using a Philips type-F X-ray diffractometer with a Ni-filtered Cu Kα radiation source (λ = 1.54 Å). While electrospun webs were attached to the metal stub and taped using a double sided carbon tape, uniform surface of β-CD powder was obtained by holding them in a glass cup, and patting them gently. The applied voltage and current used were 35 kV and 25 mA, respectively, and the diffraction intensities were measured from 2θ of 5 to 40°, at the rate of 0.05°/second. X-ray photoelectron spectroscopy experiment was performed using SPECS Flex mode XPS instrument with an MgKα anode monochromator (1254 ev) as a source with X-ray energy of 10 kV, and hemispherical analyzer PHOIBIS 150. The takeoff angle was normal to the surface with an X-ray incidence angle of ~30°, and an x-ray source to analyzer angle of ~60°. Base pressure in the analysis chamber was of the order of 10^{-10} mbar range. Energy calibration was established by referencing to adventitious Carbon (C1s line at 285.0 ev binding energy). Once the wide spectra were collected, and the elemental composition established, an in-depth higher resolution spectra was obtained for speciation analyses (C1s and O1s, in this case). CASA XPS software was used for data analyses. Gas chromatography experiments were performed using Agilent 6890N GC with a 7693A auto sampler.

3.3. Wound odor absorption test:

Simulated wound fluid was prepared by dissolving 0.58 grams each of butyric acid and propionic acid in 55 ml ethanol to prepare 2.1% solution. The prepared wound odor solution was further separated into 9 equal parts, and placed in separate vials. Small samples of nanoweb weighing about 0.2 g were cut from the mat, and placed in the vials. At designated time intervals, the samples were then taken out, and dried in a vacuum oven to remove any surface adsorbed chemical. The samples were then analyzed using XPS to determine the presence and concentration of butyric and propionic acid (in the form of carboxylic acids) and corresponding changes in the composition before and after the absorption tests. The degradation pattern of samples before and after immersion was further observed through TGA.

3.4. Results:

3.4.1 SEM morphology:

The composition of PCL/β-CD solutions and the key fiber statistics obtained from the resultant electrospun nanofibers are listed in Table.1. The representative scanning electron microscope images of electrospun neat PCL and β-CD functionalized PCL nanofibers (all at the same magnification and length scale) containing different amounts of β-CD, and the fiber diameter distributions are shown in Figures 3.2 & 3.3, respectively. The diameters of the β-CD functionalized nanofibers are only slightly greater compared to that of the neat PCL mat. Moreover, the fiber diameter distribution indicates that β-CD agglomeration possibly took place, resulting in statistical outliers increasing with the CD loading. Although solution

properties such as conductivity and viscosity are expected to improve with the increase in β-CD loading, unfortunately, agglomeration of CDs increased, especially at higher loadings. This is probably due to the turbidity of the solution which arises due to the precipitation of CDs from CFM/DMF solution mixture. It is important to note that CDs are highly insoluble in CFM, and hence should tend to precipitate.

Table 3.1: The composition of PCL/β-CD solutions, and key statistics of resulting electrospun PCL and PCL/β-CD nanofibers.

Solution	% β-CD* (w/w)	Average fiber diameter (nm)	Median (nm)	First quartile (nm)	Third Quartile (nm)
Neat PCL	-	397±158	368	265	471
PCL/10-β-CD	10	521±200	494	368	643
PCL/20—β-CD	20	500±218	478	341	625
PCL/30—β-CD	30	570±265	493	411	682
PCL/40-β-CD	40	559±260	499	367	656
PCL/50—β-CD	50	566±314	500	411	657

* % β-CD , with respect to PCL. PCL concentration used was 12% (m/v).

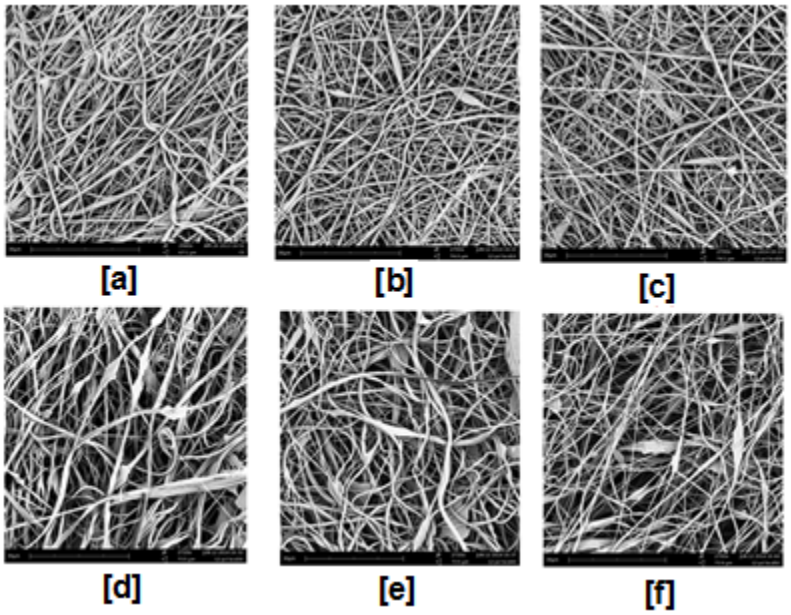

Figure 3.2: SEM images of electrospun nanofibers of (a) neat PCL, (b) PCL/10%β-CD, (c) PCL/20%β-CD, (d) PCL/30%β-CD, (e) PCL/40%β-CD, (f) PCL/50%β-CD.

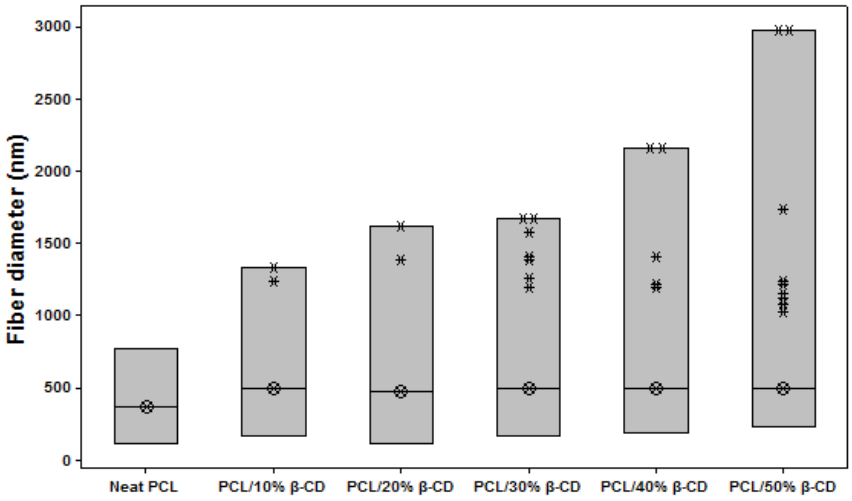

Figure 3.3: Fiber diameter distributions of electrospun neat PCL and PCL/β-CD nanofibers.

3.4.2 FTIR analysis:

FTIR spectroscopy was utilized to observe the corresponding bands of the individual components, *i.e.*, PCL and β-CD, and observe if there was any slight peak shifts which corresponded to the formation of IC. The FTIR spectra of pure β-CD, electrospun PCL nanofibers, PCL/20% β-CD, and PCL/40% β-CD are shown in Figure 3.4. In the FTIR spectrum of β-CD powder, characteristic peaks were observed at 1029 cm^{-1} due to C-O bending vibration, at 1157 cm^{-1} due to C-O stretching, and a broad absorption peak at 3347 cm^{-1} due to O-H bending vibration [47]. In the FTIR spectra of electrospun PCL nanofibers, characteristic peaks were observed at 2944 cm^{-1} and 2887 cm^{-1} corresponding to asymmetric and symmetric CH_2 stretching.

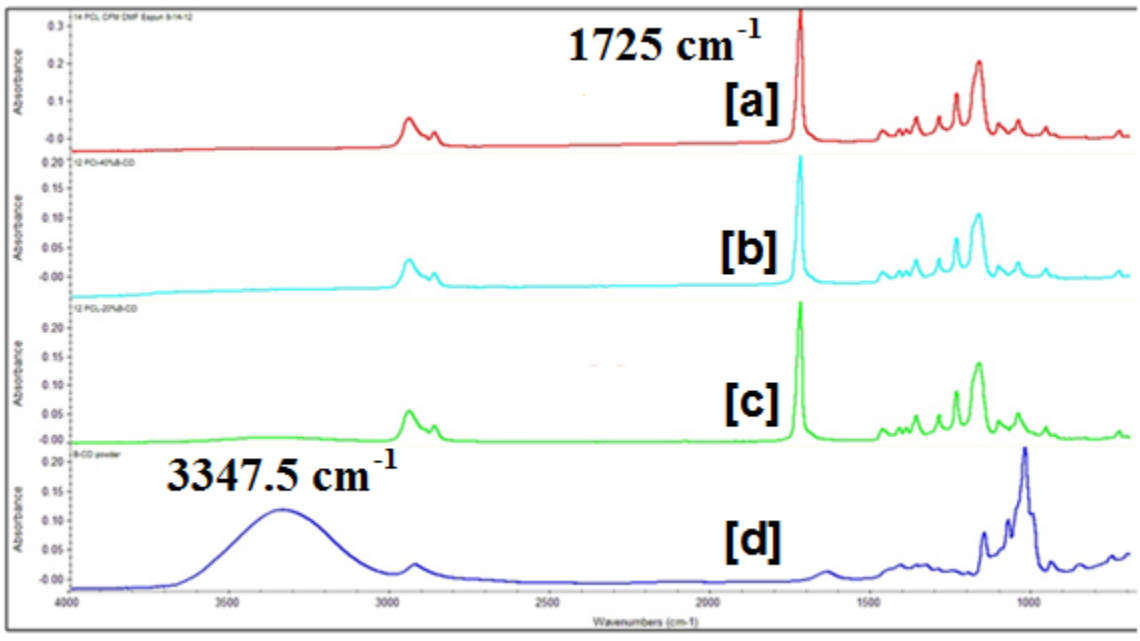

Figure 3.4: FTIR spectra of electrospun (a) PCL fibers, (b) PCL/40%β-CD, (c) PCL/20% β-CD and (d) neat β-CD powder.

The carbonyl peak, which was predominant, was observed at 1727 cm^{-1}, and another dominant peak at 1168 cm^{-1} was observed that corresponds to symmetric C-O-C stretching. Apart from these dominant peaks, several minor peaks were observed that can be attributed to PCL. However, in the electrospun PCL/CD mats, mostly dominant peaks of PCL were visible; due to overlapping between the peaks of CDs and PCL, most of the peaks that are attributed to CDs could not be identified, except for slight halo like peak at 3347 cm^{-1}. Since the ATR-FTIR typically penetrates deep into the bulk, most nanoscale properties or presence of bonds on the surface typically become invisible [46]. The presence of O-H peak at 3347 cm-1 indicates, not only the presence of CDs but also that CDs are mostly present in the surface. Accordingly, with FTIR, apart from detecting slightly the O-H peak, it is difficult to confirm or exclude the presence of CD. To overcome this, XPS was used.

3.4.3 WAXD analysis:

The XRD patterns of the pure β-CD, electrospun PCL, and functionalized PCL/ β-CD nanofibers are shown in Figure 3.5. XRD spectra of β-CD indicate series of peaks, especially between 2Θ of 17 to 34°, confirming the amorphous nature of native β-CD. PCL, being a semi crystalline material with orthorhombic crystal structure, exhibits two distinct peaks at 2Θ= 22° and 24° that corresponds to (110) and (200) lattice structures, respectively. In the case of functionalized fibers, it is clearly evident that the characteristic peaks of PCL at 2Θ= 24° has broadened, and the intensity of peak at 2Θ= 22° has decreased significantly and shifted slightly to its right. Also, in general, the visibility of the β-CD peaks diminished, and

the absence of a crystalline peak at 2Θ= 18 and 19°, expected of ICs, indicates that PCL and β-CD have not formed ICs [42a].

In a physical mixture, however, no additional peaks are expected and the peaks are expected to resemble individual components, and their intensities depending on the ratio of its components. When any interaction occurs between components, however, a decrease in peak intensity and an increase in peak widening is expected to be typically observed [42b]. Although, still a hypothesis, such results observed in our functionalized samples points out that there is some interaction between PCL and β-CD occurred.

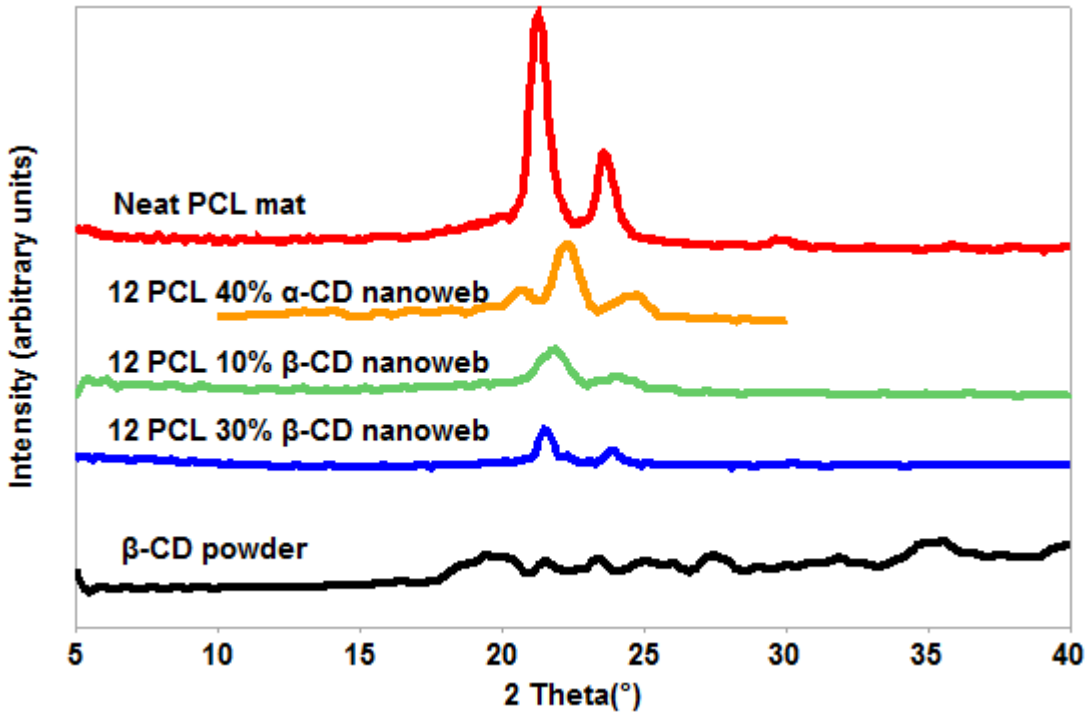

Figure 3.5: WAXD analysis of (a) pure β-CD, electrospun nanofibers of (b) neat PCL, (c) PCL/10% β-CD, (d) PCL/30% β-CD.

Formation of IC can be discarded, since corresponding IC peaks were not observed. Interestingly, different behavior was observed in our α-CD functionalized PCL nanofibers, for example. It should, however, be noted that, β-CD functionalized PCL nanofibers were electrospun at a higher feed rate (1 ml/hr compared to 0.5 ml/hr for α-CD functionalized nanofibers), which might have prevented the formation of crystal structure.

3.4.4 Thermogravimetric analysis:

TGA thermograms of neat PCL, PCL/10% β-CD, PCL/30% β-CD, and PCL/50% β-CD, obtained from 25 to 600 °C scans, and the magnified thermogram from 25 to 150 °C are shown in Figures 3.6 & 3.7, respectively. Thermogram of PCL nanofibers indicate there is no weight loss, and the degradation starts at about 370 °C and significant weight loss is observed above 400 °C. In the case of functionalized PCL nanofibers, three step degradation pattern was observed: firstly, from about 50 to 125 °C (Figure 3.7), dehydration of the nanowebs took place which indicates the presence of CDs [48a]. This is followed by degradation of CDs from 320 to about 370 °C. Beyond this, the degradation of PCL was observed. It is quite obvious that, with the addition of CDs, improvement in thermal stability is not observed, which is typically found for ICs [48b]. TGA results complement the FTIR findings about the presence of CDs, and XRD analyses about the presence of physical mixture in the fibers, rather than the ICs.

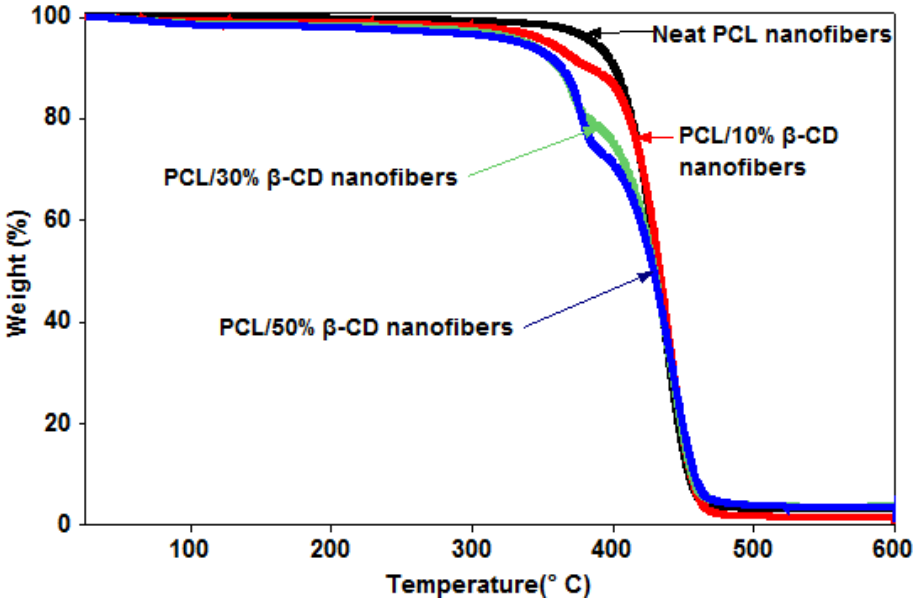

Figure 3.6: TGA thermogram of neat PCL and electrospun PCL nanofibers from 25 to 600° C.

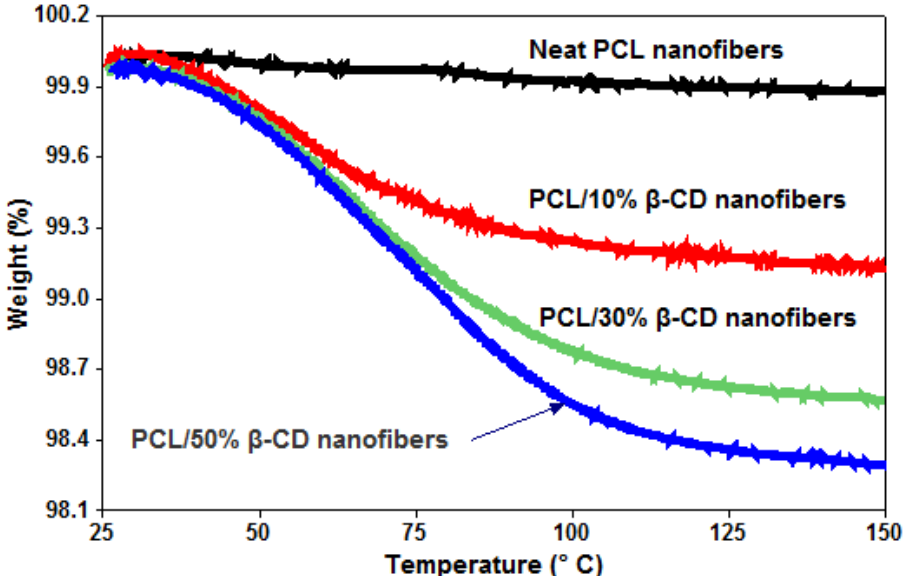

Figure 3.7: TGA thermogram of neat PCL and electrospun functionalized nanofibers from 25 to 600 °C.

3.5. Wound odor absorption:

3.5.2 X-ray Photoelectron Spectroscopy (XPS):

XPS measurements were carried out to characterize the presence of β-CDs on the PCL surface as well as to determine the uptake of butyric and propionic acids by the neat PCL and β-CD functionalized PCL fibers. As mentioned before, FTIR analysis was insufficient to characterize the presence of CDs in the fibers. Wide spectra of XPS of PCL and β-CD functionalized nanofibers exhibit the presence of C1s and O1s as elements, and their composition is given in Table.2. As expected, with the addition of β-CDs, the % content of oxygen increased considerably (17.5% for neat PCL to 24% for 20% β-CD functionalized PCL nanofibers). Also, % increase of oxygen was observed to be proportional to the % content of β-CD (24% for 20% β-CD and 27% for 40% β-CD).

Table 3.2: Elemental composition of PCL and β-CD functionalized PCL nanofibers, and corresponding components of O1s spectra.

Sample	Total carbon content %	Total oxygen content %
Neat PCL	82.47	17.53
PCL/20% β-CD	76.00	24.00
PCL/40% β-CD	73.02	26.98

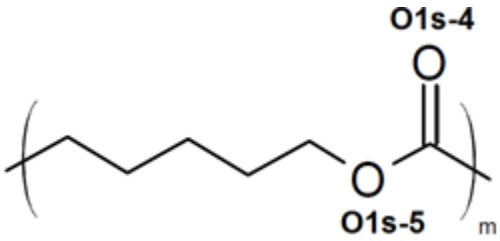

Since there were significant overlaps in the high resolution C1s spectra, O1s spectra, instead was chosen for further wound odor analyses. High resolution O1s spectra of the neat PCL, 20%, and 40% β-CD functionalized nanofibers are shown in Figure 3.8. O1s spectra of the neat PCL nanofibers indicate, two distinct peaks at ~ 531.7 and 533.4 ev, corresponding to C=O* and C-O* of the PCL, and their ratio was observed to be 55.47 and 44.43%, respectively. In the case of β-CD functional nanofibers, two new distinct peaks at ~533.15 and 535.2 ev were observed that can be attributed to the hydroxyl groups present in CDs (C-O*H) and to the water that is adsorbed both within the cavity as well as those bound on the external hydroxyl groups of the CDs.

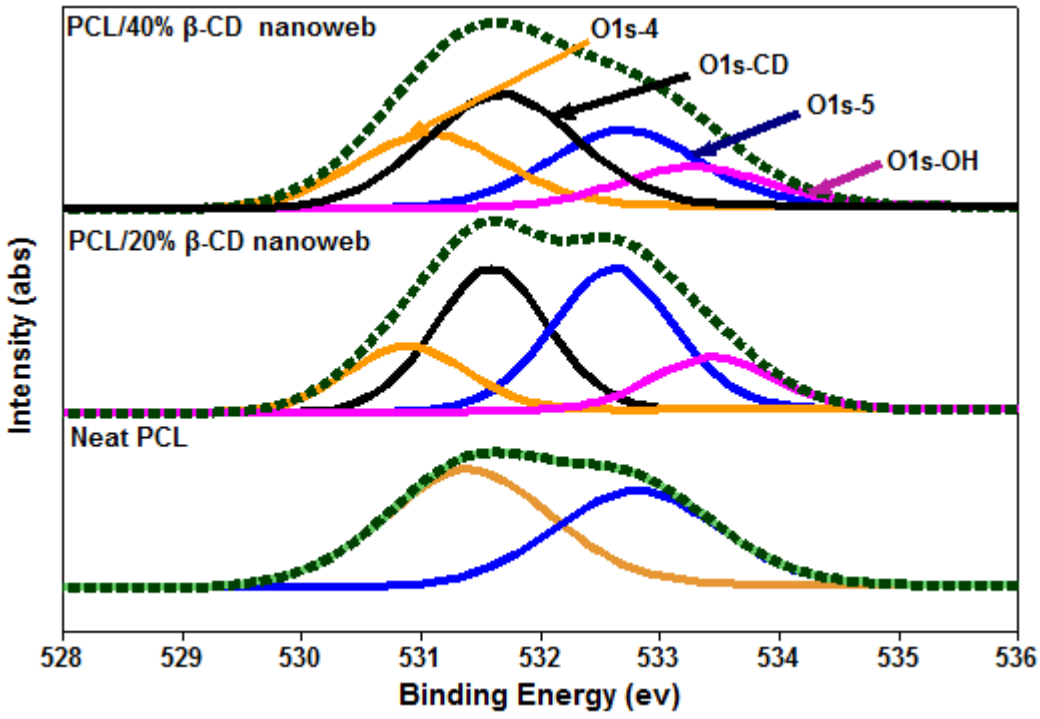

Figure 3.8: High resolution O1s spectra of PCL and β-CD functionalized PCL nanofibers.

As expected, the % content of hydroxyl groups in the functionalized nanofibers was proportional to the β-CD content (OH for 40% > OH for 20%). However, the adsorbed water content was observed to be similar for both the functionalized nanofibers (~13%). It is interesting to note that this content is far higher than those reported in the literature [43]. With the addition of CDs, decrease in the content of O1s-4 and O1s-5 was observed, and this phenomenon can simply be attributed to the dilution effects. The presence of two new peaks along with their high content indicates that most of the β-CDs are present on the surface, and hence should possess excellent encapsulation capabilities.

After immersion tests, to determine the efficiency of the nanofibers in absorbing foul odor acids, XPS measurements were carried out, and their O1s spectra obtained are shown in Figure 3.9.

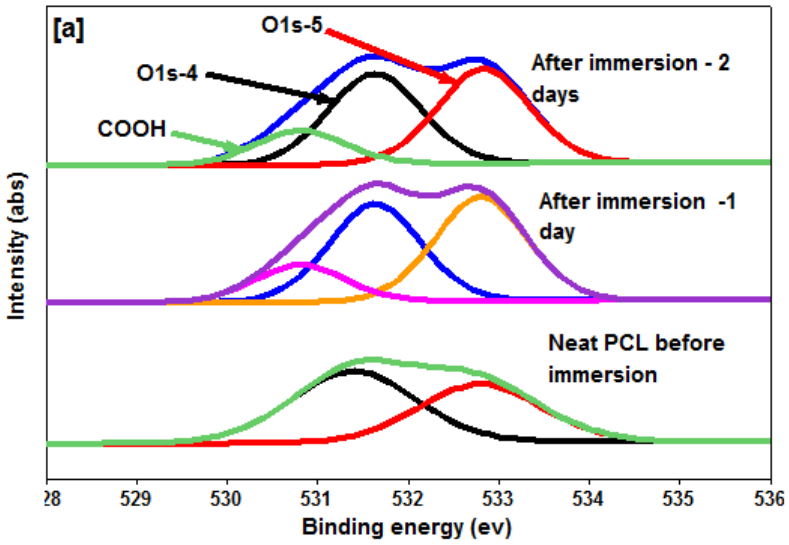

Figure 3.9: High resolution O1s spectra of Neat PCL nanofibers before and after immersion tests.

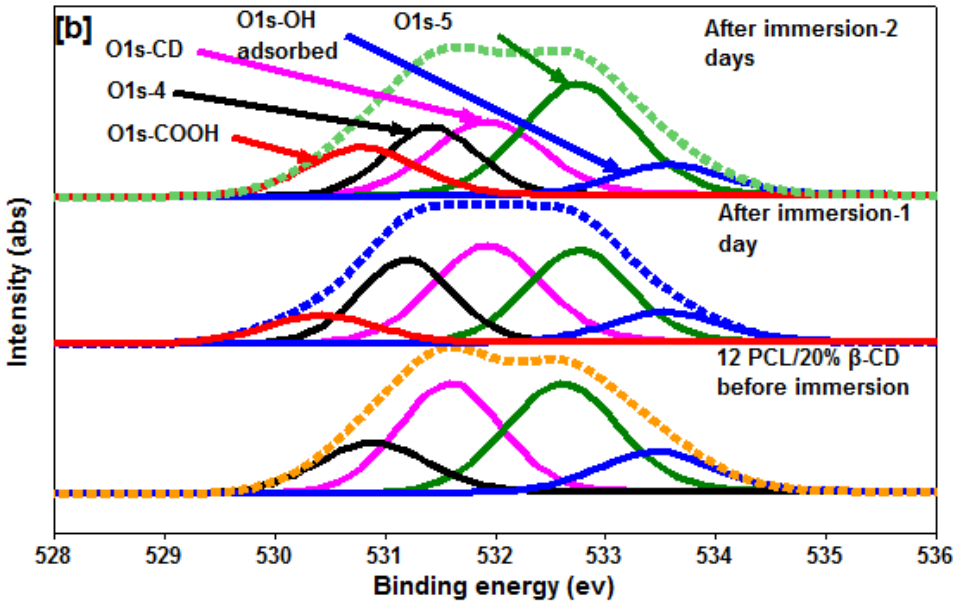

Figure 3.9b: High resolution O1s spectra of PCL/20% β-CD nanofibers before and after immersion tests.

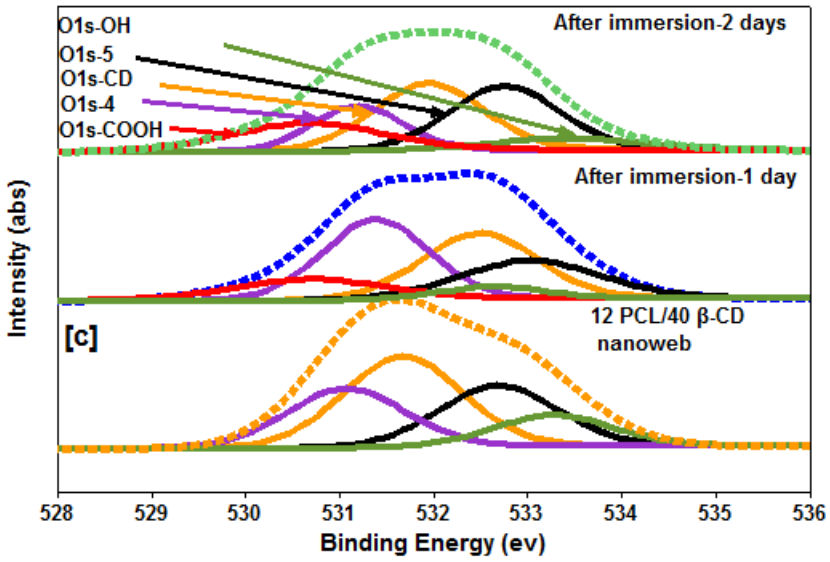

Figure 3.9c: High resolution O1s spectra of PCL/40% β-CD nanofibers before and after immersion tests.

Interestingly, in the case of PCL/20% β-CD and PCL/40% β-CD nanowebs, content of the carboxylic acids was estimated to be only about 10% and 15%, respectively, which is lower than that for neat PCL, especially the 20% β-CD nanowebs. It was also observed that in the case of β-CD functionalized nanofibers, especially for 40% β-CD nanofibers, the absorbed water content decreased sharply, indicating inclusion formation with butyric and propionic acids. After 2 days of immersion, the carboxylic content absorbed by neat PCL nanofibers still remained at about 15%, while those containing β-CDs had increased to 15 and 18% for 20 and 40% β-CD, respectively. A slight decrease in water content was observed in both functional nanofibers, but nevertheless, some water content was still observed, indicating that more room was available for the absorption of foul odors by these functionalized nanofibers.

Two points needs to be made here: firstly, the acidic environment typically retards the inclusion formation and, secondly, one of the key driving mechanisms for successful IC formation is the expulsion of high enthalpy water molecules that are present inside the CD cavity [45]. In our case, we had used ethanol as a solvent in which the butyric acid and propionic acids were dissolved, and possibly, therefore, the high enthalpy water molecules were not displaced efficiently, coupled with the fact that the acidic environment used had further decreased the efficiency of IC formation. However, in a real wound exudate, wound odors are present as aqueous solution and it typically consists of components such as cadaverine and putrescine, that are alkaline in nature, which should tend to neutralize or at the very least increase the pH of the solution. These two factors are expected to greatly increase the wound odor absorption by β-CD functionalized PCL nanofibers.

Although the neat PCL nanoweb was not expected to absorb butyric and propionic acids, it indeed did so; but, during the experiments it was observed that when the neat PCL nanoweb was removed from the solution, there was a strong odor emanating from the nanoweb which was not observed with functionalized nanofibers. This indicated the instability of the odor producing compound which was held dynamically. Since XPS measurements were carried out in vacuum, these loosely held compounds were visible in the spectra. Since, the objective of this study was to not merely absorb the wound odor chemical but mask the malodor, we can safely conclude that neat PCL fibers absorb, but do not mask the odor, while those containing β-CD do mask the odor, which was further confirmed by TGA (discussed later).

In the case of β-CD functionalized nanofibers, after two days of immersion, it was observed that the adsorbed water content was about 8 and 9%, for 20% β-CD and 40% β-CD, respectively. This high adsorbed water content values indicate, in both cases, at least half of the β-CDs are in uncomplexed form, which are expected to form ICs with wound odor, if provided sufficient time. This result was supported by GC data, where it was observed that the saturation point of uptake of the wound odors was observed to occur somewhere around 4 days (supporting information).

3.5.2 Thermogravimetric analysis of wound odor absorbed nanofibers:

TGA measurements were carried out on the nanowebs before and after the immersion tests to investigate the thermal stability of the nanofibers, which should also indicate the presence of the acids. TGA thermograms of neat PCL nanoweb, 20% β-CD, and 40% β-CD

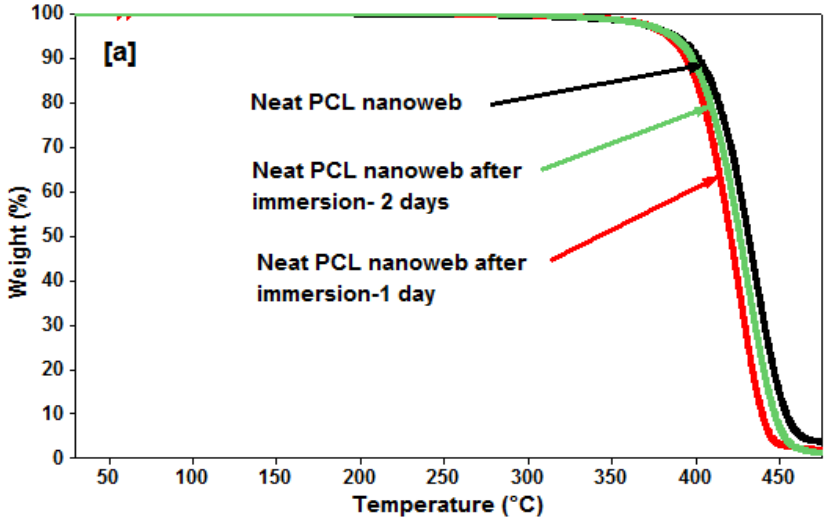

Figure 3.10: TGA thermograms of Neat PCL nanowebs before and after immersion in wound odor solution.

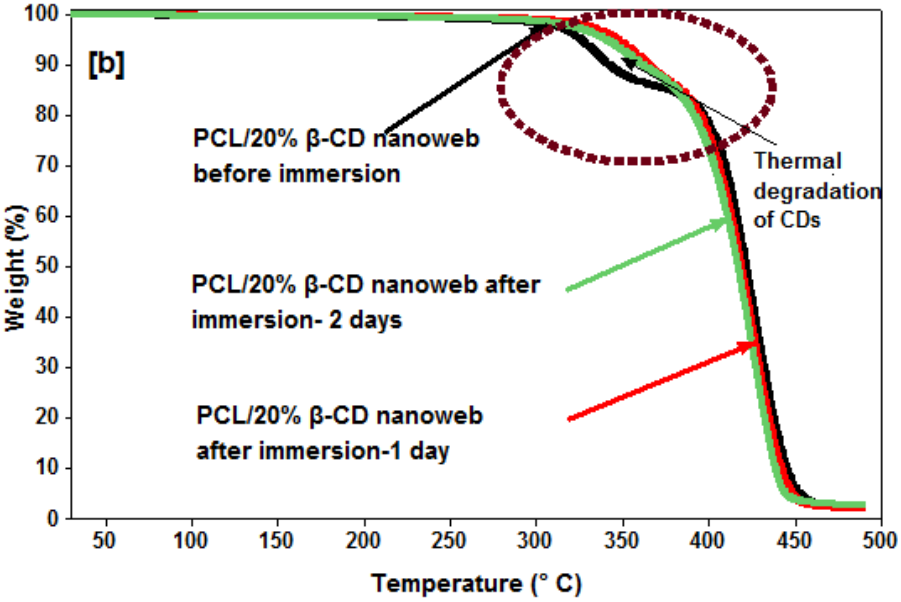

Figure 3.10b: TGA thermograms of 20% β-CD functionalized PCL nanowebs before and after immersion in wound odor solution.

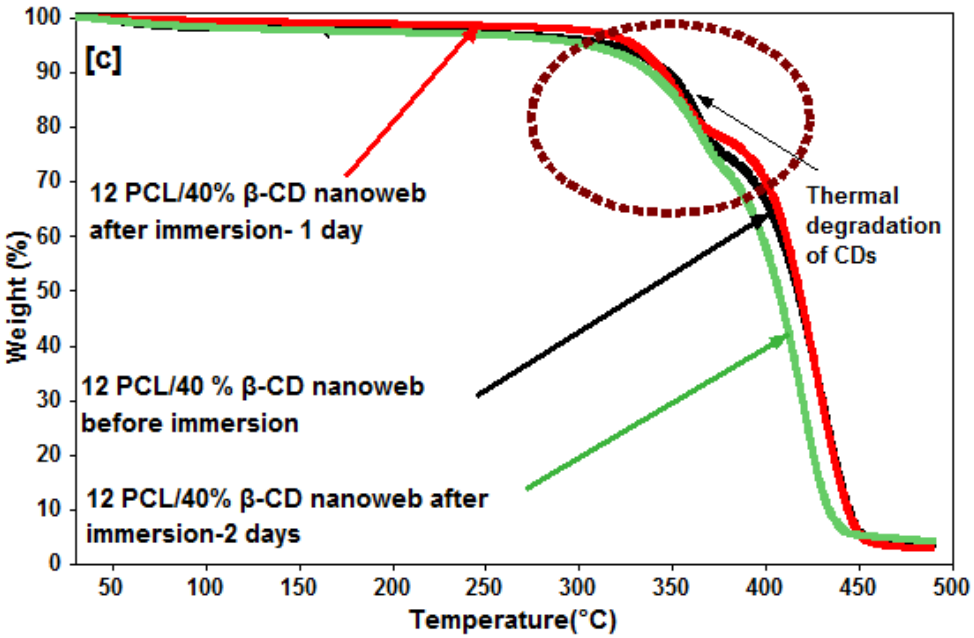

Figure 3.10c: TGA thermograms of 40% β-CD functionalized PCL nanowebs before and after immersion in wound odor solution.

functionalized fibers before and after immersion are shown in Figures 3.10a, 3.10b, and 3.10c, respectively. Thermal degradation of neat PCL nanowebs before immersion indicates, a single degradation pattern that starts at about 380 ºC, and progresses rapidly around 410 ºC at which point the complete destruction of PCL structure takes place, as reported in the literature [35]. In the case of neat PCL nanoweb, after 1 and 2 days immersion experiments, both elicit a strikingly similar degradation pattern. Although, thermal degradation of butyric or propionic acids could not be obtained from the literature, mass loss due to dehydration at 100 °C, and degradation of carboxylic acid structures are expected. But in the thermograms of neat PCL, there was no dehydration noted or any mass loss observed between 30 ºC and

400 ºC. The absence of these two patterns indicates the absence of any wound odor compounds.

However, in the case of β-CD functionalized PCL nanofibers, in addition to the thermal degradation of PCL at ~410 ºC, two more recognizable degradation steps take place. Firstly, there is a water weight loss at about 100 ºC, and, secondly, there is thermal degradation of CDs, which starts at about 320 ºC that proceeds till about 370 ºC. Further, the water loss observed for the functionalized nanofibers depended on the % β-CD content (Figures 3.6 & 3.7). The thermal degradation of β-CD is typically seen as a "slanted broad U" pattern (highlighted in the thermogram) that starts at about 320 ºC and ends with the degradation of PCL. The broadness of the "slanted U" pattern depends on the added % β-CD content, *i.e.*, the higher the β-CD content, the broader is the pattern. When the β-CD forms an inclusion compound with a small host molecule, however, the degradation pattern significantly changed; depending on the degree of IC formation, the "slanted U pattern" straightens.

From the thermograms of the functionalized nanofibers, it is clear that after immersion tests; the "slanted broad U" like pattern "straightens" progressively (highlighted in the thermograms 10b & 10c). A marked decrease in the CD degradation pattern is observed for both the nanowebs at even 1 day, and a further drastic change is observed at 2 days. It is also clear from the thermograms (10b & 10c) that, the "slanted U like pattern" did not disappear completely, meaning, there is further room for IC formation with the acids. These results support the XPS data that, neat PCL nanofibers do not mask any odor, and β-CD functionalized PCL nanofibers do so.

3.6. Discussion:

As mentioned before, this study was conducted as a proof of concept to examine the possibility of utilizing the functional fibers for removing wound odor. Since the functional nanofibers possess β-CD in the form of cage structures, slightly longer chain fatty acids such as valeric acid, which typically is a wound odor compound, cannot form ICs with CDs [49]. Hence, novel ways to electrospin the β-CDs that results in channel type structure should be investigated, as it can potentially facilitate absorption of such acids. For the matter of simplicity, only two short chain fatty acids, *viz*. butyric and propionic acids, were investigated in this study. A full factorial design experiment consisting of a simulated wound fluid should be conducted. The model fluid used could be such that it replicates wound fluids typically observed in diabetic patients. Also, in this study, ethanol was used as a solvent to dissolve the acids, whereas in the real case scenarios, wound odor compounds are present as aqueous solution.

Aqueous solution was not considered in our experiments, since the presence of water might potentially dissolve or leach the CDs. However, recently, Uyar et al had reported the formation of cross-linked electrospun polyester/ β-CD moieties, using citric acid as cross linker [41]. But, from biomedical standpoint, use of citric acid as cross linker might not be desirable, as being acidic, citric acid might hinder cell growth, as typically observed for acrylic acid-grafted polymeric systems [46]. Other option such as using glutaraldehyde for cross-linking might also not be desirable due to toxicity considerations.

UV crosslinking offers a potentially better environmentally benign, biomedically friendly route to solve this issue. Recently, Polydimethyl siloxane (PDMS) was reported to be cross-

linked using UV with benzophenone as catalyst [50]. Since PCL has methylene groups, it could be feasible to UV crosslink PCL-CD composite. Moreover, since benzophenone melts at less than 47 ºC, PCL/ β-CD could be melt processed without the destruction of nanofibrous structure, and subsequently UV crosslinked.

3.7 Conclusions:

β-CD functionalized composite nanofibers containing PCL and β-CDs have been prepared for the first time using electrospinning process. Presence of β-CDs in the mats was verified using XPS, and by water loss through TGA. Average fiber diameter of a neat PCL control web was found to be around 400 nm, while that of the composite web fibers containing β-CD was found to be about 500 nm. However, the statistical outliers were observed to increase with increase in β-CD loading.

Unlike α- and γ-CD functionalized PCL nanofibers reported in our previous study [35], TGA observations indicate the degradation patterns of β-CD functionalized materials to be a simple mixture, rather than the ICs. The result was further confirmed by the absence of IC peaks in the XRD analysis. FTIR analyses, by virtue of halo like hydroxyl peak at 3347 cm^{-1}, indicate the possibility of β-CD present in the surface, rather than in the bulk.

The absorption of wound odor solution consisting of butyric and propionic acids by neat and functionalized PCL nanofibers was examined using XPS. Although, the XPS indicated the presence of the acids in the neat PCL mats, TGA conclusively indicated absence of any such moieties. On the other hand, functionalized nanofibers, especially, those containing

40% β-CD, absorbed much higher amount of odor compounds, with the possibility of absorbing even more, if provided greater amount of time.

It would be desirable to study the absorption of simulated wound fluids containing all components such as the amines and the short chain fatty acids, using XPS. From our observations of the work with short chain fatty acids, in a real wound fluid of neutral or at least slightly higher pH, we would expect that β-CD functionalized nanofibers to perform better compared to neat PCL fibers.

Acknowledgements:

The authors acknowledge the use of the Analytical Instrumentation Facility (AIF) at North Carolina State University, which is supported by the State of North Carolina and the National Science Foundation. The authors thank Fred Stevie and Elaine Zhou, of AIF, in data analysis is also acknowledged.

References:

1. Kim B-S, Kim I-S. Recent Nanofiber Technologies. Polym.Rev. 2011; 51:235-238.

2. Frenot A, Chronakis IS. Polymer Nanofibers Assembled by Electrospinning. Curr. Opin.Colloid Interface Sci. 2003; 64-75.

3. Tong H-W, Wang M. Electrospinning of Poly (hydroxybutyrate-*co*-hydroxyvalerate) Fibrous Scaffolds for Tissue Engineering Applications: Effects of Electrospinning Parameters and Solution Properties. Journal of Macromolecular Science Part B: Physics. 2011; 50:1535-1558.

4. Bhardwaj N, Kundu SC. Electrospinning: a Fascinating Fiber Fabrication Technique. Biotechnology Advances 2010; 28: 325-347.

5. Jin L, Wang T, Zhu M-L, Leach MK, Naim YI, Corey JM, Feng Z-Q, Jiang Q. Electrospun Fibers and Tissue Engineering. J. Biomed. Nanotechnol.2012; 8:1-9.

6. McCann JT, Li D, Xia Y. Electrospinning of Nanofibers with Core-Sheath, Hollow, or Porous Structures. J. Mater Chem. 2005; 15:735-738.

7. Mehraban M, Zadhoush A, Ravandi SAH, Bagheri R, Tehrani AH. Preparation of Porous Nanofibers from Electrospun Polyacrylonitrile/Calcium Carbonate Composite Nanofibers Using Porogen Leaching Technique. Journal of Applied Polymer Science. 2013; 128: 926-933.

8. Finne-Wistrand A, Albertsson AC, Kwon OH, Chen G, Kang K, Hasuda H, Gong J, Ito Y. Resorbable Scaffolds From Three Different Techniques: Electrospun Fabrics, Salt Leaching Porous Films and Smooth Flat Surfaces. Macromol Biosci. 2008; 8: 951-959.

9. Moghe AK, Hufenus R, Hudson SM, Gupta BS. Effect of the Addition of a Fugitive Salt on Electrospinnability of Poly (ε-caprolactone). Polymer 2009; 3311-3318.

10. Celebioglu A, Uyar T. Electrospun Porous Cellulose Acetate Fibers From Volatile Solvent Mixture. Mater. Lett.2011; 65: 2291-2294.

11. Lee BN, Kim DY, Kwon JS, Park YH, Chun HJ, Kim JH, Lee HB, Min BH, Kim MS. *In vivo* Biofunctionality Comparison of Different Topographic PLLA Scaffolds. J.Biomed Mater Res A. 2012; 100: 1751-1760.

12. Moura LIF, Dias AMA, Carvalho E, De Sousa HC. In vitro Bone Exposure to Strontium Improves Bone Material Level Properties. Acta Biomater. 2013; 9:7013-7114.

13. da Silva L, Carvalho E, Cruz MT.Role of Neuropeptides in Skin Inflammation and Its Involvement in Diabetic Wound Healing.Expert Opin. Biol. Ther. 2010; 10:1427–39.

14. Enoch S, Leaper DJ. Basic Science of Wound Healing.Surgery. 2008; 26: 31-37.

15. Fromantin I, Seyer D, Watson S, Rollot F, Elard J, Escande C, De Rycke Y, Kriegel I, Garde VL.Bacterial Floras and Biofilms of Malignant Wounds Associated with Breast Cancers.J. Clin.Microbiol. 2013; 51:3368-3373.

16. Leveen HH, Falk G, Borek B, Diaz C, Lynfield Y, Wynkoop BJ, Mabunda GA, Rubricius JL, Christoudias GC.Chemical Acidification of Wounds. An Adjuvant to Healing and the Unfavorable Action of Alkalinity and Ammonia.Ann. Surg.1973; 178:745-753.

17. Rodriguez P.G, Felix F.N, Woodley D.T, Shim E.K.The Role of Oxygen in Wound Healing: A Review of the Literature. Dermatol. Surg 2008; 34:1159-1169.

18. Bradley M, Cullum N, Nelson EA, Petticrew M, Sheldon T, Torgerson D. Systematic Reviews of Wound Care Management.(2) Dressings and Topical Agents used in the Healing of Chronic Wounds. Health Technol Assess. 1999; 3:1-35.

19. Winter GD. Formation of the Scab and the Rate of Epithelization of Superficial Wounds in the Skin of the Young Domestic Pig.Nature 1962; 193:293-294.

20. Lloyd LL, Kennedy JK, Methacanon P, Paterson M, Knill CJ. Carbohydrate Polymers as Wound Management Aids. Carbohydr Polym. 1998; 37: 315–22.

21. Fonder MA, Lazarus GS, Cowan DA, Aronson-Cook B, Kohli AR, Mamelak AJ. Treating the Chronic Wound: A Practical Approach to the Care of Nonhealing Wounds and Wound Care Dressings. J Am Acad Dermatol. 2008; 58: 185–206.

22. Skorkowska-Telichowska K, Czemplik M, Kulma A, Szopa J. The Local Treatment and Available Dressings for Chronic Wounds. J Am Acad Dermatol.2011; 5:1–11.

23. Hilton JR, Williams DT, Beuker B, Miller DR, Harding KG.Wound Dressings in Diabetic Foot Disease. Clin Infect Dis. 2004; 39:100–3.

24. Lipman RDA, van Bavel D, Odor Absorbing Hydrocolloid Dressings for Direct Wound Contact.Wounds research. 2007.

25. Exuderm ® Odorshield™ Wound Dressing, the First Odor-Control Hydropolymer,Medline.Available from URL:http://www.medline.com/jump/product/x/Z05-PF00173 .

26. Szejtli J, Cyclodextrin Technology. Boston: Kluwer Academic Publishers, 1988. P. 1-15.

27. Kayacki F, Uyar T. Encapsulation of Vanillin/Cyclodextrin Inclusion Complex in Electrospun Polyvinyl Alcohol (PVA) Nanowebs: Prolonged Shelf-life and High Temperature Stability of Vanillin. Food Chem. 2012; 133: 641-649.

28. Tonelli AE. Molecular Processing of Polymers with Cyclodextrins. Adv Polym Sci. 2009; 222:115-173.

29. Huang L, Tonelli AE. Polymer Inclusion Compounds. J. Macromol. Sci., Part C: Polym. Rev. 1998; 38: 781-837.

30. Huang L, Gerber M, Lu J, Tonelli AE. Formation of a Flame Retardant-Cyclodextrin Inclusion Compound and its Application as a Flame Retardant for Poly (ethylene terephthalate). Polym. Degrad. Stab. 2001; 71: 279-284.

31. Huang L, Taylor H, Gerber M, Orndorff PE, Horton JR, Tonelli AE. Formation of Antibiotic, Biodegradable/Bioabsorbable Polymers by Processing with Neomycin Sulfate and Its Inclusion Compound with Beta-cyclodextrin. J. Appl. Polym. Sci.1999; 74:937-947.

32. Whang HS, Hunt MA, Wrench N, Hockney JE, Farin CE, Tonelli AE. Nonoxynol-9-Alpha-Cyclodextrin Inclusion Compound and its Application for the Controlled Release of Nonoxynol-9 Spermicide. J. Appl. Polym. Sci. 2007; 106:4104-4109.

33. Szente L, Szejtli J.Cyclodextrins as Food Ingredients. Trends Food Sci. Technol. 2004; 15:137-142.

34. Tonelli AE. Restructuring Polymers via Nanoconfinement and Subsequent Release. Beilstein J. Org. Chem. 2012; 1318-1332.

35. Narayanan G, Gupta BS, Tonelli AE. Poly (ε-caprolactone) Nanowebs Functionalized with α- and γ-cyclodextrins. Biomacromolecules.2014.DOI: 10.1021/bm501158w

36. Huang L, Allen E, Tonelli AE. Study of the Inclusion Compounds Formed Between α-cyclodextrin and High Molecular Weight Poly (ethylene oxide) and Poly (ϵ-caprolactone). Polymer. 1998; 39:4857-4865.

37. Rusa CC, Fox J, Tonelli AE. Competitive Formation of Polymer−Cyclodextrin Inclusion Compounds. Macromolecules.2003; 36:2742-2747.

38. Shuai X, Porbeni FE, Wei M, Bullions T, Tonelli AE. Inclusion Complex Formation Between α, γ-cyclodextrins and a Triblock Copolymer and the Cyclodextrin-Type-Dependent Microphase Structures of Their Coalesced Samples. Macromolecules. 2002; 35:2401-2405.

39. Williamson BR, Tonelli AE.Constrained Polymer Chain Behavior Observed in their Non-Stoichiometric Cyclodextrin Inclusion Complexes. J. Inclusion Phenom. Macrocyclic Chem. 2012; 72:71-78.

40. Chan S-C, Kup S-W, Chang F-C.Synthesis of the Organic/Inorganic Hybrid Star Polymers and their Inclusion Complexes with Cyclodextrins.Macromolecules.2005; 38: 3099-3107.

41. Kayaci F, Aytac Z, Uyar T. Surface Modification of Electrospun Polyester Nanofibers with Cyclodextrin Polymer for the Removal of Phenanthrene from Aqueous Solution. J. Hazard. Mater. 2013; 261:286-294.

42a. Gao J, Yu S, Zheng B, Song Q, Peng X, Lin Y et al. Inclusion Complexes Synthesized From an ABA Triblock Polymer and β-cyclodextrins: Amplification of Hydrophobic Interaction Along a Hydrophilic Polymer Chain. RSC Adv. 2014; 4: 36675-366681.

42b. Jia Y-T, Gong J, Gu X-H, Kim H-Y, Dong J, Shen X-Y. Fabrication and Characterization of Poly (vinyl alcohol)/Chitosan Blend Nanofibers Produced by Electrospinning method. Carbohydr Polym. 2007; 67:403-409.

43. Kayaci F, Uyar T.Electrospun Polyester/Cyclodextrin Nanofibers for Entrapment of Volatile Organic Compounds. Polym. Eng. Sci.2014. Available from URL: http://onlinelibrary.wiley.com/doi/10.1002/pen.23858/pdf (DOI: 10.1002/pen.23858).

44. Yatsimirskii KB, Nemoskalenko VV, Aleshin VG, Bratushko YI, Moiseenoo EI.X-ray Photoelectron Spectra of Mixed Oxygenated Cobalt(II)-Amino Acid-Imidazole Complexes. Chem Phys Lett. 1997; 52:481-484.

45. Yu J-S, Wei F-D, Zhao C-Thermodynamic Study on the Effects of β-Cyclodextrin Inclusion with Berberine. Spectrochim. Acta, Part A. 2002; 58:249-256.

46. Gupta B, Plummer C, Bisson I, Frey P, Hilborn J. Plasma-Induced Graft Polymerization of Acrylic Acid onto Poly (ethylene terephthalate) Films: Characterization and Human Smooth Muscle Cell Growth on Grafted Films. Biomaterials.2002; 23:863-871.

47. Uyar T, Havelund R, Hacaloglu J, Zhou X, Besenbacher F, Kingshott P. The Formation and Characterization of Cyclodextrin Functionalized Polystyrene Nanofibers Produced by Electrospinning.Nanotechnology.2009; 20:125605-125619.

48a.Uyar T, Rusa CC, Hunt MA, Aslan E, Hacaloglu J, Tonelli AE.Reorganization and Improvement of Bulk Polymers by Processing with Their Cyclodextrin Inclusion Compounds. Polymer 2005; 46:4762-4775. 48b. Porbeni FE, Edeki EM, Dan Shin I, Tonelli AE. Formation and Characterization of the Inclusion Complexes Between Poly (dimethylsiloxane) and Polyacrylonitrile with γ-Cyclodextrin. Polymer. 2001; 16:6907-6912.

49. Huang L, Tonelli AE. Inclusion Compounds Formed Between Cyclodextrins and Nylon 6. Polymer. 1999; 40: 3211-3221.

50. Bhagat AAS, Jothimuthu P, Paputsky I.Photodefinable Polydimethylsiloxane (PDMS) For Rapid Lab-on-a-chip Prototyping. Lab Chip. 2007; 7: 1192-1197.

3.8 Supporting information:

Table S-1: Summarized GC data of PCL/ 50% β-CD functionalized nanofibers observed at different intervals.

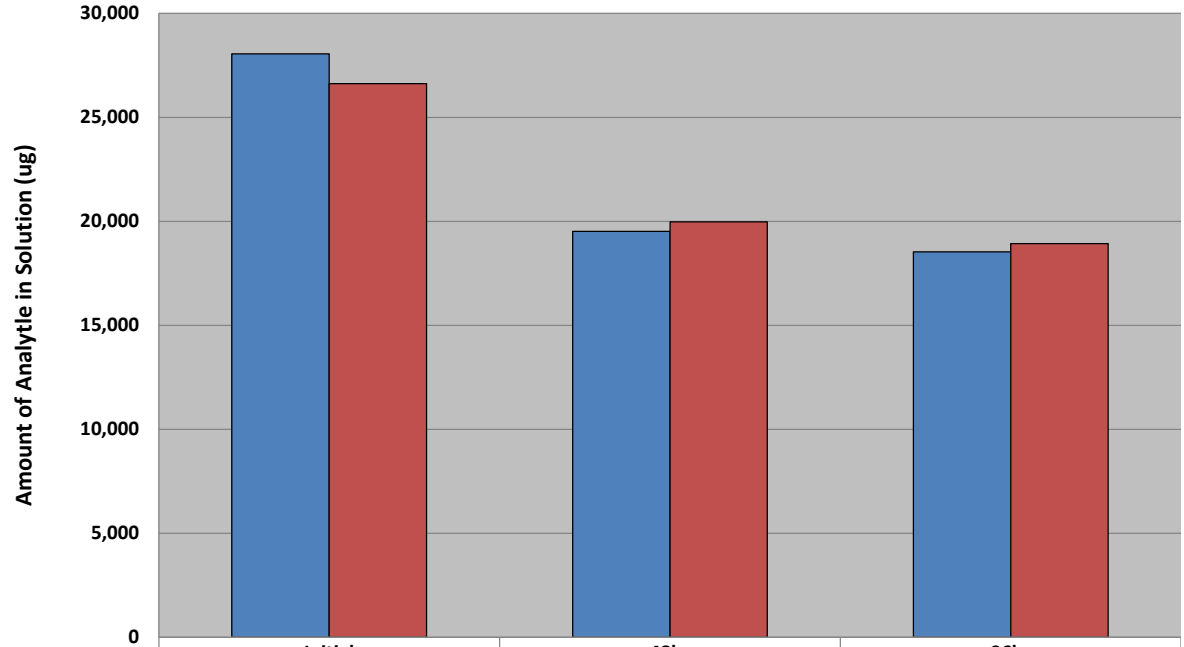

	Initial	48hr	96hr
Propionic Acid	28,050	19,514	18,531
Butyric Acid	26,621	19,981	18,929

Table S-2: Gas Chromatogram of the wound odor chemical solution after 2 days of immersion

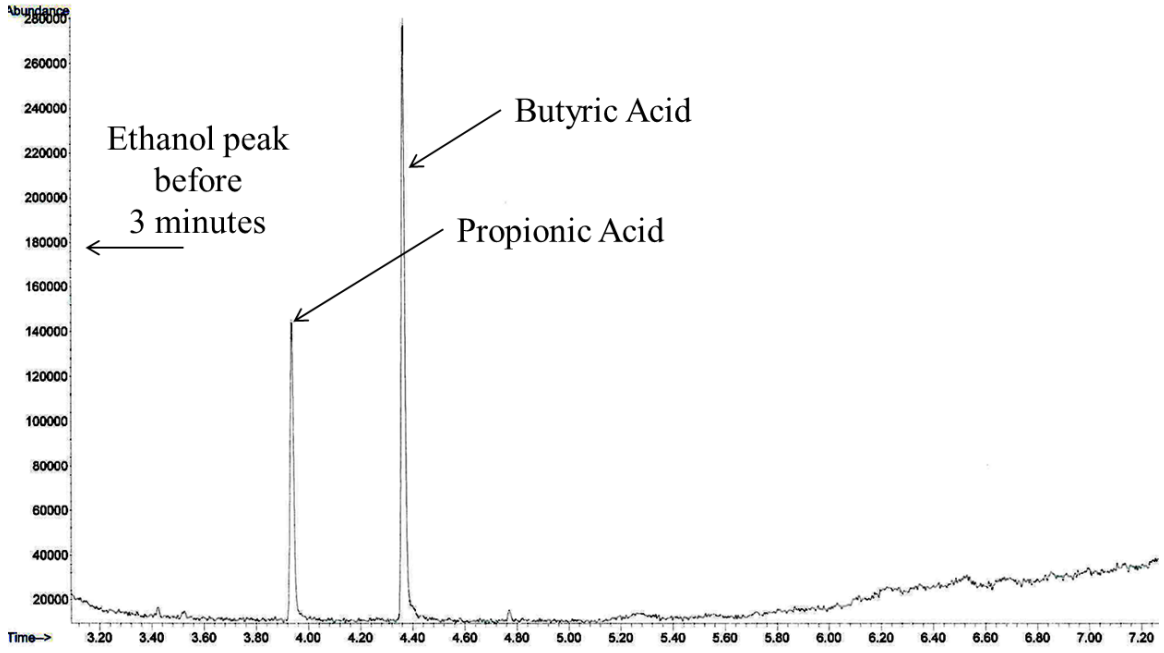

Chapter 4: Enhanced Mechanical Properties of Poly (ε-caprolactone) Nanofibers with the Addition of Non-stoichiometric Inclusion Complexes of Poly (ε-caprolactone) and α-Cyclodextrin.

Abstract:

The effects of α-cyclodextrin-polycaprolactone inclusion complexes (PCL-α-CD-ICs) on the thermal behavior and mechanical properties of electrospun PCL nanofibers have been investigated in this study. Non-stoichiometric inclusion complexes [(n-s) PCL-α-CD-ICs] with various stochiometries were prepared by threading host α-CDs onto guest PCL chains, and PCL/ (n-s)-PCL-α-CD-IC composite nanofibers were obtained by an electrospinning process. The stochiometric ratios of the (n-s) PCL-α-CD-ICs, % loadings of the (n-s) PCL-α-CD-ICs, and the concentration of the PCL solutions were varied. SEM indicates that at lower concentration (12%) of PCL, in all of the (n-s) PCL-α-CD-ICs, up to 15% loading (with respect to PCL), fibers were obtained with no significant beads. However, at 14% PCL concentration, bead-free fibers occurred only up to 10% loading; beyond this loading some beads were observed. DSC analyses indicates that the melting and the crystallization temperatures of the PCL/(n-s) PCL-α-CD-ICs increased significantly compared to that of the 0neat PCL nanofibers, indicating the presence of (n-s) PCL-α-CD-ICs, not dethreaded PCL and α-CDs. The presence of (n-s) PCL-α-CD-ICs is also confirmed by absence of water loss and enhanced thermal stability of α-CDs, as observed by TGA analyses. Mechanical properties of the composite webs were studied using stress-strain measurements profiles

obtained on an Instron. With the addition of the ICs, the tensile modulus and ultimate tensile strength of the composite fibers increased significantly over those of the neat PCL or PCL/α-CD mixture nanofibers. These novel nanocomposite fibers, which are non-toxic, but biodegradable and biocompatible, with better mechanical and stiffness properties, could be an ideal candidate for scaffolds used in applications such as bone tissue engineering, which typically require superior mechanical properties.

4.1. Introduction:

Electrospinning is one of the simplest, most inexpensive and straightforward technique to make submicron fibers [1]. In the electrospinning process, a high electric potential difference is applied between two electrodes, one being the syringe or vessel containing either polymer melt or solution, and the other being the collector. As the fiber size decreases, several interesting properties such as increased surface to volume ratio and various fiber surface functionalities can be achieved, compared to those found in fibers made by the traditional fiber processing methods. These fibers have high potential in biomedical applications, such as tissue engineering, wound healing, drug delivery, and in various other applications, such as filtration, photonics, and sensors, to name a few [2-3].

Wide range of polymers, including synthetic and naturally occurring materials have been electrospun and reported. Some of the naturally occurring polymers electrospun include chitosan, gelatin, collagen, silk fibroin, zein, and cellulose acetate: a synthetically derivative of cellulose [4-10]. Many synthetic biodegradable polymers have also been electrospun and extensively studied, including poly (ε-caprolactone) [PCL], poly (lactic acid), poly (glycolic

acid), copolymers of poly (lactide-co-caprolactone), poly (lactide-co-glycolide); several of these are projected for use in biomedical field [11-15]. Being environmentally friendly, both natural and synthetic polymers have attracted much attention due to their biocompatibility, low toxicity and biodegradability, and they have emerged as promising materials for biomedical applications, such as cartilage repair, bone tissue engineering, and nerve regeneration [14-15].

Although PCL has some ideal features as a biomaterial, it has poor mechanical properties. The mechanical properties of PCL are typically enhanced by adding minerals such as nano hydroxyapatite, collagen, and gelatin or by reinforcing them with nanomaterials, such as cellulose nanowhiskers or carbon nanotubes [20-23]. Other than the naturally derived minerals and cellulose nanowhiskers, the effect of fillers such as carbon nanotubes on the environment still remains controversial [23a]. Thus there exists a need to develop novel nucleating materials for reinforcing from natural or synthetic sources that are biocompatible, biodegradable, and not cytotoxic.

Cyclodextrins (CDs) are cyclic (α-1,4) oligosaccharides that are typically made by bacterial degradation of starch sources [26]. The CDs consists of at least six glucose units with a truncated cone like structure with a hydrophilic surface and a hydrophobic inner cavity, which can hold guests that can be either short or long molecules, including polymer chains. The most widely used CDs are from 6 to 8 glucose units and they are named, α-, β- and ɤ-CD, respectively, and are schematically shown in Figure 4.1 [27]. Harada et al, first reported the formation of cyclodextrin inclusion complexes with guest polymers (polymer-

CD-ICs), using polyethylene glycols (PEG) of various molecular weights and ever since the interest in these novel supramolecules has increased [29]. Tonelli et al, reported preparation of cyclodextrin inclusion complexes with various homo- and copolymers as guest molecules including poly (ε-caprolactone) [30], nylon [31], poly (ethylene oxide) (PEO) [32], poly (ethylene terephthalate) [33] and PCL-PEO-PCL tri-block copolymer [34].

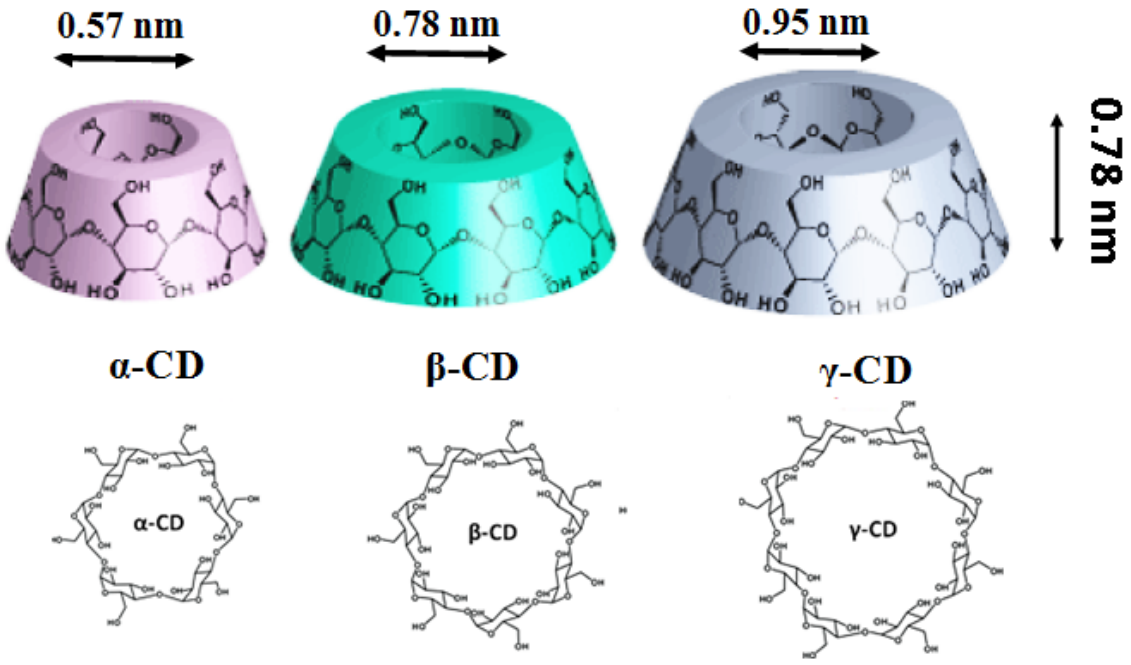

Figure 4.1: Chemical structures and schematic representation of α-β- and γ-cyclodextrins.

Non stoichiometric polymer inclusion [(n-s)-polymer-CD-IC] is formed when the stoichiometry of CD: polymer is less than that required for complete guest polymer coverage [37]. The schematic illustration of preparing such (n-s)-polymer-CD-ICs is shown in Figure

4.2. It was shown by Tonelli *et al.* [38] & Inoue *et al.*[39] that when these non-stoichiometric inclusion complexes are used as nucleating agents for bulk polymers, they result in enhanced mechanical properties as evidenced by increase in tensile strength from tensile testing, and storage modulus from dynamic mechanical analysis.

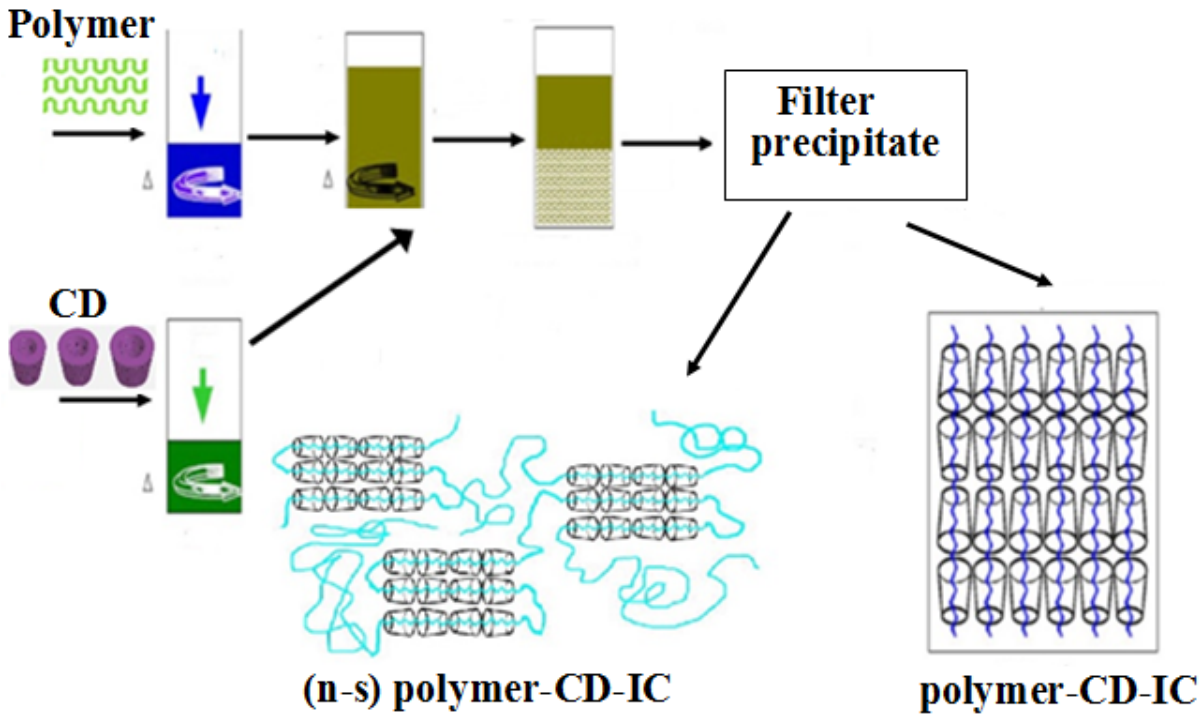

Figure 4.2: Schematic illustration of CD-IC or (n-s)-polymer-CD-IC preparation.

However, achieving such properties in nanofibers through the electrospinning process remains a challenge. There have been only few a reports of electrospinning of such systems, but those systems employed low molecular weight polymer (PEGs) or molecules such as, drugs, fragrances, etc. we report here the successful electrospinning of such nanocomposites

consisting of high molecular weight (n-s)-PCL-CD-ICs embedded in a PCL nanoweb. Advantages of such system include simple fabrication, *i.e.,* PCL forms nonstoichiometric inclusion complexes with α-CD relatively easily, which can then be electrospun with PCL. Another interesting aspect is (n-s)-PCL-CD-ICs can also be used as effective nucleants for compatible polymers, such as poly butylene succinate (PBS).

In chapter 2, we have reported the efficient nucleation capabilities of CDs on electrospun PCL nanofibers which provided improved hydrophilicity and the ability to capture wound odor agents, without forming ICs [41-42]. In this study, we report the enhanced mechanical and thermal properties of electrospun PCL fibers reinforced with nonstoichiometric inclusion complexes of PCL and α-CD. These novel inclusion complexes offer an alternative to conventional reinforcement methods requiring use of carbon nanotubes, clays, etc. whose toxicity is questionable.

4.2. Experimental:

4.2.1 Materials:

Poly (ε-caprolactone) (PCL)with a molecular weight (M_n) of 60,000-80,000, chloroform (CFM) (99.5% pure), N, N-Dimethyl Formamide (DMF)(anhydrous 99.8%) and acetone (99.5% pure) were purchased from Sigma-Aldrich, MO, US. α-CD (pharma grade) was obtained as a gift from Wacker Chemie, Michigan US.

4.2.2 Preparation of PCL-α-CD-ICs:

PCL-α-CD-IC formation was performed according to the procedures adopted by Tonelli et al. in the past [43] In general, 0.75 grams of PCL (in pellet form) is dissolved in 150 ml of acetone and, 15 grams of α-CD is dissolved in 75 ml of deionized water. The two solutions are then stirred and heated using a hot plate at 60° C for 3 hours till complete dissolution occurs. The α-CD solution is then added in a drop-wise fashion, and the solution was continuously heated and stirred at 60° C. To aid in and expedite the IC formation process, the combined solution is sonicated at room temperature, using an ultrasonicator for 5 minutes. The solution is then heated and stirred using a hot plate at 60° C for 1 hour, and then stirring continued for 36 hours at room temperature. The solution is allowed to rest for 24 hours and then filtered, washed with acetone and water, to remove uncomplexed PCL and α-CD. The white precipitate (PCL-α-CD-IC) is dried under vacuum for 48 hours.

(N-S)-PCL-α-CD-ICs were prepared similarly, except that depending on the stochiometry required, the ratio of CD: PCL was changed. For example, IC-6 was made by dissolving 1.5 g of PCL in 300 ml of acetone, and 2 g of α-CD in 12 ml of DI H_2O. These were then combined and stirred on a hot plate at 60 °C for 3 hours that causes complete dissolution to take place. The rest of the procedure was similar to that of making the completely covered stoichiometric PCL-α-CD-IC. Various ICs were made in this study and are described in Table 4.1.

Table 4.1: Solution ratios of α-CD and PCL, and their theoretical and estimated host-guest stochiometric ratios in the IC.

Sample	PCL& CD solution		Theoretical host-guest stochiometry ratio	Estimated host-guest stochiometric ratio [a]
	PCL/acetone solution ratio	α-CD/DI water solution ratio	PCL:CD	PCL:CD
PCL-IC-1	0.75g/150 ml	15g/75 ml	1:2	1:1
PCL IC-2	0.75g /150 ml	4g/25 ml	2:1	-[c]
PCL IC-6 [b,d]	1.5g/300ml	2g/8ml	6:1	5:1
PCL IC-3	1.5g/300ml	4g/16ml	3:1	-[c]
PCL IC-4 [b,d]	1.5g/300 ml	3g/12 ml	4:1	4:1

[a] Estimation of stochiometry was performed using ^{1}H-NMR, and integration of peaks at 4.7 ppm (α-CD) and 3.7 ppm (PCL).

[b] IC-6 & IC-4 means theoretical stochiometry ratio (PCL: CD) of 6:1 & 4:1, respectively.

[c] ^{1}H-NMR was not performed on these samples as the motivation of this work is to study ICs with lesser coverage.

[d] ^{1}H-NMR spectra and the estimated ratios are shown in supporting information.

4.3 Electrospinning of PCL/PCL-IC composite fibers:

4.3.1 Solution preparation:

PCL solutions were prepared by dissolving the required quantities of PCL in 6 ml of CFM and then the (n-s)-PCL-α-CD-IC mixture were prepared by suspending appropriate quantities of the (n-s)-PCL-α-CD-ICs in 4 ml DMF. PCL solutions and (n-s)-PCL-α-CD-ICs suspensions were then mixed together to form combined PCL/ (n-s)-PCL-α-CD-IC

suspensions. For control experiments, PCL solutions were made by dissolving PCL in a mixture of CFM and DMF. Once the solutions were prepared, they were agitated using a magnetic stirrer overnight at room temperature.

4.3.2 Electrospinning of composites fibers:

The solutions/suspensions were placed in a commercial 10 ml syringe (Becton Dickinson and company) attached with a blunted 21 gauge needle. The electrospinning process was performed using a high precision pump (New Era Pump Systems) that pumps the fluid at a preset rate and applying high voltage between the tip of the needle and the collector using a Gamma High Voltage Research instrument. In this study, a rotating drum was used as collector. The collector was made of stainless steel and had an outer diameter of 1.5 in; it was rotated at 280 rpm. The collector was positioned at a distance of 30 cm from the tip of the needle. The electrospinning process was carried out at a potential difference of 15 kV and at a solution feed rate of 0.5 mL/hr. The non-woven nanomats obtained were allowed to dry in a clean vacuum oven (for a week) to remove unevaporated solvents.

4.4. Characterization of Analytical properties:

4.4.1 PCL-IC characterization:

4.4.2 FTIR:

Infrared spectral studies were conducted using a Nicolet 470 FTIR infrared spectrophotometer in the frequency range of 4000-400 cm^{-1} with a resolution of 4 cm^{-1} and

64 scans collected for each sample. A Nicolet OMNI Germanium crystal ATR was used as sampling head, with the automatic ATR correction applied.

4.4.3 DSC:

Thermal transitions of the PCL-α-CD-ICs were determined using a Perkin Elmer diamond 7 DSC instrument. In this procedure, a small amount of sample (3-5 mg) was placed in a sealed aluminum pan, and the heating-cooling-heating cycles were applied between 0 and 80 °C. After the first heating cycle, the sample was held at 80° C for 1 min before cooling it to 0 °C. First heating was carried out at 20 °C/min, with the successive cooling and heating cycles out at 10 ° C/min.

4.4.4 TGA:

TGA was performed using a Perkin Elmer Thermogravimetric analyzer. Nitrogen gas was used to purge the furnace. Samples of 5-8 mg were placed in a pan and heated from 25 ° to 600 °C at a rate of 10 °C per minute. The Pyris software was used to analyze the data.

4.4.5 ^{1}H-NMR:

NMR spectra were collected on a Bruker 500 MHz NMR spectrometer and the data were analyzed using ACD spec manager software. For this, the PCL-α-CD-IC was dissolved in DMSO-d_6 at 80 °C overnight and then the testing performed at 30 °C.

4.5 Characterization of electrospun PCL/PCL-α-CD-IC composite nanofibers:

4.5.1 SEM:

Scanning electron microscopy (SEM) was performed using a phenom world G1 model microscope at an acceleration voltage of 10 KV to examine fiber morphology and to determine fiber diameters. The samples (0.5 inch in size) were cut and attached onto a metal stub using double sided carbon tape. These were coated with gold using a Polaron SC7620 Mini Sputter Coater (Quorum technologies) for about 45 seconds that yielded a coating of about 10 nm. SEM images were obtained at various magnifications and the fiber diameter was estimated using ImageJ software. A minimum of 100 fibers were measured and an average is reported as fiber diameter.

4.5.2 Tensile testing:

Mechanical properties were determined using a universal testing machine (Instron model 5544) with the Bluehill software version 2.0 used to calculate the modulus and also automatically generate a report at the end of tests on a batch of samples. Tensile tests were carried out on the electrospun PCL control, PCL/α-CD web, and those containing IC-4 and IC-6. The testing was conducted on a sample, 1 cm wide with a gauge length of 2 cm. The average thicknesses of the sample were measured at different sample locations using an electronic thickness gauge (Marathon electric). The samples were stretched to failure at a speed of 0.2 cm/minute at room temperature. Tests were conducted on a minimum of 10 specimens. Stress and strain coordinates for the entire curve were recorded, from which the

values for ultimate strain and tensile modulus were determined, and displayed as mean ± standard deviation.

4.5.3 Statistical analysis:

Statistical analyses of tensile modulus and elongation at break values for neat PCL, stoichiometric and PCL/(n-s)-PCL-α-CD-IC nano-composites were performed by student *t*-tests using Mintab® version 17. The variances were assumed to be equal, and P values less than 0.05 ($P<0.05$) at the 95% confidence level were assumed to be significantly different.

4.6 Results and Discussion:

4.6.1 Formation and Characterization of PCL-α-CD-ICs:

The formation of PCL-α-CD-ICs was characterized by FTIR, DSC, and the host-guest stochiometries were estimated using ^{1}H NMR. FTIR is frequently used to characterize CD-ICs as a rapid test to confirm the presence of both components, *i.e.*, PCL and α-CD. FTIR can sometimes be used to distinguish CD-ICs from a physical mixture by virtue of peak shifts and or suppression. In FTIR, as shown in Figure 4.3, PCL exhibits characteristic peak at 1727 cm^{-1}, and all of the (n-s)-PCL-α-CD-ICs, irrespective of the host-guest stochiometries, exhibit an intense peak at 3356 cm^{-1} which corresponds to the secondary hydroxyl group (OH-) present in CDs . In the case of the present (n-s) PCL-α-CD-ICs, it is seen clearly that as more of the PCL chains get confined within the α-CD cavity, the carbonyl peak of PCL observed at 1727 cm^{-1} disappears or is severely suppressed (a), which indicate

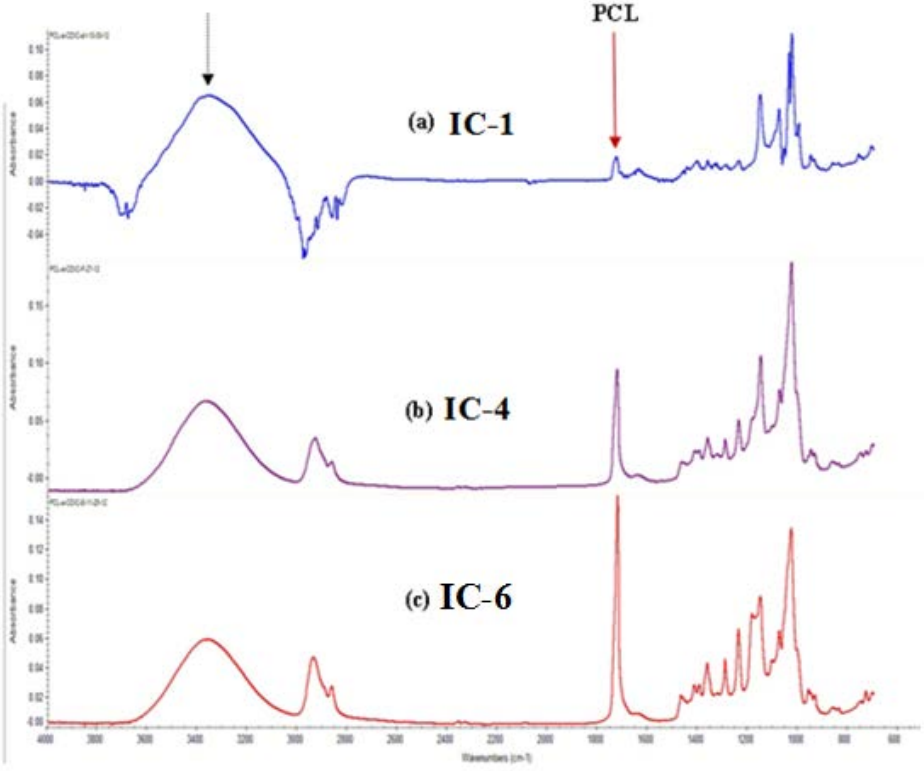

Figure 4.3: FTIR spectra of PCL-ICs. (a) IC-1, (b) IC-4, (c) IC-6.

that the stochiometric ratio is 1. The samples that that have more dangling PCL chains outside of the α-CD cavities would have more prominent carbonyl peaks; this is seen in (b), & (c), which indicates the PCL: CD stochiometry is higher.

Figures 4.4 & 4.5 shows the DSC heating and cooling cycles of neat PCL and their ICs with α-CD, with various stochiometries. The melting temperature of neat PCL was observed to be 59° C. Upon the formation of ICs as seen in 4.4, one observes that the fully covered ICs do not elicit melting transition, the latter suppressed due to the chains being inside the CD cavity. However, the ICs that are not completely covered (samples c and d in Figure 4.4)

show melting transitions, but at elevated temperatures of 65.5 and 66.2° C, respectively, for IC-4 and IC-6. This indicates that the increase in melting temperature depended on the coverage by α-CD, *i.e.*, the higher the coverage, the higher the melting temperature. This phenomena is due to the fact that, the PCL chain portions inside the α-CD cavity, hinder the melting of the PCL chain portions that are present outside the α-CD cavity. As expected, the melting enthalpies decrease, with increase in coverage.

The crystallization behavior of the neat PCL and the ICs measured by the cooling cycle in DSC is shown in Figure 4.5. The crystallization temperature and the crystallization enthalpy of the neat PCL was observed to be 24.97 °C and -54.40 J/g, respectively. As the behavior in the heating cycle, disappearance of crystallization peak is observed upon IC stochiometric formation (IC-1), indicating that the crystallization of PCL has been suppressed due to the chains within the CD cavities, with little or no chains freely available to crystallize. However, in case of partial ICs, crystallization of PCL is observed, but at elevated temperatures and with lower crystallization enthalpies. The behavior in heating and cooling cycles seen in the DSC results confirms the formation of IC and also indicates that the stochiometries of the ICs produced here are different, similar to observations made by Tonelli *et al.* [44] and Inoue *et al* [45].

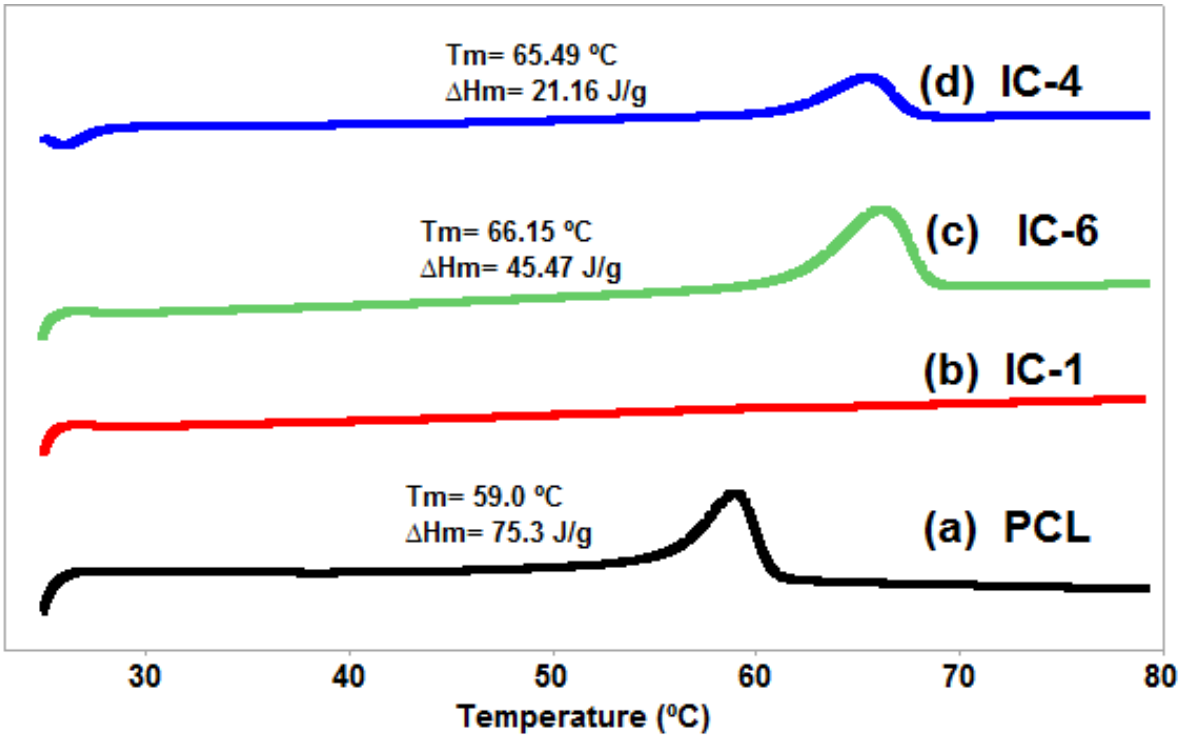

Figure 4.4: Heating cycle of neat PCL and its inclusion complexes with α-CD.

From the results of FTIR and DSC, it is quite evident that the stochiometries of the ICs made were different. The stochiometry of each IC was estimated through ^{1} H-NMR by the ratio of resonance intensities, corresponding to the CH_2 groups that is present adjacent to the ester group of the PCL repeat unit (δ 3.7 ppm) and (C_1H) of α-CD (δ 4.7 ppm) (See Supporting Information).

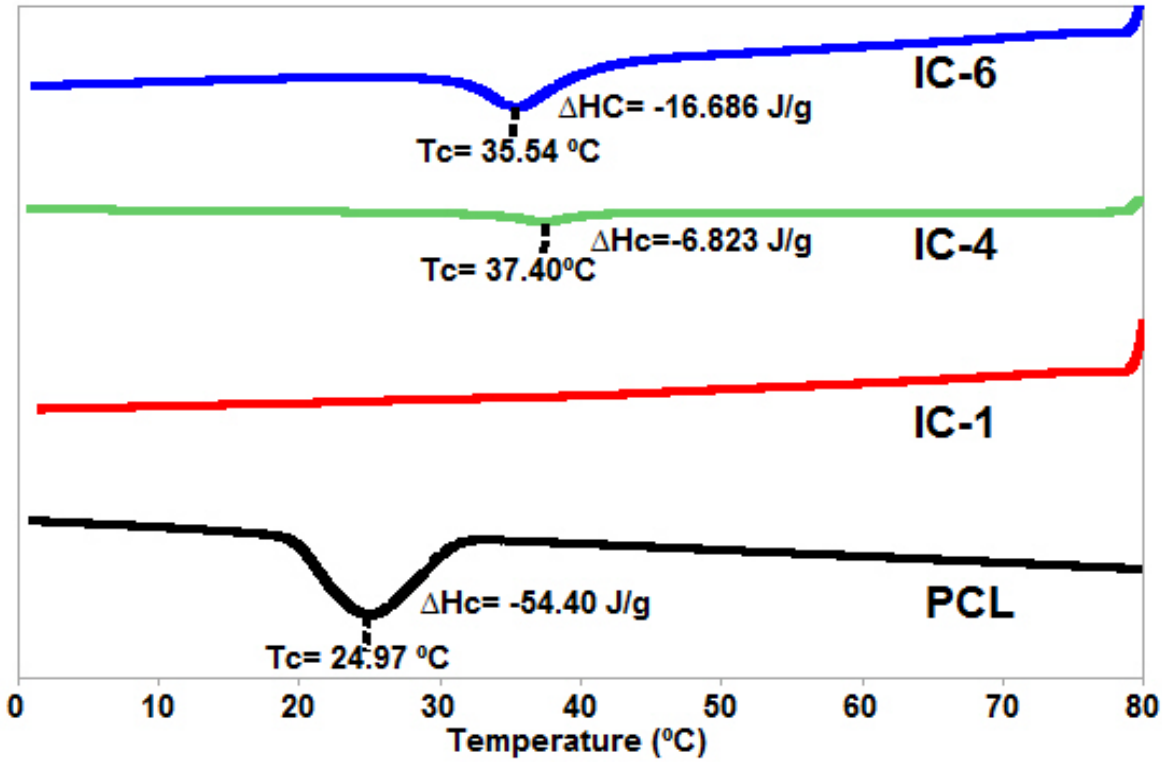

Figure 4.5: DSC non isothermal crystallization behavior of Neat PCL and its inclusion complexes with α-CD.

4.7: Characterization of electrospun PCL/IC composites:

4.7.1 Scanning Electron Microscopy:

To optimize the electrospinning process with respect to the addition of (n-s)-PCL-α-CD-ICs, initially the IC with a lower coverage of PCL (IC-6) was chosen and electrospinning conducted at a set PCL concentration of 14%, with loading of IC was varied from 5-15%, with respect to PCL. IC with a lower coverage (IC-6) was chosen, because the dangling chains had a better possibility of forming gel with the solvent mixture than those with higher coverage. The representative SEM images are shown in Figure 4.6. As generally observed

with electrospinning of PCL/CD systems, slightly thicker fibers with some beads are observed, especially at higher IC loadings (15%). Beyond 15% loading, frequent clogging of the needle occurred, and hence IC loading beyond 15% was not studied. The average fiber diameter of the IC-6 loaded PCL nanofibers was observed to be: 444 ±267 nm, 543 ± 249 nm, 589 ± 316 nm, for 5, 10, and 15% IC loadings, respectively. Results from SEM suggested that lower PCL concentration provided better nanofibers; accordingly, the concentration was decreased to 12%. In this case, the type of ICs was also varied. The representative SEM images and fiber distribution of IC-4 and IC-6 nucleated PCL nanofibers at PCL concentration of 12% are shown in Figures 4.7 & 4.8, respectively.

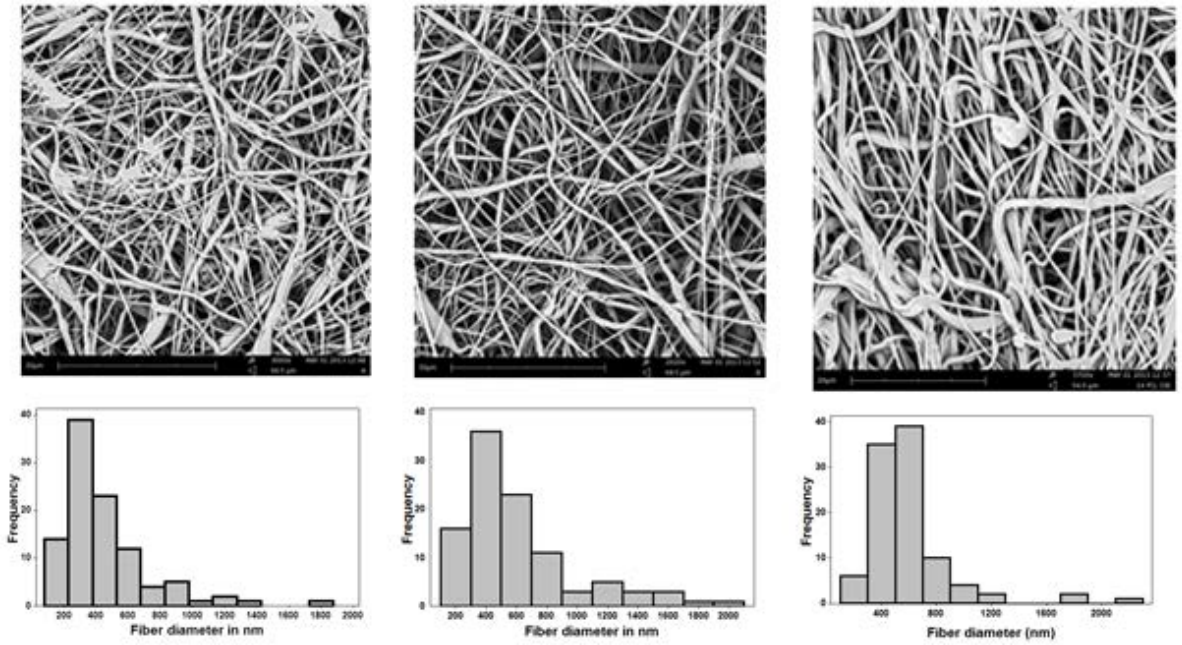

Figure 4.6: Representative images of PCL/PCL-IC-6 nanofibers obtained from 14% PCL solution. (a) 5% IC-6, (b) 10% IC-6, (c) 15% IC-6.

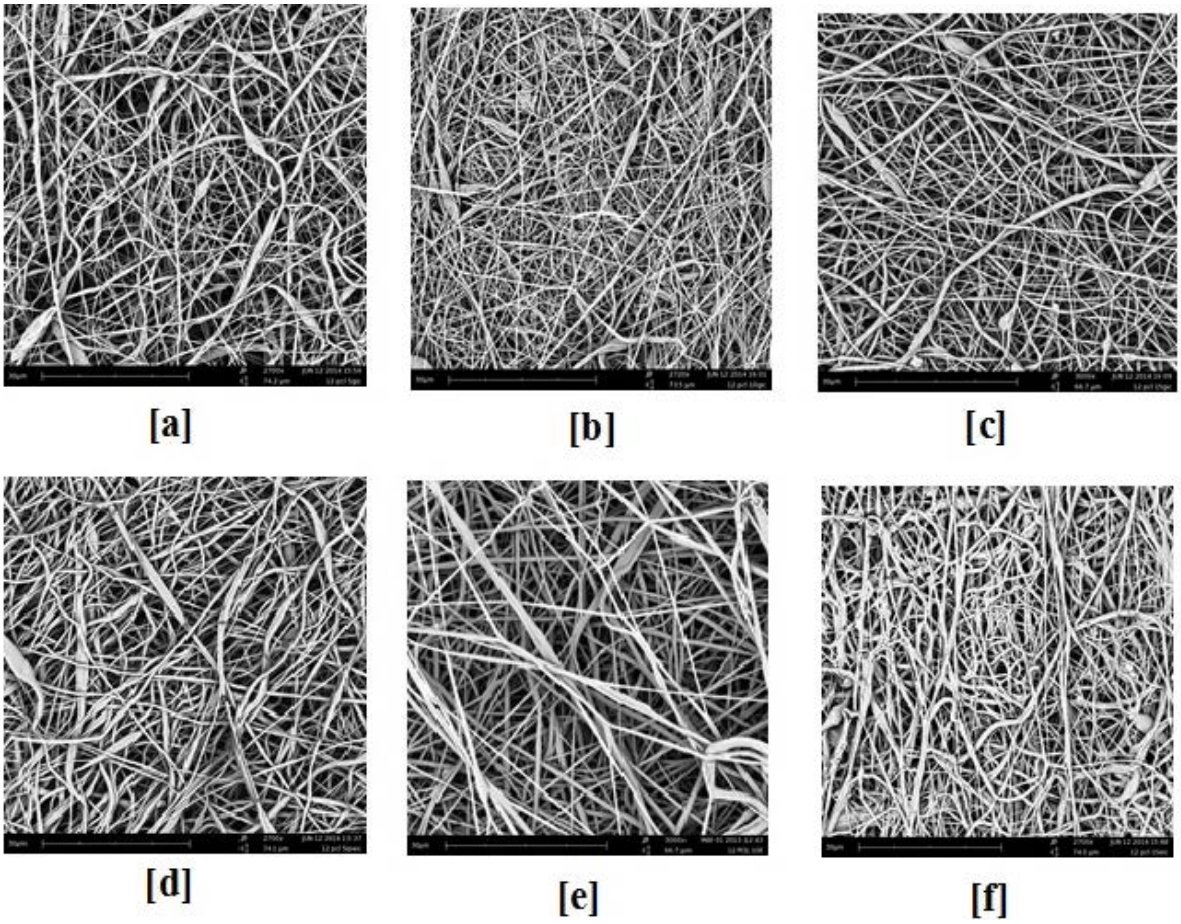

Figure 4.7: SEM images of PCL/PCL-IC fibers electrospun at 12 % PCL. (a) 5% IC-4, (b) 10% IC-4, (c) 15% IC-4, (d) 5% IC-6, (e) 10% IC-6, (f) 15% IC-6.

Although not expected, IC-4 nucleated nanofibers have smaller diameters compared with IC-6. In the case of IC-6, the solubility of longer dangling PCL chain portions would be higher, and in turn increases viscosity of the solution/suspension. Whereas, in the case of IC-4, the dangling chain portions are shorter, leading to a smaller increase in the viscosity. As with the previous observation at 14% PCL, beyond 10% concentration, slight beads or

agglomerates were observed for both cases, which in turn could be due to their being in suspension.

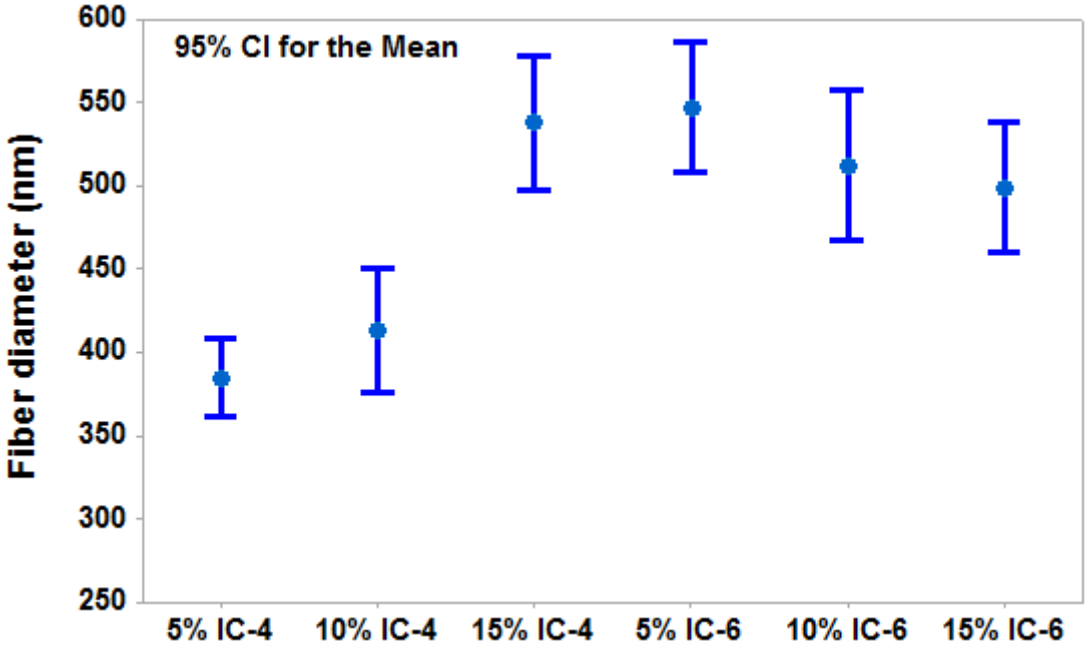

Figure 4.8: Fiber diameter of PCL/PCL-IC fibers electrospun at 12 % PCL.

From the SEM images and average fiber diameter measurements, it is quite clear that it is possible to electrospin PCL and (n-s)-PCL-α-CD-ICs. However, a serious question still remains, do the ICs exist as an IC or have α-CDs dethreaded from the PCL chains. DSC and TGA analyses were performed on these electrospun mats to analyze if the ICs have dethreaded during solution preparation or electrospinning.

4.7.2 Differential Scanning Calorimetry (DSC):

DSC analyses were performed to study the influence of ICs on the melting and subsequent crystallization behavior from the melt, and to compare with that of neat PCL and those containing mixture of PCL with α-CDs. Figure 4.9, shows the DSC thermograms of neat PCL nanofibers, PCL/PCL-IC nanofibers, and PCL/α-CDs; their enthalpy values are summarized in Table 4.1. It is seen that the T_m values of PCL and those containing α-CD are almost the same (~ 60° C), whereas the value of those containing ICs, there is a significant change in the T_m values (~5 ° C). This is due to the presence of hard IC segments, which delay the melting of the neat PCL chains portions outside the α-CD cavities as well as in the neighboring region. This behavior is not observed in the case of those PCL nanowebs nucleated by α-CD alone. The melting enthalpy of neat PCL nanofiber was observed to be 75.30 J/g, and those containing ICs with high coverage (IC-4) had almost the same enthalpy as that of neat PCL. However, those containing lower coverage (IC-6) had significantly

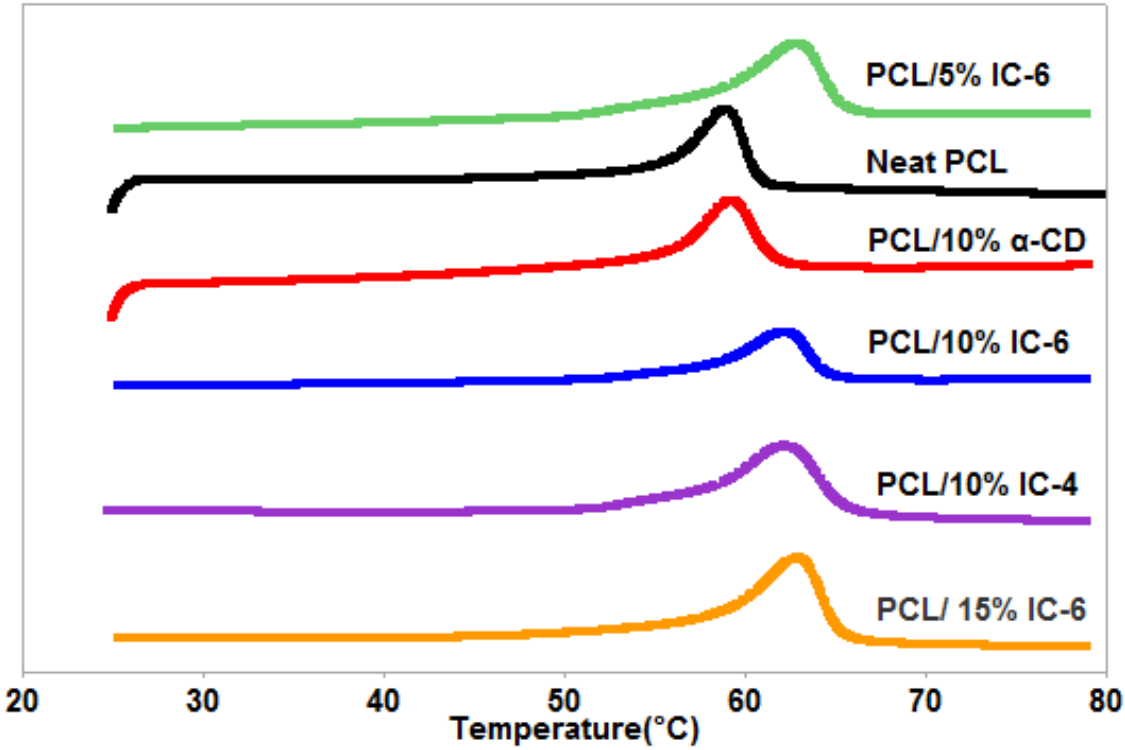

Figure 4.9: DSC thermograms of neat PCL, PCL/CD, PCL/PCL-IC nanofibers.

Table 4.2: Melting and crystallization temperatures, melting and crystallization enthalpies of neat PCL, and PCL/PCLICs obtained from DSC.

	First heating cycle		First cooling cycle	
Sample	**Tm (°C)**	**ΔHm (J/g)**	**Tc (°C)**	**ΔHc (J/g)**
Neat PCL	59.20	75.30	25.68	-49.70
12 PCL/ 10% IC-4	62.19	75.87	31.27	-45.72
12 PCL / 5% IC-6	62.84	68.03	30.95	-41.68
12 PCL /10% IC-6	64.58	58.50	31.77	-42.40
12 PCL /15% IC-6	62.85	62.28	31.75	-41.34

lowered enthalpy (~60 J/g). Even more pronounced was seen in those containing higher IC loadings (10 and 15%). These findings are comparable to those reported in the literature, although, the latter were obtained from films [45].

Figure 4.10 shows the non-isothermal crystallization behavior of neat PCL and PCL/PCL-IC composites, obtained from the cooling cycle of the DSC experiment. The crystallization temperatures and their corresponding enthalpies of PCL and PCL/PCL-ICs are summarized in Table 4.2. The crystallization temperature (Tc) of neat PCL was observed to be about 25.68°C, while those containing ICs exhibited crystallization at elevated temperatures, indicating the nucleating capability of the ICs on PCL. After the addition of unthreaded α-CD or ICs, not only the crystallization temperatures increased, but also the peaks tended to become narrower, which is consistent with the observations reported in the literature on films and melt spun fibers [37, 47]. Another interesting observation made was that the sharpness of the crystallization peaks tended to increase with that of the IC loading, and the most effective nucleant was IC-6 at 15% loading.

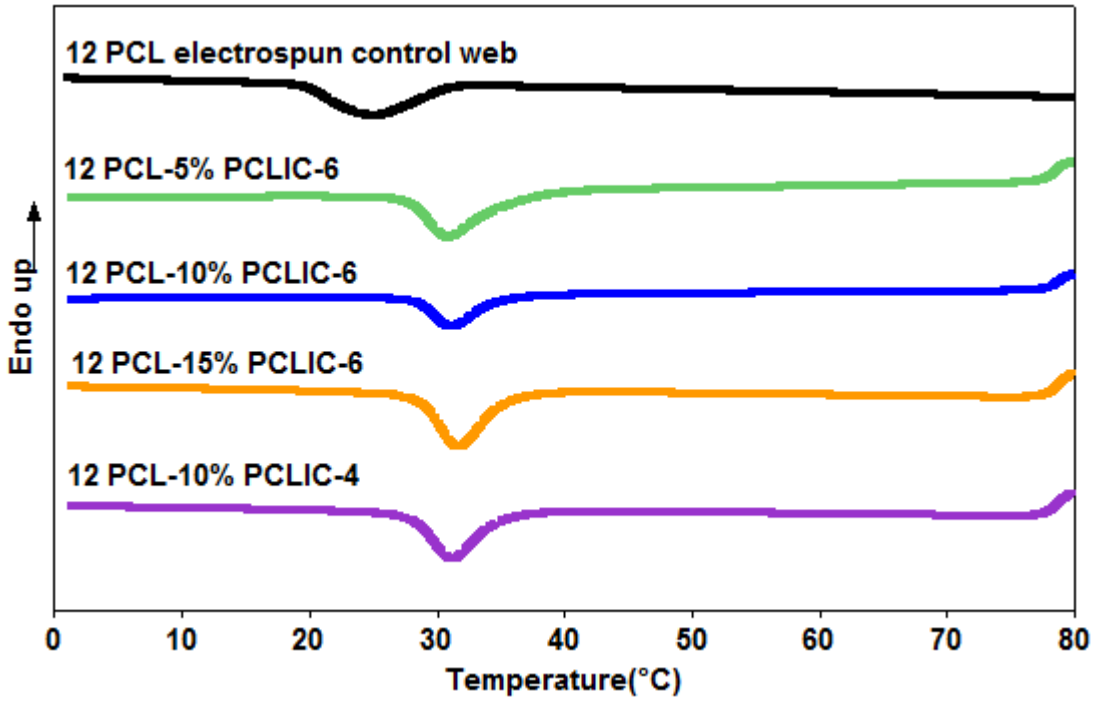

Figure 4.10: DSC first cooling thermograms of PCL and PCL/PCL IC nucleated nanofibers.

4.7.3. Thermogravimetric Analyses (TGA):

The thermal stability of the α-CD, neat PCL and PCL/PCLIC nanofibers was investigated by thermogravimetric analysis (TGA), and the results are shown in Figure 4.11. α-CDs exhibited two stage degradation: the first related to a significant water loss from 60 to 120° C (~10 %), and the second to degradation of the CD structure from 315 to 350 °C. The final residue at 500° C was observed to be about 10%. In the case of the neat PCL mat, there a one-step degradation was observed starting at about 410° C, and the final residue measured at 500° C was only about 2.5%. In the case of the IC nucleated nanofibers, however, two step degradation patterns were observed: the first step attributed mainly to the decomposition of

α-CD, followed by second step in which the decomposition of the dangling PCL chain portions and bulk neat PCL occurred. Interestingly, no water loss was observed (~<0.05%) in these cases, which indicates that the α-CD cavity had been threaded by PCL chains, and therefore no loss of weight due to water could occur. Also, the weight loss that is attributed to the α-CD has shifted significantly, instead of 315° C, the degradation started at 350° C, which is also a strong indication of the presence of ICs, instead of unthreaded α-CDs. Further, the final residues of IC containing nanofibers were observed to be 3.2%, 4.7%, and 6% for 5, 10, and 15% IC loading, respectively. These values are higher than that of neat PCL alone (2.5%), but less than that of α-CD powder. The melting and crystallization characteristics obtained from DSC, along with the thermal degradation characteristics obtained from TGA indicate that in these nanofibers, PCL and CDs are in threaded form.

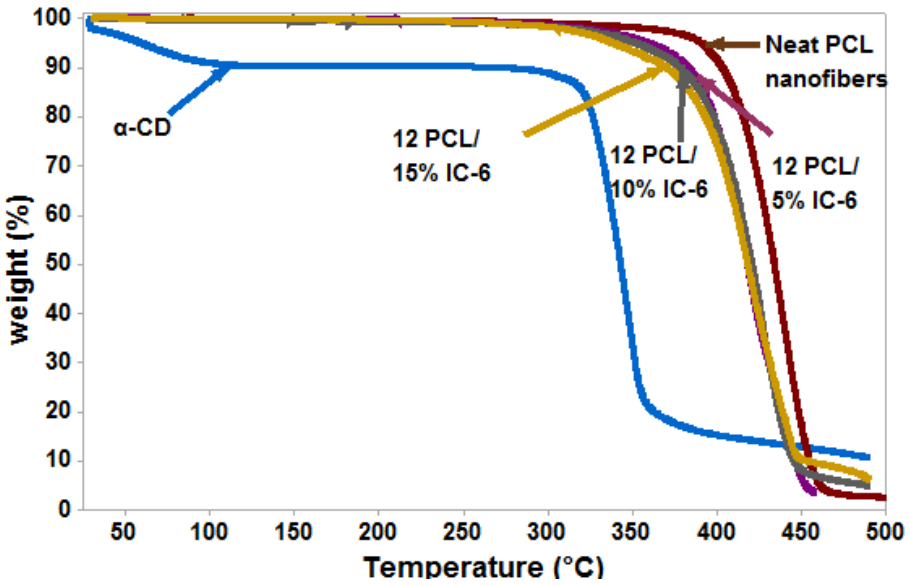

Figure 4.11: TGA thermograms of a-CD, neat PCL, and PCL/PCL-IC composites.

4.7.4 Mechanical properties:

Tensile properties of the neat PCL nanofiber mat and nanofiber mats containing ICs-4 & 6 at various loadings are shown in Table 4.3**.** For clarification again, ICs 4 & 6 indicate the theoretical stochiometric ratio between PCL and CD, for example, IC-6 indicates the ratio of 6:1. The stress-strain plots for the structures containing ICs 4 & 6 are shown in Figures 4.12 and 4.13, respectively, along with neat PCL control and those containing neat α-CD for comparison.

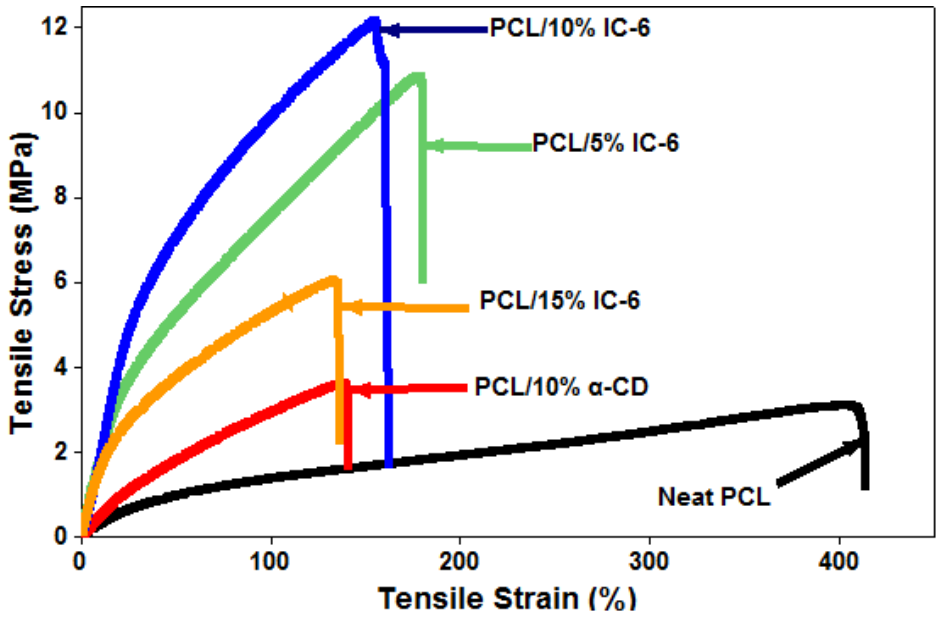

Figure 4.12: Stress-strain plots of Neat PCL, PCL/α-CD, and PCL/IC-6 composites.

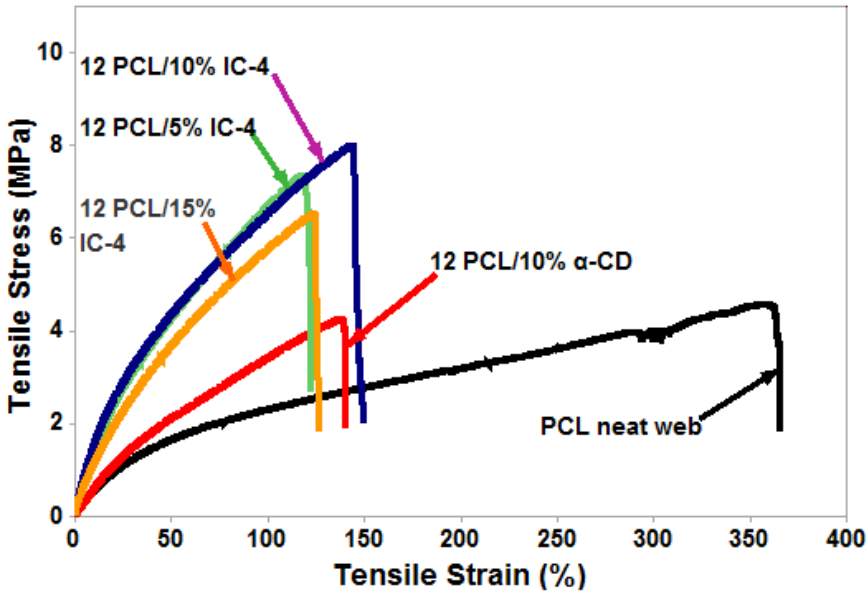

Figure 4.13: Stress-strain plots of Neat PCL, PCL/α-CD, and PCL/IC-4 composites.

Table 4.3: Tensile modulus and elongation at break values of neat PCL, PCL/αCD, and PCL/IC composites.

Sample	Tensile Modulus (MPa)	Elongation at break (%)
PCL neat control	2.55±0.86	390±66
PCL/α-CD	5.06±1.044	124±21
PCL/5% IC-6	13.90±4.57	149±50
PCL/10% IC-6	15.16±4.97	172±41
PCL/15% IC-6	9.46±2.01	132±21
PCL/5% IC-4	9.98±2.11	121±19
PCL/10% IC-4	10.24±1.23	165±22
PCL/15% IC-4	8.22±1.14	143±29

The neat PCL web was observed to have a tensile modulus of 2.55 ±0.9 MPa and elongation of 390± 67 %. It was observed through DSC analysis that a simple addition of α-CD elevated the crystallization temperature of the PCL, indicating the nucleating ability of the α-CD on PCL chains. Although, addition of 10% α-CDs resulted in an elevated modulus ($P<0.05$), its elongation at break and maximum load bearing capability decreased extensively, indicating, it more likely encountered the classical problem associated with nanoparticles, *i.e.*, agglomeration and diffusion [46]. Also, due to the incompatibility of PCL and α-CD, bonding between the PCL and α-CD is retarded, which also causes the mechanical properties, to be poor, in general. However, with the addition of ICs into the PCL matrix, marked increases in ultimate tensile strengths and moduli are observed, although with a decrease elongation at break. In the case of the IC-6 nucleated composite fibers, superior modulus was observed at 5 and 10% IC loadings. At 15% loadings, however, the increase in modulus was far too less. It is interesting to note that at 5 and 10% loadings, the modulus values are statistically similar ($P>0.05$), but at 15% loading, statistically the value is significantly lower ($P<0.05$).

Elongation at break values are, however, quite different. 5% and 15% IC-6 loading have similar values ($P>0.05$), and 10% loading has higher value. These results suggest that at 10% IC loading, there is an excellent physical interaction between the PCL chains protruding from α-CD cavities and the adjacent unthreaded PCL chains, and possibly also presence of hard segments consisting of PCL chains in the α-CD cavities. As the material is stretched, the covered regions provide the tie points with the uncovered regions extending and bonding.

This results in high mechanical properties. In contrast, in PCL and PCL/α-CD, as the strain increases, shear yielding and followed by necking occurs, which results in the destruction of the composite. At 15% loading, due to significant agglomeration of the IC particles, interaction between the IC particles are higher, which causes the composite to yield and neck much easily than for 5 and 10% IC loading, resulting in lower elongation and modulus values. As pointed out earlier, the 10% IC loading has higher elongation at break values compared to not only 15% IC loading, but also 5% loading ($P<0.05$). At 5% IC loading, possibly tie points are too few whereas at 15% loading, the latter exceed the optimum value.

In case of the composites nucleated by IC-4, higher moduli and elongation at break are observed for 10% loading, similar to that for PCL/IC-6 composites. However, relatively marked decrease in modulus values are observed ($P<0.05$). The possible reason is that, since the availability/lengths of the dangling chains are far less compared to that in IC-6, much less interaction occurs; this decreases the modulus values. Further, of all the IC nucleated composites, lowest modulus values were observed for IC-4 composites at loadings similar to those in IC-6 composites. The trend of elongation at break values for PCL/ IC-4 composites were similar to those for IC-6 composites. With 5 and 15% IC-4 loadings, the composites exhibited statistically lower ($P>0.05$), and with10% IC-4 higher elongation values ($P<0.05$).

In summary, the stress-strain measurements indicate that the ultimate mechanical properties are influenced by both type of IC loading as well as the % loading. In general, 10% IC loading seem to be optimal, and the longer the unthreaded dangling IC chains, *i.e.*, the less coverage, the better the tensile properties.

4.8 Conclusions:

PCL-α-CD-ICs with varying stochiometries were prepared and characterized using FTIR, DSC, and their stochiometries estimated by ^{1}H-NMR. Composite nanofibers containing PCL and PCL-α-CD-ICs with varying stochiometric ratios were prepared using electrospinning process from a 6:4 mixture of CFM/DMF. Average fiber diameters of the composite fibers were observed to depend on both the stochiometric ratios as well as the % loading. Composite fibers containing IC-4, with shorter un-included PCL chain portions, exhibited much smaller fiber diameters, and at 5% loading (400 nm) the fiber diameter was statistically similar to that of control PCL nanofibers. However, when the % loading was increased beyond 5%, the fiber diameter increased, with the value at 15% loading being 550 nm. Interestingly, for the composite nanofibers containing IC-6, even at 5% loading, the fiber diameter was 550 nm. Since IC-6 contains longer un-included PCL chain portions, the addition of these ICs could have increased the viscosity, resulting in larger fiber diameters.

DSC analyses indicated that, irrespective of the stochiometries of the ICs, the addition of the PCL-α-CD-ICs increased the melting temperatures of the composites. Also, similar to unthreaded neat CDs, ICs also enhanced the crystallization temperatures, indicating the nucleating ability of these ICs on the PCL matrix. Through TGA, enhanced thermal stability of α-CD in the composites containing PCL-α-CD-ICs was observed which indicate dethreading did not occur, and the structure of the IC has been retained in the composites. This result was further corroborated by the absence of water loss from 75 to 125^{o} C, indicating IC structures in the composites to be intact.

The stress strain measurements illustrated that there is substantial increase in modulus, tensile strength, and maximum load, the composites can withstand. Increased modulus combined with lowered elongations at break indicates the increase in the stiffness of these composites. The maximum tensile properties were observed for those containing IC-6 over those containing IC-4, at same % loadings. This was likely due to the longer un-included PCL chain portions in IC-6, which are better able to interact with the unthreaded matrix PCL chains. Also, in both cases, 10% loading was observed to be optimal. In this study, only two (n-s)-PCL-α-CD-ICs were considered. From this limited comparison, it seems that higher stoichiometric PCL CD ratios elicit better properties. Thus, it would be interesting to study composites containing higher stochiometries, because even better mechanical properties can be achieved.

Acknowledgements:

The writer would like to thank his colleague, Hammad Cheema, in Fiber & Polymer Science program, for his help with ^{1}H-NMR data analysis and CHEM-DRAW drawings of CDs and PCL structures.

References:

1. Reneker DH, Yarin AL, Zussman E, Xu H. Electrospinning of Nanofibers from Polymer Solutions and Melts. Adv. Appl. Mech.2007; 43-197.

2. Huang ZM, Zhang Y-Z, Kotaki M, Ramakrishna S. A Review on Polymer Nanofibers by Electrospinning and their Applications in Nanocomposites. Compos. Sci. Technol.2003; 63:2223-2253.

3. Li D, Xia Y. Electrospinning of Nanofibers: Reinventing the Wheel. Adv Mater.2004; 16:1141-1170.

4. Jin L, Wang T, Zhu M-L, Leach MK, Naim YI, Corey JM, Feng Z-Q, Jiang Q. Electrospun Fibers and Tissue Engineering. J. Biomed. Nanotechnol.2012; 8:1-9.

5. Homayoni H, Ravandi SAH, Valizadeh M. Electrospinning of Chitosan Nanofibers: Processing Optimization. Carbohydr. Polym. 2009; 77: 656-661.

6. Huang Z-M, Zhang YZ, Ramakrishna S, Lim CT. Electrospinning and Mechanical Characterization of Gelatin Nanofibers. Polymer.2004; 45:5361-5368.

7. Matthew JA, Wnek GE, Simpson DG, Bowlin GL. Electrospinning of Collagen Nanofibers. Biomacromolecules.2002; 3:232-238.

8. Min BM, Lee G, Kim SH, Nam YS, Lee TS, Park W-H. Electrospinning of Silk Fibroin Nanofibers and its Effect on the Adhesion and Spreading of Normal Human Keratinocytes and Fibroblasts *in vitro*.Biomaterials.2004; 25:1289-1297.

9. Kayaci F, Uyar T. "Electrospun Zein Nanofibers Incorporating Cyclodextrins. Carbohydr. Polym. 2012; 90:558-568.

10. Sarioglu OF, Yasa O, Celebioglu A, Uyar T, Tekinay,T. Efficient Ammonium Removal from Aquatic Environments by Acinetobacter Calcoaceticus STB1 Immobilized on Electrospun Cellulose Acetate Nanofibrous Web. Green Chem. 2013; 15: 2566-2572.

11. Li, WJ, Danielson KG, Alexander PG, Tuan RS.Biological Response of Chondrocytes Cultured in Three-dimensional Nanofibrous Poly(epsilon-caprolactone) Scaffolds.J.Biomed.Mater.Res A.2003; 67:1105-1114.

12. Patra SN, Easteal AJ, Bhattacharya D. Parametric Study of Manufacturing Poly(lactic) acid Nanofibrous Mat by Electrospinning. J.Mater.Sci.2009; 44: 647-654.

13. Boland ED, Wnek GE, Simpson DG, Pawlowski K.J, Bowlin G.L. Tailoring Tissue Engineering Scaffolds Using Electrostatic Processing Techniques: A Study of Poly(Glycolic Acid). J. Macromol. Sci.,Part A: Pure Appl.Chem. 2001; 38: 1231-1241.

14. Chung S, Moghe AK, Montero GA, Kim SH, King MW. Nanofibrous Scaffolds Electrospun from Elastomeric Biodegradable Poly(l-lactide-co--caprolactone) copolymer. Biomed. Mater.2009; 4:1-9.

15. Bini TB, Gao S, Tan, TC, Wang S, Lim A, Hai LB, Ramakrishna S. Electrospun Poly (L-lactide-co-glycolide) Biodegradable Polymer Nanofibre Tubes for Peripheral Nerve Regeneration. Nanotechnol. 2004; 15:1459-1464.

16. Mahoney C, Mccullough MB, Sankar J, Bhattarai N. Nanofibrous Structure of Chitosan for Biomedical Applications. J Nanomedic Biotherapeu Discover.2012; 2:1000102.

17. Xie J, Zhong S, Ma B, Shuler FD, Lim CT. Controlled Biomineralization of Electrospun Poly(ε-caprolactone) Fibers to Enhance their Mechanical Properties. Acta Biomater.2013;13:5698-5707.

18. Okhawa K, Cha D, Kim H, Nishida A, Yamamoto H. Electrospinning of Chitosan. Macromol. Rapid Commun.2004; 25:1600-1605.

19. Steyaert, Iline, Lien Van der Schueren, Karen De Clerck, et al. "Blend Electrospinning of Chitosan / Polycaprolacton Nanofibres." *11th European Symposium on Polymer Blends, Book of Abstracts*. San Sebastian, Spain: Universidad des Pais Vasco, 2012. 75-76.

20. Tyagi P, Catledge SA, Stanishevsky A, Thomas V, Vohra YK. Nanomechanical Properties of Electrospun Composite Scaffolds Based on Polycaprolactone and Hydroxyapatite. J. Nanosci. Nanotechnol.2009; 9:4839-4845.

21. Powell HM, Boyce ST. Engineered Human Skin Fabricated using Electrospun Collagen–PCL Blends: Morphogenesis and Mechanical Properties. Tissue Eng., Part A. 2009; 8: 2177-2187.

22. Saeed K, Park S-Y, Lee H-W, Baek J-B, Huh W-S. Preparation of Electrospun nanofibers of Carbon Nanotube/Polycaprolactone Nanocomposite. Polymer.2006; 47: 8019-8025.

23. Kolbuk D, Sajkiewicz P, Maniura-Weber K, Fortunato G. Structure and Morphology of Electrospun Polycaprolactone/Gelatine Nanofibres. Eur. Polym. J. 2013; 49:2052-2061.

23a.Blaise C, Gagné F, Fêrard JF. Ecotoxicity of Selected Nano-materials to Aquatic Organisms. Environ Toxicol;2008, 23:591-598.

24. Mark EJ, Polymer Data Handbook.Oxford University Press 1999

.

25. Mano JF, Sousa RA, Boesel LF, Neves NM, Reis RL. Bioinert, Biodegradable and Injectable Polymeric Matrix Composites for Hard Tissue Replacement: State of the Art and Recent Developments. Compos. Sci. Technol.2004; 64:789-817.

26. Du Y-Z, Xu J-G, Wang L, Yuan H, Hu F-Q. Preparation and Characteristics of Hydroxypropyl-β-cyclodextrin Polymeric Nanocapsules Loading Nimodipine Euro.Polymer.J.2009; 29:1397-1402.

27. Rusa CC, Fox J, Tonelli AE. Competitive Formation of Polymer-Cyclodextrin Inclusion

Compounds.Macromolecules.2003; 36:2742-2747.

28. Lu J, Mirau PA, Tonelli AE. Dynamics of Isolated Polycaprolactone Chains in their Inclusion Complexes with Cyclodextrins.Macromolecules.2001; 34:3276-3284.

29. Harada A, Kamachi M. Complex Formation Between Poly (ethylene glycol) and α-Cyclodextrin. Macromolecules.1990; 23:2821-2823.

30. Rusa CC, Luca C, Tonelli AE. Polymer−Cyclodextrin Inclusion Compounds: Toward New Aspects of Their Inclusion Mechanism.Macromolecules.200; 34:1318-1322.

31. Huang L, Allen E, Tonelli AE. **I**nclusion Compounds Formed Between Cyclodextrins and Nylon 6.Polymer.1999; 40:3211-3221.

32. Huang L, Allen E, Tonelli AE. Study of the Inclusion Compounds Formed Between α-Cyclodextrin and High Molecular Weight Poly (ethylene oxide) and Poly(ε-caprolactone).Polymer.1998; 39:4857-4865.

33. Vedula J, Tonelli AE. Reorganization of Poly (ethylene terephthalate) Structures and Conformations to Alter Properties. J. Polym. Sci., Part B: Polym. Phys.2007; 45:735-746.

34. Wei M, Tonelli AE. Compatiblization of Polymers via Coalescence from Their Common Cyclodextrin Inclusion Compounds.Macromolecules.2001; 34:4061-4065.

35. Wei M, Shuai X, Tonelli AE. Melting and Crystallization Behaviors of Biodegradable Polymers Enzymatically Coalesced from Their Cyclodextrin Inclusion Complexes. Biomacromolecules.2003; 4:783-792.

36. Tonelli AE. Organizational Stabilities of Bulk Neat and Well-mixed, Blended Polymer Samples Coalesced from their Crystalline Inclusion Compounds Formed with Cyclodextrins. J. Polym. Sci., Part B: Polym. Phys. 2009; 47:1543-1553.

37. Williamson B, Tonelli AE. Constrained Polymer Chain Behavior Observed in their Non-stoichiometric Cyclodextrin Inclusion Complexes. J Incl Phenom Macrocycl Chem.2012; 72:71-78.

38. Tonelli AE. Non-Stoichiometric Polymer-Cyclodextrin Inclusion Compounds: Constraints Placed on Un-Included Chain Portions Tethered at Both Ends and Their Relation to Polymer Brushes. Polymers.2014; 6:2166-2185.

39. Dong T, Mori T, Pan P, Kai W, Zhu B, Inoue Y. Crystallization Behavior and Mechanical Properties of Poly (ε-caprolactone)/Cyclodextrin Biodegradable Composites.

J. Polym. Sci.2009; 2351–2357.

40. Luo H, Liu Y, Yu Z, Zhang S, Li B. Novel Biodegradable Shape Memory Material \ Based on Partial Inclusion Complex Formation between α-Cyclodextrin and Poly(ϵ-caprolactone).Biomacromolecules.2008; 9:2573-2577.

41. Narayanan G, Gupta BS, Tonelli AE. Poly(ε-caprolactone) Nanowebs Functionalized with α- and γ-Cyclodextrins. Biomacromolecules.2014; 15:4122-4133.

42. Narayanan G, Gupta BS, Tonelli AE. Efficient Wound Odor Removal by β-Cyclodextrin Functionalized Poly (ε-caprolactone) Nanofibers. Biomacromolecules, submitted.

43. Williamson BR, Krishnaswamy R, Tonelli AE. Physical Properties of Poly(ε-caprolactone) Coalesced from its α-Cyclodextrin Inclusion Compound.Polymer.2011;52: 4517-4527.

44. Mohan A, Joyner X, Kotek R, Tonelli AE. Constrained/Directed Crystallization of Nylon-6. I. Nonstoichiometric Inclusion Compounds Formed with Cyclodextrins Macromolecules.2009; 42:8983-8991.

45. Dong T, He Y, Zhu B, Shin KM, Inoue Y. Nucleation Mechanism of α-cyclodextrin-Enhanced Crystallization of some Semicrystalline Aliphatic Polymers. Macromolecules.2005; 38:7736-7744.

46. Bilotti E, Fischer HR, Peijs T. Polymer Nanocomposites Based on Needle-like Sepiolite Clays: Effect of Functionalized Polymers on the Dispersion of Nanofiller, Crystallinity, and Mechanical Properties. J.Polym.Sci. 2008; 107:1116-1123.

47. Vogel R, Tandler B, Haussler L, Jehnichen D, Brunig H. Melt Spinning of Poly (3-hydroxybutyrate) Fibers for Tissue Engineering Using α-Cyclodextrin/Polymer Inclusion Complexes as the Nucleation Agent. Macromol. Biosci.2006; 6:730–736.

Supporting information:

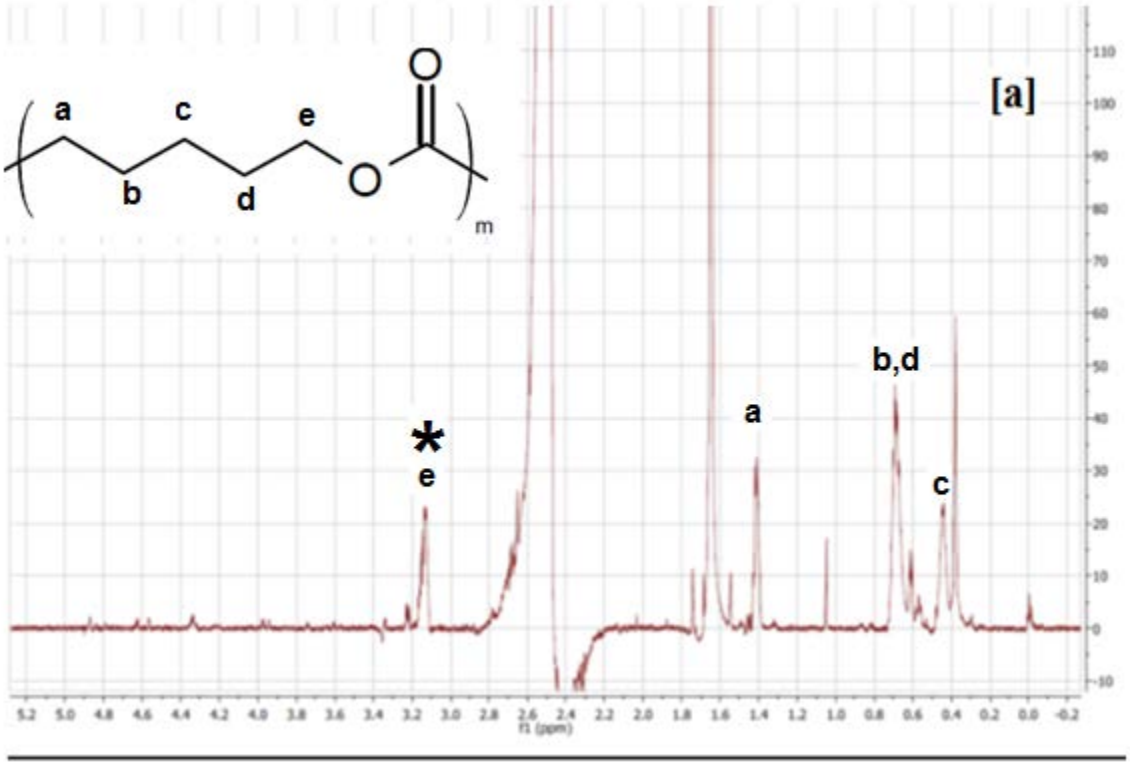

Figure S-1: 1H-NMR spectrum of PCL dissolved in d-DMSO at 80º C.

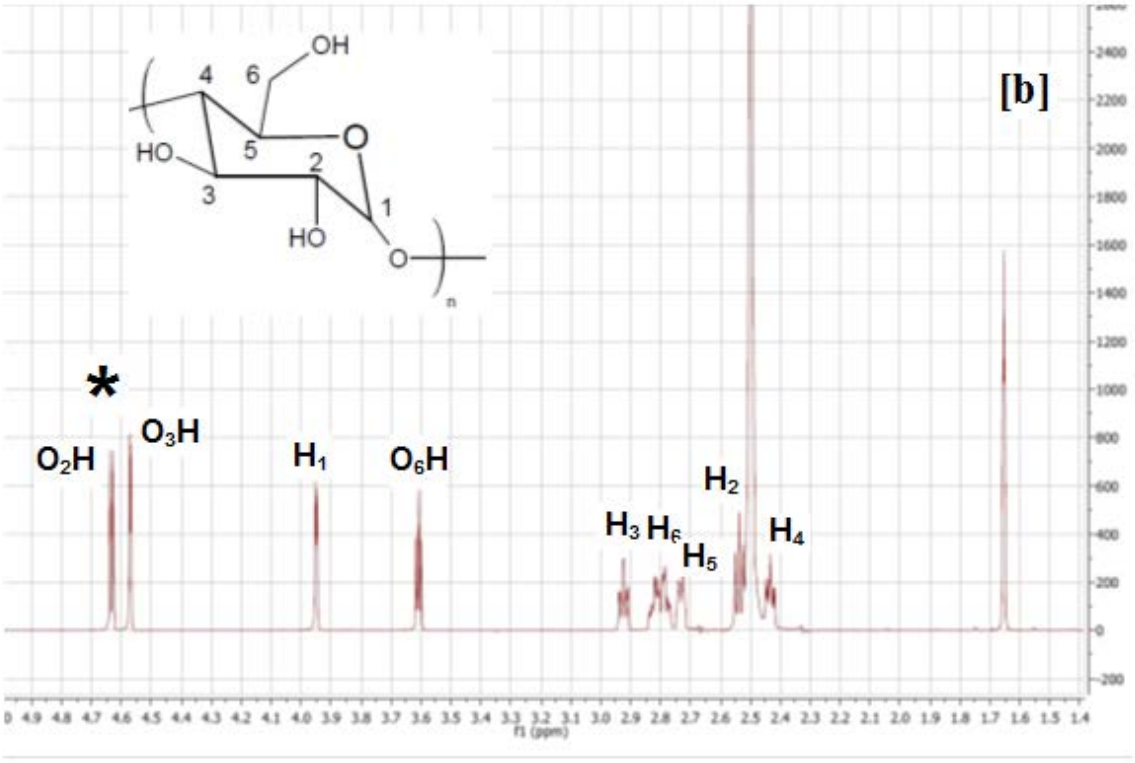

Figure S-2: 1 H-NMR spectrum of α-CD dissolved in d-DMSO.

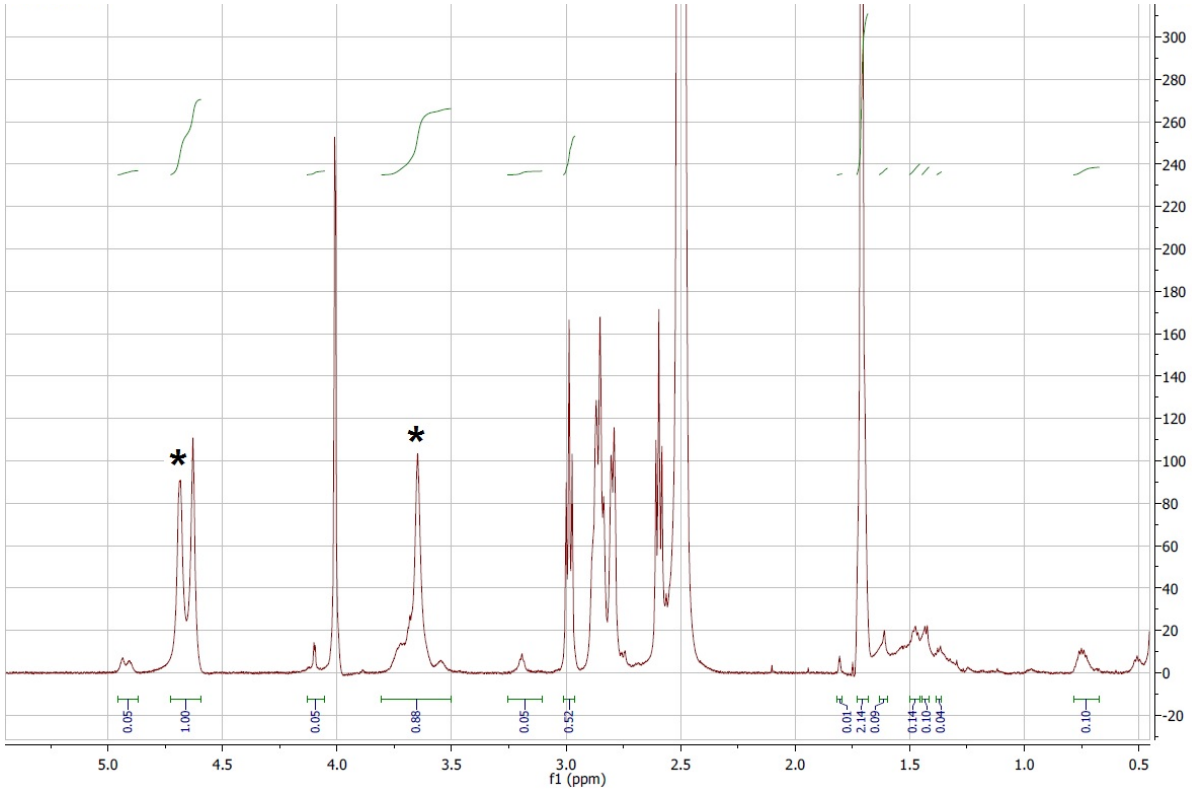

Figure S-3: 1H-NMR spectrum of IC-6 dissolved in d-DMSO at 80º C. Tests were performed at room temperature.

Stochiometric calculation:

α-CD intensity= 1.00 (doublet of O_2H and O_3H protons)

PCL intensity= 0.88 (two protons corresponding to methylene group)

Ratio of intensities= (0.88/2)/ (1/12) = 5.28

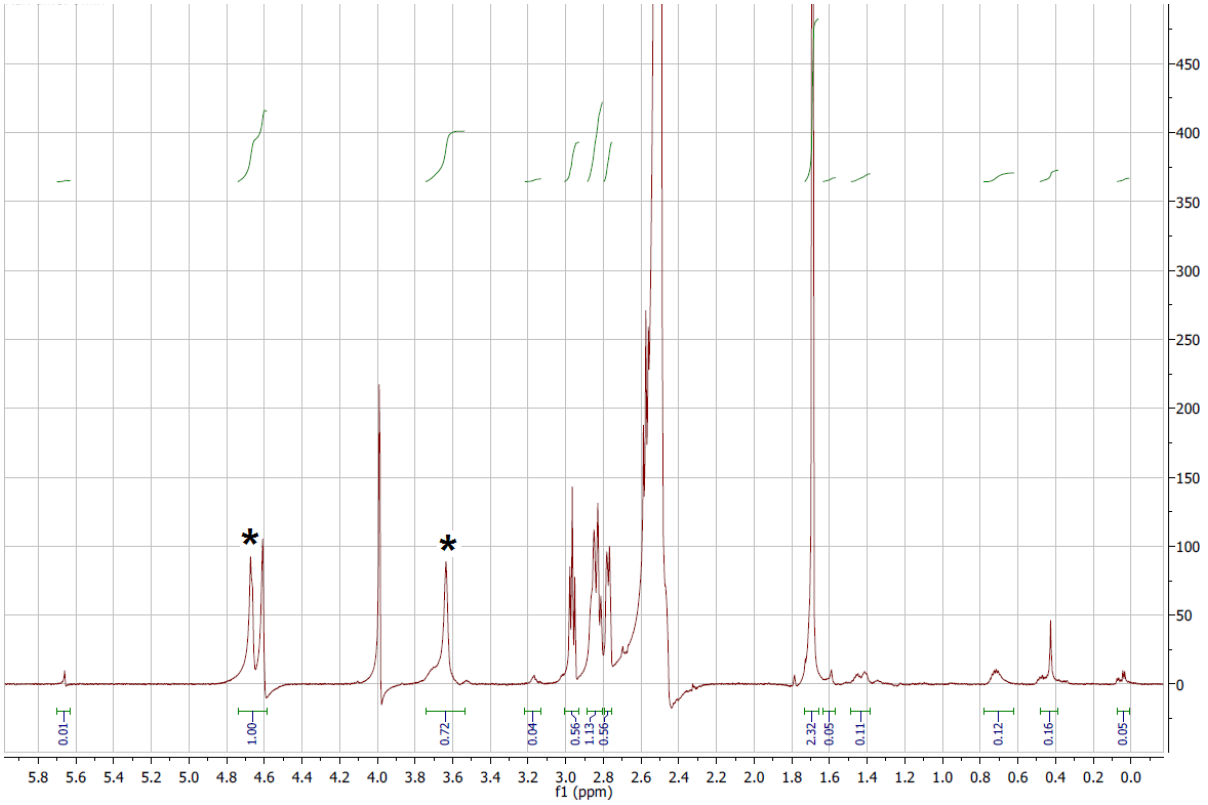

Figure S- 4: 1H-NMR spectrum of IC-4 dissolved in d-DMSO at 80º C. Tests were performed at room temperature.

Stochiometric calculation:

α-CD intensity= 1.00 (doublet of O_2H and O_3H protons)

PCL intensity= 0.72 (two protons corresponding to methylene group)

Ratio of intensities= (0.72/2)/ (1/12) = 4.32

Chapter 5: Summary and Conclusions:

5.1 Summary:

The goal of this work was to functionalize polymeric nanofiber scaffolds using CDs or ICs with desired properties for variety of applications. Although, a few studies on electrospinning polymer/CD have been reported in the literature, those systems were simple and complicated polymeric system such as PCL have never been studied before. Therefore, the objectives of the current research were to (1) develop PCL nanofiber surfaces functionalized with α- and ɤ-CDs, (2) since PCL is a biodegradable and biocompatible material, find an innovative application where the hollow cavities of CDs can be utilized for small molecular encapsulation, (3) engineer the PCL nanofibers with enhanced mechanical properties using (n-s)-PCL-α-CD-ICs, which might address the drawbacks of neat PCL nanofibers.

Initial studies were aimed at identifying the solvent or combination of solvents that might be suitable for electrospinning PCL/CD systems. It was observed that a binary solvent mixture is a must for electrospinning PCL/CD systems, since PCL and CD do not have a single solvent that can dissolve them. Various solvent combinations such as acetone/water, acetone/DMF, THF/DMF, chloroform/water, chloroform/DMF, to name a few, were tried as solvents for PCL and CD, respectively. It was found that lesser precipitation of, possibly ICs, occurred in chloroform/DMF solvent mixture, and hence was chosen for the electrospinning study.

As mentioned before, aliphatic polyesters have not been done before because of two reasons: primary reason is due to the rapid formation of ICs or (n-s) ICs, and the secondary reason is the potential complication of electrospinning from immiscible solvent mixtures. To optimize the electrospinning process and to obtain finer bead free fibers, solution studies were conducted. It was observed that, minimum PCL concentration of 12% was required, and unlike polymer/CD systems reported in the literature, significant change in surface tension or conductivity values were not observed. At PCL concentration of 14%, larger fiber diameters were obtained (800 nm), and with slight reduction in PCL concentration (12%), finer fiber diameters (600 nm) were obtained and also higher CD concentrations were possible. However, with such increased CD loadings, agglomerations of CDs were noted, which is unfortunately unavoidable.

Prepared PCL/CD systems were subsequently characterized by analytical techniques such as FTIR, TGA, DSC, and WAXD, to understand surface, thermal, crystal structure of these hybrid structures, respectively. Those studies indicated that at higher loadings, there was formation of (n-s)-ICs, which was confirmed by both WAXD and TGA. However, with the addition of CDs, significant improvement in the crystallinity of the PCL was also observed. Moreover, with the addition of CDs, even at 5% CD loading, a drastic reduction in water contact angle was observed. To test the availability of unthreaded CDs, molecular encapsulation studies were performed using phenolphthalein (PhP) as a model compound. Nanowebs with higher CD loadings resulted in enhanced PhP encapsulation. Based on these

observations, a simple hypothetical model was created which could potentially serve as a guideline for similar polymer/CD systems.

In the case of PCL/β-CD structures, a slight change in the electrospinning process was necessitated, as precipitation of β-CD was observed, especially at higher loadings. To overcome the precipitation of β-CDs, solution feed rate was increased to 1 mL/hr, rather than 0.5 mL/hr which was used for PCL/α-CD or PCL/ɤ-CD systems. But increase in the feed rate resulted in the increase of fiber diameter statistical outliers, especially at higher CD loadings. Moreover, in the WAXD analyses, with the addition of β-CDs, slight distortion of PCL crystal structures were observed. The surface functionalities of these nanowebs were assessed using XPS spectra. It was found that increase in the CD loading resulted in the nanofibers with increased oxygen content. It was expected, as when two immiscible materials are mixed, the low molecular weight compound typically aggregates on the surface, in this case CDs.

A potential application of this hybrid nanofiber structures in absorbing wound odor was investigated using a model compound of combination of butyric and propionic acids in ethanol. All the nanowebs, including neat PCL, were found to absorb these acids; however, neat PCL was not observed to mask the odor. But, PCL/β-CD structures were observed not only to adsorb these volatile fatty acids but also mask those foul smelling odors.

Due to poor interaction between PCL and CDs (α-β- and ɤ-CDs), significant improvements in the mechanical properties of the prepared nanowebs are not expected. To improve the mechanical properties of the nanowebs and thereby to make these materials

suitable for bone tissue engineering applications, composite fibers comprising PCL and (n-s)-PCL-α-CD-ICs were prepared. Prior to electrospinning, the (n-s)-PCL- α-CD-ICs were characterized using FT-IR, DSC, and its stochiometry estimated using ^{1}H-NMR. Of the various ICs prepared, only two ICs with PCL: CD stochiometries of 6:1 and 4:1 were chosen for this study.

Based on our previous observations with PCL/CD systems, PCL concentration of 14% was chosen and the IC loading varied from 5 to 15%. Similar to PCL/CD systems, at 14% PCL concentration, beaded fibers were obtained, especially at higher IC loadings. However, when the PCL concentration was set at 12%, bead-free fibers were obtained upto 15% IC loading. Thermal analyses indicated, with the addition of ICs, there was a significant increase in the melting temperatures of the composites (~ 65 °C for the composite fibers vs 59 °C for the neat PCL and PCL/α-CD fibers). Moreover, the degradation patterns observed by TGA indicated the presence of ICs, rather than simple mixtures.

Instron testing was performed to study the mechanical properties of these nanowebs. Addition of ICs was observed to have a profound effect on the mechanical profile of these nanowebs. Especially, those with a higher stochiometry (IC-6), exhibited higher tensile modulus (15.16±4.97 MPa for the 10% IC-6 loading vs 2.55 ±0.86 MPa for the neat PCL fibers) of the nanowebs, and also caused a decrease in elongation values (172±41 for 10% IC-6 loading vs 390±66 for the neat PCL fibers). Another key observation observed was that, although bead-free fibers were made at 15% IC-loading, it did not translate into stronger fibers. In fact, for both IC-4 and IC-6 based composites, stronger fibers were obtained at 10%

IC-loading, rather than 15% loading. This suggested that10% loading to be the most ideal loading ratio to improve the mechanical properties of the PCL nanowebs.

5.2 Conclusions:

The major conclusions that can be derived from this investigation are as follows:

- For the preparation of bead-free PCL/CD (all three CDs) composite fibers with higher CD loadings, a maximum solution concentration of 12% PCL was required. This was necessary to ensure sufficient entanglements of the PCL chains are available for the preparation of the composite fibers. Above this concentration, slightly beaded fibers were obtained and, below which, higher CD loadings were not possible.
- With the addition of CDs (α- and ɤ-CDs), a significant increase in crystallinity as well as faster crystallization of PCL was noted. Also observed was the drastic reduction in the water contact angle measurements in CD containing nanowebs. However, at higher loadings, some of the PCL chains might have threaded through the CD cavities; more so, in the case of α-CD functionalized PCL nanofibers.
- PhP absorption measurements indicated ɤ-CD functionalized PCL nanofibers to absorb PhP at much faster rates. One possible reason could be due to the threading of PCL chains through the α-CD cavity.
- Unlike α- and ɤ-CD functionalized PCL nanofibers, those containing β-CDs were found to be not threaded by PCL chains, which are expected to result in enhanced molecular absorption capabilities. The surface analyses indicated aggregation of

PCL surface by the CDs, and the model wound odor absorption test indicated, composite fibers with higher CD loading to be capable of masking the wound odor.

- With the addition of ICs instead of plain CDs, composite fibers were found to exhibit higher melting temperatures, but similar crystallization temperatures. Also, the higher degradation temperature of the ICs indicated that the ICs are present intact in the nanofibers, rather as dethreaded CDs. This was further confirmed by the absence of any water loss.
- Mechanical testing indicated, both type of IC as well as % loading of the ICs played a role in improving the mechanical properties. Especially, IC-6 resulted in higher modulus values compared to IC-4, at all loadings. Also, in both cases, 10% IC-loading was found to be optimal and had slightly higher value than 5% IC-loading; but had significantly higher modulus values than those containing 15% IC-loading.

As a general conclusion based on the results of this investigation, it can be stated that PCL and CDs can be combined in different ways using electrospinning method to produce nanostructures with contrasting properties and applications. As expected prior to the start of the work, these nanostructures exhibit enhanced surface or mechanical properties than found in neat-PCL nanofibers alone.

Chapter 6: Recommendations for Further Research:

This research demonstrated that CDs can be utilized to surface functionalize the PCL nanofibers. Such structures offer immense potential for further surface modification, due to the presence of abundant hydroxyl groups in CDs. The surface modification of hydroxyl groups with suitable functional groups, including biological molecules, could be carried out. For the PCL surface to be biologically active, PCL is plasma treated and then grafted with a spacer molecule, which could then interact with natural polymers, such as collagen or gelatin. Having CDs on the surface would likely make the plasma treatment unnecessary. Additionally, by virtue of its capability to include smaller molecules, CDs, as reported in this study, could also be used in applications such as wound odor absorbance.

In this study, only butyric and propionic acids were examined. However, in a real exudate, various other components, such as cadaverine and putrescine, are present as well. It would be of interest to conduct a detailed study on a simulated wound fluid containing all of its common components, and if the results are promising, an animal study might also be considered. The effect of CDs on wound healing was not investigated in this study. As a follow up study, effects of CDs on wound healing could be investigated using neo-natal or adult Human Dermal Fibroblasts (HDF) cells.

In this study, only two (n-s)-ICs were used to increase the mechanical properties of the PCL nanowebs, and the general trend indicated, higher the stochiometry between the PCL and CD caused an increase in tensile modulus and decreased elongation values. It is quite

possible to make (n-s)-ICs with a much higher stochiometries, hence a detailed study involving those (n-s)-ICs should be carried out. The goal of this work was to generate a scaffold for bone tissue engineering; hence, cell differentiation studies in osteogenic pathway should be conducted. Since, a scaffold with better mechanical properties have been known to result in better cell differentiation of stem cells into osteoblasts, those scaffolds containing (n-s)-ICs with enhance properties are expected to differentiate better than neat PCL control.

Appendix:

Statistical analyses of tensile modulus values (2-sample t-test):

Control PCL and α-CD

Sample	N	Mean	StDev	SE Mean
1	10	2.550	0.866	0.27
2	10	5.06	1.04	0.33

Difference = μ (1) - μ (2)

Estimate for difference: -2.510

95% CI for difference: (-3.412, -1.609)

T-Test of difference = 0 (vs ≠): T-Value = -5.85 **P-Value = 0.000** DF = 18

Both use Pooled StDev = 0.9592

a-CD and 5% IC-6

Sample	N	Mean	StDev	SE Mean
1	10	5.06	1.04	0.33
2	20	13.90	4.58	1.0

Difference = μ (1) - μ (2)

Estimate for difference: -8.84

95% CI for difference: (-11.87, -5.81)

T-Test of difference = 0 (vs ≠): T-Value = -5.98 **P-Value = 0.000** DF = 28

Both use Pooled StDev = 3.8175

5% IC-6 and 10% IC-6

Sample	N	Mean	StDev	SE Mean
1	20	13.90	4.58	1.0
2	14	15.16	4.97	1.3

Difference = μ (1) - μ (2)

Estimate for difference: -1.26

95% CI for difference: (-4.62, 2.11)

T-Test of difference = 0 (vs ≠): T-Value = -0.76 **P-Value = 0.452** DF = 32

Both use Pooled StDev = 4.7416

10% IC-6 and 15% IC-6

Sample	N	Mean	StDev	SE Mean
1	14	15.16	4.97	1.3
2	13	9.47	2.02	0.56

Difference = μ (1) - μ (2)

Estimate for difference: 5.69

95% CI for difference: (2.64, 8.74)

T-Test of difference = 0 (vs ≠): T-Value = 3.84 **P-Value = 0.001** DF = 25

Both use Pooled StDev = 3.8470

15% IC-6 and 5% IC-6

Sample	N	Mean	StDev	SE Mean
1	20	13.90	4.58	1.0
2	13	9.47	2.02	0.56

Difference = μ (1) - μ (2)

Estimate for difference: 4.43

95% CI for difference: (1.67, 7.19)

T-Test of difference = 0 (vs ≠): T-Value = 3.28 **P-Value = 0.003** DF = 31

Both use Pooled StDev = 3.7973

15% IC-6 and 5% IC-4

Sample	N	Mean	StDev	SE Mean
1	10	9.98	2.12	0.67
2	13	9.47	2.02	0.56

Difference = μ (1) - μ (2)

Estimate for difference: 0.514

95% CI for difference: (-1.287, 2.315)

T-Test of difference = 0 (vs ≠): T-Value = 0.59 **P-Value = 0.559** DF = 21

Both use Pooled StDev = 2.0590

5% IC-4 and 10% IC-4

Sample	N	Mean	StDev	SE Mean
1	10	9.98	2.12	0.67
2	9	10.24	1.23	0.41

Difference = μ (1) - μ (2)

Estimate for difference: -0.261

95% CI for difference: (-1.962, 1.441)

T-Test of difference = 0 (vs ≠): T-Value = -0.32 **P-Value = 0.751** DF = 17

Both use Pooled StDev = 1.7557

10% IC-4 and 15% IC-4

Sample	N	Mean	StDev	SE Mean
1	10	8.22	1.14	0.36
2	9	10.24	1.23	0.41

Difference = μ (1) - μ (2)

Estimate for difference: -2.020

95% CI for difference: (-3.169, -0.871)

T-Test of difference = 0 (vs ≠): T-Value = -3.71 **P-Value = 0.002** DF = 17

Both use Pooled StDev = 1.1855

Statistical analyses of Tensile Strain:

Neat PCL and α-CD

Sample	N	Mean	StDev	SE Mean
1	6	390.0	66.8	27
2	6	124.3	21.3	8.7

Difference = μ (1) - μ (2)

Estimate for difference: 265.7

95% CI for difference: (202.0, 329.5)

T-Test of difference = 0 (vs ≠): T-Value = 9.29 **P-Value = 0.000** DF = 10

Both use Pooled StDev = 49.5571

α-CD and 5% IC-6

Sample	N	Mean	StDev	SE Mean
1	6	124.3	21.3	8.7
2	19	149.3	21.3	4.9

Difference = μ (1) - μ (2)

Estimate for difference: -24.99

95% CI for difference: (-45.61, -4.37)

T-Test of difference = 0 (vs ≠): T-Value = -2.51 **P-Value = 0.020** DF = 23

Both use Pooled StDev = 21.2850

5% IC-6 and 10% IC-6

Sample	N	Mean	StDev	Mean
1	19	149.3	50.4	12
2	13	172.8	41.1	11

Difference = μ (1) - μ (2)

Estimate for difference: -23.5

95% CI for difference: (-58.0, 10.9)

T-Test of difference = 0 (vs ≠): T-Value = -1.39 **P-Value = 0.173** DF = 30

Both use Pooled StDev = 46.8983

10% IC-6 and 15% IC-6

Sample	N	Mean	StDev	SE Mean
1	19	132.4	21.1	4.8
2	13	172.8	41.1	11

Difference = μ (1) - μ (2)

Estimate for difference: -40.4

95% CI for difference: (-63.0, -17.8)

T-Test of difference = 0 (vs ≠): T-Value = -3.66 **P-Value = 0.001** DF = 30

Both use Pooled StDev = 30.6928

5% IC-4 and 10% IC-4

Sample	N	Mean	StDev	SE Mean
1	10	121.8	19.5	6.2
2	9	165.3	22.0	7.3

Difference = μ (1) - μ (2)

Estimate for difference: -43.53

95% CI for difference: (-63.62, -23.45)

T-Test of difference = 0 (vs ≠): T-Value = -4.57 **P-Value = 0.000** DF = 17

Both use Pooled StDev = 20.7221

10% IC-4 and 15% IC-4

Sample	N	Mean	StDev	SE Mean
1	9	143.1	29.4	9.8
2	9	165.3	22.0	7.3

Difference = μ (1) - μ (2)

Estimate for difference: -22.2

95% CI for difference: (-48.2, 3.7)

T-Test of difference = 0 (vs ≠): T-Value = -1.82 **P-Value = 0.088** DF = 16

Both use Pooled StDev = 25.9579